Dark Solitons in Optical Communication Systems

Katherine M. Allen

Doctor of Philosophy

The University of Aston in Birmingham

October 1995

The University of Aston in Birmingham

Dark Solitons in Optical Communications.

Katherine M. Allen

Doctor of Philosophy

1995

This thesis presents experimental and theoretical work on the use of dark optical solitons as data carriers in communications systems. The background chapters provide an introduction to nonlinear optics, and to dark solitons, described as intensity dips in a bright background, with an asymmetrical phase profile. The motivation for the work is explained, considering both the superior stability of dark solitons and the need for a soliton solution suitable for the normal, rather than the anomalous (bright soliton) dispersion regime.

The first chapters present two generation techniques, producing packets of dark solitons via bright pulse interaction, and generating continuous trains of dark pulses using a fibre laser. The latter were not dark solitons, but were suitable for imposition of the required phase shift by virtue of their extreme stability.

The later chapters focus on the propagation and control of dark solitons. Their response to periodic loss and gain is shown to result in the exponential growth of spectral sidebands. This may be suppressed by reducing the periodicity of the loss/gain cycle or using periodic filtering. A general study of the response of dark solitons to spectral filtering is undertaken, showing dramatic differences in the behaviour of black and 99.9% grey solitons. The importance of this result is highlighted by simulations of propagation in noisy systems, where the timing jitter resulting from random noise is actually enhanced by filtering. The results of using sinusoidal phase modulation to control pulse position are presented, showing that the control is at the expense of serious modulation of the bright background.

It is concluded that in almost every case, dark and bright solitons have very different properties, and to continue to make comparisons would not be so productive as to develop a deeper understanding of the interactions between the dark soliton and its bright background.

Additional key words and phrases

Nonlinear optics, transmission systems.

for George and Mary Allen

Acknowledgements

These acknowledgements come in no particular order, and to thank everyone who deserves it would be an impossible task, but at least here I have the opportunity to mention just a few of the many people who have kept me sane, and made working for a PhD an interesting and worthwhile experience.

Firstly I must thank both Ian Bennion and Nick Doran, Ian for first suggesting that I might be interested in research, and Nick for carrying on his good work, and being a paragon among supervisors: only there when I needed him for something ...

Among the post-doctoral students in our group, two stand out as having put in far more time and effort into my well-being than any call of duty could demand. John Williams and Nick Smith managed between them to not only keep me on the straight and narrow, but even keep me interested in what I was doing, and without them this thesis would be a lot briefer.

I must acknowledge John Williams again, and also Philippe Emplit of the Université Libre de Bruxelles, Belgium for concluding the experimental work on dark soliton generation via bright pulse collision when I was unable to.

This work was supported by an award from the James Watt Memorial Trust, and a CASE award from BT. My work at BT was guided by Keith Blow and Alistair Poustie, and I am grateful to them both for their advice and encouragement.

Finally, I would like to thank my friends and family, without whose unfailing support I might not have survived the joys of research. In particular I would like to mention Iain Brown, Jason Price, Finlay Knox, Amanda Moorhouse and Kate Sugden, for being there and listening. Thanks also to Karl Brabbin and to Patrick Hearn, without whom I would never have met the Asher sisters or Ergoda.

Contents

List of Figures

Chapter 1

Linear and nonlinear fibre optics.

Dark optical solitons have long been considered an interesting mathematical phenomenon, but in the last few years improvements in analytical and experimental tools have allowed workers to demonstrate some of their more practical uses. Generally described as intensity dips in a bright background, they possess in addition an asymmetric phase profile. This is an unusual feature of a stable pulse and one which is responsible for many of their unique responses.

Solitons form as a result of interplay between linear and nonlinear effects, both of which are considered problems in traditional communication systems. Bright soliton research is very much more advanced than the dark soliton work, and bright solitons are widely regarded as elegant and 'natural' carriers for high-speed data communications, with dark solitons having been largely ignored until recently.

However, many of the key features of the success of bright solitons are due to their generic soliton properties, not specifically to their form as bright pulses of

light. Studies have shown that dark solitons can exhibit greater stability than the more familiar bright solitons in some situations. Also, for those fibre communication systems currently in place unsuitable for bright solitons, changing to solitons as the data carriers (with all the advantages of stability this can bring) would mean implementing a dark soliton solution.

This chapter provides a background to basic linear and nonlinear optics, as applied to optical communications. It includes discussions of loss, dispersion, and the various effects resulting from the nonlinear response of silica to high-intensity electro-magnetic fields. It concludes with the modelling of these effects using the nonlinear Schroedinger equations, and the derivation of the bright and dark soliton solutions to this equation.

1.1 Introduction

It is now widely recognised that optical fibre technology provides the fastest and most secure method of transmitting large amounts of data very cheaply. With the recent huge growth in demand for Internet services such as electronic mail and the World Wide Web, any techniques for increasing bandwidth and reliability of communications systems are of great commercial value. One such technique is based on optical soliton technology, which uses the nonlinear properties of the interaction between light and silica to produce either bright or dark optical pulses (dips in a bright background) with remarkable stability.

In addition to their obvious commercial importance, the methods considered here are also of considerable mathematical interest, since the study of solitons is a branch of nonlinear physics. Solitons provide one of the first clear examples that the complexity of nonlinear systems could be harnessed and put to good use.

To understand the properties of dark temporal solitons it is first necessary to consider the behaviour of light in optical fibres. There are various different forms of this behaviour, which can be broadly separated into linear and nonlinear responses. Linear effects, such as loss and chromatic dispersion, will be observed independent of the optical power in the signal, whereas the various nonlinear effects are functions of power.

1.2 Linear Propagation

Early work with optical fibres concentrated exclusively on the linear response of glass to light[1]. At the very simplest level, a linear system will produce a predictable quantity $Y * x$ in response to an input x. If the input x is larger, whether it be a pulse of light entering a fibre, the pressure applied to the accelerator pedal or money owed to the bank at a fixed rate of interest, the corresponding output will change by the same percentage, resulting in more light at the output of a fibre, an increase in engine speed, or more debt.

When studying linear propagation in fibres there are two main effects of concern to systems designers; loss of power during transmission, and chromatic dispersion. The former results from a combination of many different effects, and the latter is due to the wavelength dependence of the speed of light in most media, well illustrated by the splitting of white light by a prism.

1.2.1 Loss

The loss in power which a signal suffers during propagation depends mainly on the wavelength of the light. Various effects contribute to this wavelength dependence. These include intrinsic attenuation due to absorption of energy

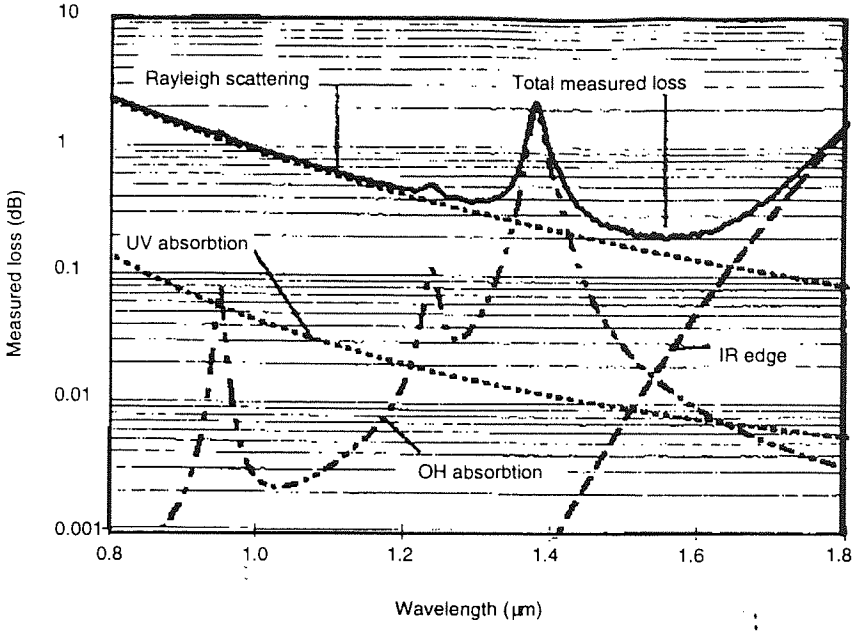

Figure 1.1: The importance of the different loss mechanisms to the wavelength dependent loss profile of silicon glass.

by the silica atoms, extrinsic attenuation due to the presence of impurities introduced into the fibre, and Rayleigh scattering.

The lower limit on loss for a given type of fibre is determined by the minimum absorption of energy by the basic fibre material at a given wavelength. For example, the minimum loss in pure silica fibre is 0.15 decibels per kilometre, and occurs at a wavelength of 1.55μm. This minimum results from the combination of the losses from the electron absorption bands at short wavelengths and losses related to the atomic vibration bands at long wavelengths (see figure 1.1).

In addition to intrinsic fibre losses there is the possibility of absorption by materials which have been introduced into the fibre, deliberately or otherwise, during manufacture. The most significant external contribution to the overall fibre loss results from the presence of OH^- ions. In the early days of fibre manufacture this was the main limitation on performance, but improvements in maintaining a dry atmosphere during forming and pulling have greatly reduced

these losses. Figure 1.1 (solid line) shows a typical loss profile for standard fibre. Notice the OH^- peak at 1.4μm, which separates the low-loss region into two areas, the second and third telecommunications windows. (The first, centred around 0.9μm, was of greater importance when water losses were high.)

Rayleigh Scattering is the final significant mechanism resulting in wavelength dependent loss and dominates at short wavelengths. It is caused by microscopic variations in the fibre composition, which produce variations in refractive index over scales which are short with respect to the wavelength of the light. These local fluctuations scatter light in all directions. The same effect can be seen on a clear day, where scattering of the shorter wavelengths makes the sky look blue.

1.2.2 Loss Compensation Techniques.

Fibre loss presents a significant limit to the distance over which signals can be transmitted and received without error. Various techniques have been proposed to restore signal energy lost during propagation. Traditionally, long-haul optical systems have used electronic transceivers to detect incoming signals and transmit clean pulses into the next span of fibre (see figure 1.2). The maximum span between transceivers is then a function of input power, fibre loss and receiver sensitivity.

There are various disadvantages to electronic regeneration of optical signals. Upgrading the system to a higher data rate means replacing all the regenerators in the line, and the time taken to detect and retransmit presents a transmission bottleneck caused by the maximum response speed of the electronic components. Systems which use multiple wavelengths in the same fibre to increase the total data flow rate must use wavelength splitters and recombiners at each stage, as well as circuitry designed to respond to each of the wavelengths used.

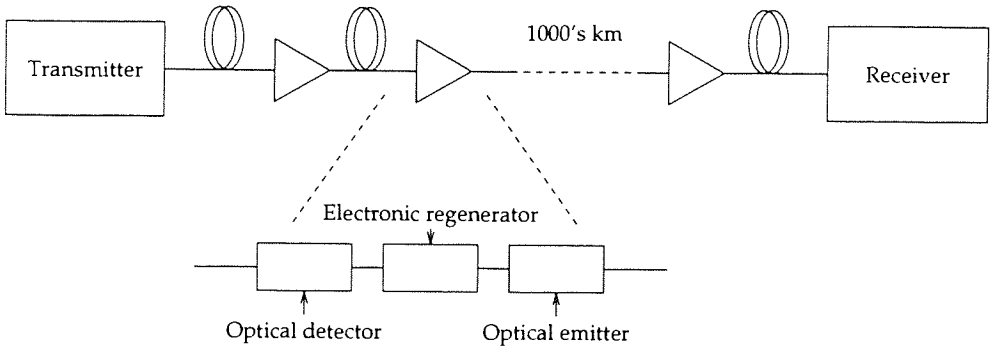

Figure 1.2: Schematic of a traditional long-haul transmission system, showing the repeated use of detection and retransmission to reduce the effects of loss.

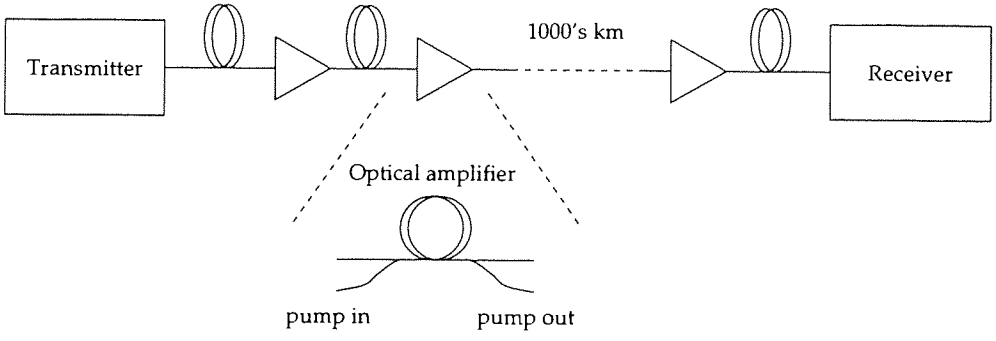

Figure 1.3: Schematic of transmission system using in-fibre amplification.

With the advent of rare-earth doped fibre technology it has become possible to amplify optical signals in-fibre (see figure 1.3). The most commonly used dopant is erbium, which emits over a range of up to 120nm, centred about the third telecommunications window at 1550nm[2],[3]. The use of all-optical amplifiers neatly removes the problems of data-rate and wavelength dependency associated with earlier schemes, and so the problem becomes one of maintaining pulse profiles over very long distances without the reshaping function originally provided by the electronics.

The most significant effects in pulse reshaping during propagation are due to dispersion, spontaneous emission noise produced and amplified at each amplifier and, at higher powers, the nonlinear response of the medium. The success of erbium-doped fibre amplifiers in extending the potential of optical communications has meant that attention is now being focused on solutions which combine linear and nonlinear effects to produce pulses with high stability.

1.2.3 Dispersion.

Chromatic dispersion.

Chromatic dispersion originates from the characteristic resonances at which a material absorbs electro-magnetic radiation. Effectively, the response of the medium, and therefore the speed of propagation is related to the optical frequency ω of the field in question. Since pulses of light are a combination of a range of different optical frequencies this results in pulse broadening. The most important result of this for communications systems is the very severe limits which it presents in terms of maximum bit rate and pulse spacing before the overlap of broadened pulses causes receiver errors.

The effects of fibre dispersion can be approximated by expanding the mode

propagation constant β about the centre frequency ω_0 as follows.

$$\beta(\omega) = n(\omega)\frac{\omega}{c} = \beta_0 + \beta_1(\omega - \omega_0) + \frac{1}{2}\beta_2(\omega - \omega_0)^2 + \cdots \tag{1.1}$$

where $n(\omega)$ is the refractive index of the material ω and c is the speed of light in a vacuum. The parameters β_1 and β_2 can be found from the refractive index and its derivatives. The rate of movement of a pulse envelope, the group velocity, is given by $v_g = 1/\beta_1$.

$$\beta_1 = \frac{1}{c}\left(n + \omega\frac{dn}{d\omega} = \frac{1}{v_g}\right) \tag{1.2}$$

$$\beta_2 = \frac{1}{c}\left(2\frac{dn}{d\omega} + \omega\frac{d^2n}{d\omega^2}\right) \tag{1.3}$$

Signals for which the group velocity dispersion parameter β_2 is positive are said to experience normal dispersion, and signals beyond this point experience anomalous dispersion. The changeover wavelength is known as the zero dispersion point, and in standard fibres occurs at a wavelength around 1.27μm. The phenomenon of waveguide dispersion (see section 1.2.3) can be used to move the zero dispersion point towards longer wavelengths.

It is normally only necessary to consider the effects of β_1, and β_2, unless the signal pulse width is very short (sub-picosecond) or the signal wavelength is close to the zero dispersion point.

There is a third dispersion parameter, D_2 which defines pulse broadening as a function of wavelength rather than optical frequency. It is often used in the literature instead of β_2, and both terms will be used in this work.

$$D_2 = -\frac{2\pi c}{\lambda^2}\beta_2 \tag{1.4}$$

Waveguide Dispersion.

Waveguide dispersion occurs because a single mode fibre is made up of a core, in which approximately 80% of the optical power will propagate, and a cladding of a lower refractive index, which forms the waveguide used to contains the signal. This small difference in refractive index means that the effective mode index is slightly less than the core index, and the zero dispersion point is shifted towards longer wavelengths. The specific change produced is wavelength dependent, and can be controlled by careful design of the fibre profile, for example using multiple cladding layers.

This is often done deliberately to produce fibres with a zero dispersion point around the minimum loss region near 1.5μm, to produce very high dispersion fibre for use in dispersion tailoring, or to produce dispersion flattened fibre.

For the remainder of this work, the term dispersion will refer to the combined effects of both waveguide and material dispersion at any wavelength.

1.2.4 Dispersion and Pulse Propagation.

The important feature of dispersion from a communications standpoint is the effect of the group velocity dispersion (GVD) parameter β_2 on pulse shape during propagation. As was mentioned in section 1.2.3, a pulse of light is made up of a range of optical frequencies, rather than a single discrete frequency, and each of these will experience a slightly different response from the material through which the pulse is travelling.

The phase of each spectral component will be changed relative to the central frequency, resulting in a retardation of some and an acceleration of others which translates in the time domain into a broadening of the pulse. No new spectral

components are generated. The amount of broadening will depend on the sign of the dispersion parameter at the wavelength concerned, and also on any initial chirp on the pulse.

It is useful to introduce a length scale over which such effects become important and a commonly used scale is the dispersion length L_D. This is given by:

$$L_D = T_{FWHM}^2/(1.33|\beta_2|) \tag{1.5}$$

where T_{FWHM} is the pulse width at the point of half maximum intensity. This corresponds to the distance over which the pulse width of an initially unchirped gaussian pulse increases by a factor of $\sqrt{2}$. For pulses with non-gaussian profiles, the length L_D is used as defined in equation 1.5, although the broadening rate will vary depending on the exact profile.

Taking the example of propagation in the anomalous dispersion regime, the blue (or short wavelength) spectral components of a pulse will be advanced in phase compared to the longer wavelength components. This results in a net time delay between the different frequencies with blue components shifting towards the leading edge of the pulse and the red moving towards the trailing edge, and hence a broader pulse. The chirp $\delta\omega$ will be positive at the leading edge of the pulse and negative at the trailing edge, a down-chirped pulse. Figure 1.4 shows the variation in instantaneous frequency across such a pulse, while figure 1.5 shows the same pulse following propagation in the normal dispersion regime. The pulse broadening experienced in both cases is the same, but the sign of the chirp has been reversed.

If a laser at this wavelength produces up-chirped pulses, that is with red spectral components at the leading edge of the pulse, the initial effect of GVD will be to narrow the pulse, retarding the red and advancing the blue. Obviously, in the long run the pulse will broaden again, as the spectral components move past each other. This effect can be used deliberately as a pulse compression

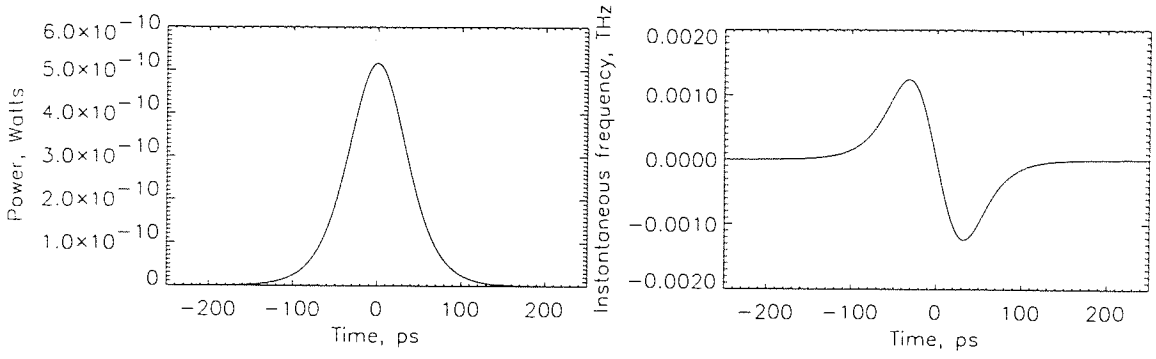

Figure 1.4: Pulse profile and instantaneous frequency across the pulse after propagation in the anomalous dispersion regime. Notice the variation in frequency across the pulse, as a result of GVD.

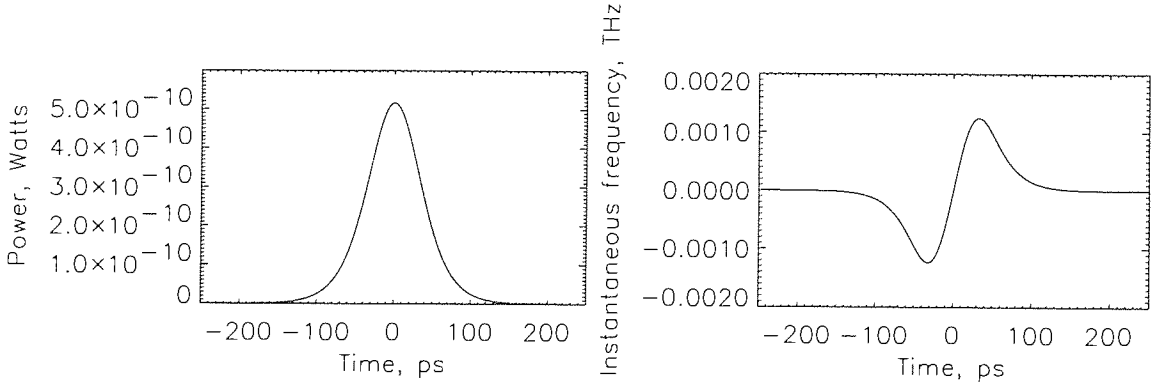

Figure 1.5: Pulse profile and instantaneous frequency across the pulse after propagation in the normal dispersion regime. Note that the high-frequency components are now advanced in time with respect to the low-frequencies

technique[4], where the initial pulse is passed through a grating to provide a large chirp, then propagated in fibre of the appropriate sign of dispersion to the distance where the prechirping is just cancelled by the GVD induced chirp.

The amount of temporal pulse broadening for the case of an unchirped gaussian pulse is independent of the sign of dispersion, and can be calculated from

$$T_1 = T_{FWHM}\left[1 + \left(\frac{z}{L_D}\right)^2\right]^{\frac{1}{2}} \tag{1.6}$$

where L_D is the dispersion length as given above, and included the dispersion parameter β_2, T_{FWHM} is the initial pulse width at half maximum and T_1 the pulse width after propagating a distance z.

(This relation has been derived assuming a gaussian pulse shape, which is straightforward to manipulate. The derivation is less simple for the pulse shape of interest in this work, the hyperbolic secant, but numerical simulations have shown that in terms of GVD-induced pulse broadening this can be approximated successfully with a gaussian pulse.)

For optical communications, where data is transmitted as patterns of pulses over increasingly large distances, GVD is one of the most important limits on data transmission rates. Some way must be used to keep the pulses clearly separated from each other, either by keeping them so far apart that pulse broadening does not cause an overlap, or by some form of reshaping at regular intervals during propagation. The third alternative is to use nonlinear effects to maintain the pulse shape. This solution to the problem is the driving force behind the work presented here.

1.3 Nonlinear Propagation.

Many systems appear linear at first glance. However, closer examination generally reveals a change in response when the input values become extreme. Such nonlinearities can add stability, for example by responding less as the accelerator pedal is pressed closer to the floor, limiting the increase in engine speed. Alternatively, they may cause the system to become progressively more and more unstable, for example with increasingly higher rates of interest as the overdraft becomes larger. The nonlinearity discussed in this work is rather more subtle, but of very great importance when studying the behaviour of pulses in optical fibre communications. It was first observed in the mid-60's, when the advent of powerful lasers made it possible to study the behaviour of high intensity light beams in various materials, including glass[5], though its origins were not fully understood for another ten years[6].

To improve the system model, extra terms must be added to the equations used to describe it, based on what is known of the mechanisms causing the nonlinearity. Most of the effects discussed here originate from the intensity dependence of the refractive index of silica. When a high intensity field interacts with any dielectric the response of the bound electrons becomes anharmonic and the induced polarisation $\mathbf{P}$ is described by:

$$\mathbf{P} = \epsilon_0 \left(\chi^{(1)} \cdot \mathbf{E} + \chi^{(2)} : \mathbf{EE} + \chi^{(3)} : \mathbf{EEE} + \cdots \right) \tag{1.7}$$

where ϵ_0 is the vacuum permittivity and $\chi^{(j)} (j = 1, 2, \cdots)$ is the jth order susceptibility.

The effects of first order susceptibility are accounted for by the refractive index and the attenuation coefficient. Because SiO_2 is a symmetric molecule, second order effects due to $\chi^{(2)}$ do not normally occur in silica fibre, and so this susceptibility will be ignored for the purposes of this work.

The third order susceptibility $\chi^{(3)}$ produces the lowest order nonlinear effects. It is related to the refractive index by the equations:

$$\overline{n}\left(\omega, |E|^2\right) = n(\omega) + n_2|E|^2 \tag{1.8}$$

where $n(\omega)$ is the linear refractive index far from the resonances of the silica, $|E|^2$ is the optical intensity inside the fibre and n_2 is the nonlinear coefficient, which is related to $\chi^{(3)}$ by the relation:

$$n_2 = \frac{3}{8n}\chi^{(3)}_{xxxx} \tag{1.9}$$

Only one component $\chi^{(3)}_{xxxx}$ of the fourth rank tensor is included in the definition of n_2, since it is assumed that the field is linearly polarised.

Again, to keep the maths as straightforward as possible, assumptions are made about the importance of the different nonlinear terms, and this model is still only an approximation of the real systems. The approximations must be made in terms of the accuracy required and the specific data to be studied, and any assumptions made in the work described here have been justified in context.

1.3.1 Self-phase Modulation (SPM)

The presence of a very small nonlinear component in the response of silica to an electro-magnetic field has important consequences as the peak powers in transmitted pulses are increased. The phases of the higher and lower intensity parts of the pulse will vary, an effect known as self-phase modulation (SPM), and for relatively low intensities, the phase change produced can be of a similar scale to those produced by group velocity dispersion. The two effects combine in a complex manner to produce dramatic differences in pulse propagation behaviour.

In the absence of any other pulse shaping effects, self-phase modulation (SPM) will give rise to an intensity dependent phase shift while leaving the temporal pulse shape unchanged.

The phase shift means that the instantaneous optical frequency will vary across the pulse, producing a frequency chirp and a correspondingly broader pulse spectrum. The magnitude of this phase shift will depend on the distance propagated and the intensity of the optical field, and can be found by observing that the phase of an optical field changes as:

$$\phi = \overline{n} k_0 L = \left(n + n_2 |E|^2\right) k_0 L \tag{1.10}$$

where L is the fibre length and $k_0 = 2\pi/\lambda$. The effect of the SPM is seen in the intensity dependent term

$$\phi_{NL} = n_2 k_0 L |E|^2 \tag{1.11}$$

This result comes from the equations describing propagation in a dielectric medium, which can in turn be derived from Maxwell's equations. A good treatment of this derivation can be found in Chapter 2 of [7].

As with dispersive effects, it is useful to define a length scale over which nonlinear effects become important. This distance is defined as

$$L_{NL} = 1/\gamma P_0 \tag{1.12}$$

where γ is the nonlinearity coefficient defined as

$$\gamma = \frac{n_2 k_0}{A_{eff}} \tag{1.13}$$

and c is the speed of light and A_{eff} is the effective area of the fibre considered. P_0 is the peak power of the incident pulse, in the case of bright pulses, and the cw level supporting the pulses in the case of dark pulses.

L_{NL} corresponds physically to the distance over which the nonlinear phase changes by one radian, which corresponds approximately to a spectral broadening by a factor of two (depending on pulse shape).

As the input power increases the nonlinear length L_{NL} decreases. This is an important limit on the maximum propagation distance in a lossy system, since it means signal power cannot be increased indefinitely to avoid the need for reamplification. However, as a consequence of the intensity-dependent variation in frequency across a pulse, it is possible by careful selection of pulse shape to cancel out the linear variation in frequency caused by group velocity dispersion.

The appropriate pulse profile may be defined by solving the equation describing propagation in each dispersion regime. This takes the form of the Nonlinear Schroedinger Equation, and the stable pulse solutions are known as solitons. In the anomalous dispersion regime they take the form of bright pulses with a shape defined by a hyperbolic secant, and have been the subject of many studies. In the normal dispersion regime, the soliton solution is a dark pulse, with the shape of an inverted hyperbolic secant. Bright solitons are discussed in more detail in section 1.4, and an introduction to dark solitons is given by chapter 2.

1.3.2 Cross-phase Modulation (XPM).

When studying the propagation of signal pulses at two different wavelengths there are two effects to take into account. In addition to the intensity dependent phase shift observed due to self phase modulation of a pulse, there is the phenomenon of cross phase modulation to consider. Although no energy is exchanged between pulses, the presence of a high energy pulse in the fibre will produce small changes in the refractive index which will affect the propagation of a pulse at a different wavelength.

A pulse copropagating with another at a different wavelength will see a nonlinear phase shift:

$$\phi_{NL} = n_2 k_0 L \left(|E_1|^2 + 2|E_2|^2 \right) \tag{1.14}$$

Comparing this with equation 1.11, it can be seen that the first term shows the effect of the pulse upon itself, and the second term the response to the presence of a second field. It is interesting to note that for fields of the same intensity, the effect of cross phase modulation is twice that of self-phase modulation.

These effects occur only when the pulses overlap in time. Because of the frequency dependence of the group velocity v_g (see above) pulses at different frequencies will travel through the fibre with different velocities and will eventually walk through each other and separate.

The distance over which this walk-through takes place for a pair of sech^2 pulses can be calculated as:

$$L_w = \frac{T_{FWHM}}{1.76|d_{12}|} \tag{1.15}$$

with d_{12} given by the respective group velocities as:

$$d_{12} = \beta_1(\lambda_1) - \beta_1(\lambda_2) = v_g^{-1}(\lambda_1) - v_g^{-1}(\lambda_2) \tag{1.16}$$

The effect of cross phase modulation has been used to develop many useful devices, including the Nonlinear Optical Loop Mirror discussed below.

Nonlinear Optical Loop Mirror

The Nonlinear Optical Loop Mirror, or NOLM, was first proposed in 1988 as a device to perform all-optical switching [8], a key goal in the development of ultra-high speed optical systems. It consists of a fibre directional coupler having splitting ratio $\alpha : (1 - \alpha)$ and with its output ports spliced together.

(see figure 1.6) This forms a very stable interferometric device, since the signals in each arm propagate in the same piece of fibre and so problems of variations between lengths etc of the two arms are eliminated.

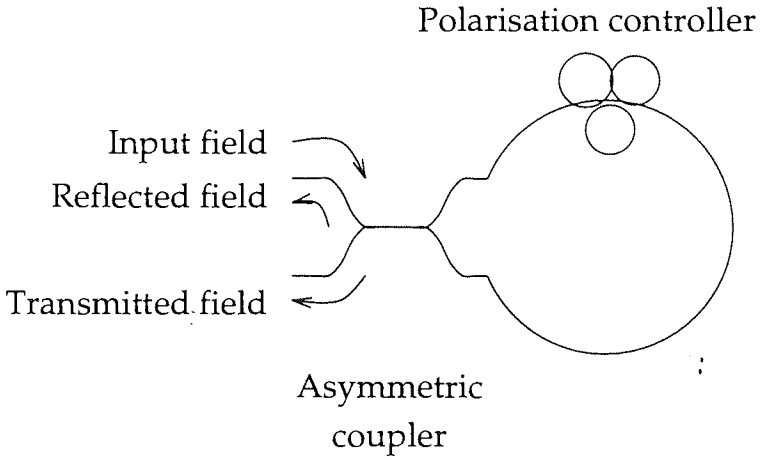

Figure 1.6: Schematic representation of a Nonlinear Optical Loop Mirror

With a coupling ratio of 50% no nonlinear behaviour is expected and the device acts as an all-fibre mirror. To observe a nonlinear response, it is necessary to introduce some asymmetry into the system, either by changing the coupling ratio, or by arranging for the signal in each direction to see different gain or loss. A third method is to include within the loop a signal at a different wavelength, propagating in one direction only and affecting the copropagating signal via cross-phase modulation.

For the case of an unbalanced coupler, the response of the NOLM can be analysed by first examining the case where the pulses do not significantly disperse, and are shorter than the loop length. It is assumed that there is only one input, which is divided in some way between the two arms of the coupler.

After propagation round the loop, and returning through the coupler, the final outputs are described as the reflected and transmitted fields, whose power is

given, respectively, by:

$$\begin{aligned} P_r &= 2\alpha(1-\alpha)\left\{1+\cos\left[(1-2\alpha)\phi_{NL}\right]\right\}P_i \\ P_t &= P_{in}-P_r \end{aligned} \tag{1.17}$$

where ϕ_{NL} is the nonlinear phase change due to self-phase modulation.

The power transmitted at each part of the pulse is dependent on the phase shift acquired by that part of the pulse, which in turn is a function of the power at that point. For typical 'non-square' pulses, which do not have a flat profile, switching will be incomplete, as different parts of the pulse see different phase shifts.

We now consider the case of bright soliton propagation in a NOLM[9]. One property of bright solitons (see Section 1.4) is that the balance between the two opposing chirps produced by SPM and GVD means they have a flat phase profile. They will thus switch as a single entity, rather than in parts depending on power. This feature can be used to remove unwanted radiation between pulses[10].

Another interesting use of the nonlinear optical loop mirror is for pulse shaping, using the interaction between the signal in one arm and a copropagating pulse at a second wavelength to impose phase changes of a specific shape on the signal. [11] With a high powered copropagating pulse A, of the form

$$A(t) = U\,\mathrm{sech}(t) \tag{1.18}$$

then the nonlinear phase change induced on the signal B is given by

$$\phi(t) = U^2\left[\frac{\tanh(t)-\tanh(t-\Delta\beta_1 L)}{\Delta\beta_1}\right] \tag{1.19}$$

where L is the length of fibre over which the interaction takes place, and $\Delta\beta_1$ is the difference between the group velocities at each wavelength, and relates

to the walk-off length as $l_w = 1/\Delta\beta_1$. It can be seen that by careful control of the loop length and the selection of the second wavelength a variety of phase profiles may be imposed on B, and therefore a variety of amplitude profiles produced at the output of the NOLM.

1.3.3 Four-wave Mixing

Four-wave mixing is a parametric process, known as such because it results from the light-induced modulation of a medium parameter, in this case refractive index. It can be understood by considering the third-order polarisation term of equation 1.7, which causes an induced nonlinear polarisation $\mathbf{P}_{NL}$ given by:

$$\mathbf{P}_{NL} = \epsilon_0 \chi^{(3)} \vdots \mathbf{EEE} \tag{1.20}$$

where $\mathbf{E}$ is the electric field and ϵ_0 the vacuum permittivity. If the electric field is made up of four waves at frequencies ω_1, ω_2,ω_3 and ω_4, linearly polarised along the same axis x and propagating in the same direction z, the total field may be written as:

$$\mathbf{E} = \hat{x}\frac{1}{2}\sum_{j=1}^{4} E_j \exp[i(k_j z - \omega_j t)] + c.c. \tag{1.21}$$

where:

$$k_j = n_j \omega_j / c \tag{1.22}$$

and n_j is the refractive index. Substituting equation 1.21 into equation 1.20 allows the expression of the induced nonlinear polarisation as the sum of the effects of the four waves, as:

$$\mathbf{P}_{NL} = \hat{x}\frac{1}{2}\sum_{j=1}^{4} p_j \exp[i(k_j z - \omega_j t)] + c.c. \tag{1.23}$$

Expanding this and solving for P_j reveals contributions to the induced nonlinear polarisation from many different combinations of one or more of the four fields, including the origin of SPM and XPM discussed in sections 1.3.1 and 1.2.4. For a given j, P_j will be contain a term proportional to E_j, which includes contributions from the other three fields, plus a large number of terms involving the products of the other three fields only. It is these terms which are responsible for four-wave mixing.

Each term includes a relative phase between the fourth field, E_j and P_j, determined by both the frequencies and wave vectors of all four waves. For significant four-wave mixing to occur, this phase must be vanishingly small, and so both the frequencies and wave vectors must be matched, satisfying this condition being referred to a phase-matching. When this occurs, photons from one or more waves can be annihilated, and new photons created at different frequencies such that the net momentum and energy are conserved, as a result of the modulation of the refractive index by the original waves.

The type of four-wave mixing of the greatest importance in optical fibre occurs when two photons at ω_1 and ω_2 are annihilated with the simultaneous creation of new photons at frequencies ω_3 and ω_4:

$$\omega_3 + \omega_4 = \omega_1 + \omega_2 \tag{1.24}$$

with the phase-matching requirement $\Delta_k = 0$ where:

$$\Delta k = k_3 + k_4 - k_1 - k_2 \tag{1.25}$$

$$= (n_3\omega_3 + n_4\omega_4 - n_1\omega_1 - n_2\omega_2)/c \tag{1.26}$$

This is easy to satisfy if $\omega_1 = \omega_2$, a partially degenerate case where a strong

pump wave at frequency ω_1 creates sidebands located symmetrically at ω_3 and ω_4, with a frequency shift:

$$\Omega_s = \omega_1 - \omega_3 = \omega_4 - \omega_1 \tag{1.27}$$

The sidebands may either be seeded by noise, if only the pump signal is incident on the fibre, or a signal at ω_3 or ω_4 may be amplified in this way. This is referred to as parametric gain.

Phase matching can be achieved experimentally in single mode fibres in a number of ways, with the parametric gain peaking when the net wavevector mismatch $\kappa = 0$. This term is given by:

$$\kappa = \Delta k_M + \Delta k_W + \Delta k_{NL} \tag{1.28}$$

where Δk_M, Δk_W and Δk_{NL} represnt the mismatch occurring as a result of material dispersion, waveguide dispersion and nonlinear effects. Approximate phase-matching can be obtained by reducing the material and nonlinear contributions, using small frequency shifts and low pump powers. Alternatively, when operating near the zero-dispersion wavelength, Δk_W nearly cancels $\Delta k_M + \Delta k_{NL}$, again resulting in near-phase matching. Operating in the anomalous GVD regime is another solution, since Δk_M is the negative and can cancel with $\Delta k_W + \Delta k_{NL}$. The final experimental solution to satisfying the phase-matching requirements for four-wave-mixing is to use birefingent fibres. Waves in such polarisation-sensitive fibres propagating with orthogonal polarisations have different effective indices, with index difference δn. This dominates the waveguide contribution to the wavevector mismatch. The nonlinear contribution is also different to the polarisation independent case, and is negligible compared to Δk_M and Δk_W. Phase matching occurs when the two terms cancel,

with the sign of Δk_W controlled by launching the pump wave polarised either along the slow or fast axis of the fibre.

1.4 Solitons

1.4.1 The Nonlinear Schroedinger Equation

Various references have already been made in this work to solitons, describing them as pulses which by a combination of linear and nonlinear effects are able to propagate unchanged over great distances. This is a fairly simplistic view, and to understand some of the complex behaviour which can be observed a more rigorous mathematical treatment is required. The discussion which follows highlights the key stages in analysing the propagation of light in nonlinear materials, and the soliton solutions which emerge from such an analysis.

A model of propagation in optical fibre can be built up by considering the various responses of the material and field. Having considered loss, dispersion and nonlinearity separately, the effects of each, and the interactions between them may be combined in equation 1.29. This describes the propagation of the slowly-varying envelope A of a pulse in a frame of reference moving at the group velocity v_g of the pulse.

$$i\frac{\partial A}{\partial z} = -\frac{i}{2}\alpha A + \frac{1}{2}\beta_2\frac{\partial^2 A}{\partial T^2} - \gamma|A|^2 A \tag{1.29}$$

where α is the loss coefficient, and γ is the nonlinearity coefficient defined by equation 1.13

In the absence of the loss term $-\frac{i}{2}\alpha A$ this is referred to as the Nonlinear Schroedinger Equation (NLS). It was shown almost simultaneously by Zakharov

and Shabat[12], and by Hasegawa and Tappert[13][14] that this equation is integrable, and can be solved exactly using the inverse scattering method, providing useful insight into the behaviour of high power pulses in optical fibres. Details of this method are available in many texts, good examples being references [7] and [15] and so only the results will be discussed here.

It is useful to normalise equation 1.29, by introducing:

$$U = \frac{A}{\sqrt{P_0}}, \; \xi = \frac{z}{L_D}, \; \tau = \frac{T}{T_0} \tag{1.30}$$

which gives:

$$i\frac{\partial U}{\partial \xi} = sgn(\beta_2)\frac{1}{2}\frac{\partial^2 U}{\partial \tau^2} - N^2|U|^2U \tag{1.31}$$

where P_0 is the peak power, T_0 is the width of the incident pulse and the parameter N is defined by $N^2 = L_D/L_{NL}$. The dispersion length L_D was defined by equation 1.5, and the nonlinear length L_{NL} by equation 1.12.

There is an infinite variety of soliton forms associated with the general solution to the nonlinear Schroedinger equation. However, there is set of solutions of particular importance, those whose form at distance $\xi = 0$ is given by:

$$u(0, \tau) = N \operatorname{sech}(\tau) \tag{1.32}$$

where the soliton order N is an integer. The power required to launch an N-th order soliton is N^2 times that required for the fundamental ($N = 1$) soliton.

Of principal interest to the communications engineer are the two stable single-pulse solutions. In the anomalous dispersion regime ($\beta_2 < 0$), the NLS takes the form :

$$i\frac{\partial U}{\partial \xi} = -\frac{1}{2}\frac{\partial^2 U}{\partial \tau^2} - N^2|U|^2U \tag{1.33}$$

and has as one of its solutions the fundamental bright soliton (see figure 1.7):

$$u(\xi, t) = \operatorname{sech}(\tau)\exp(i\xi/2) \tag{1.34}$$

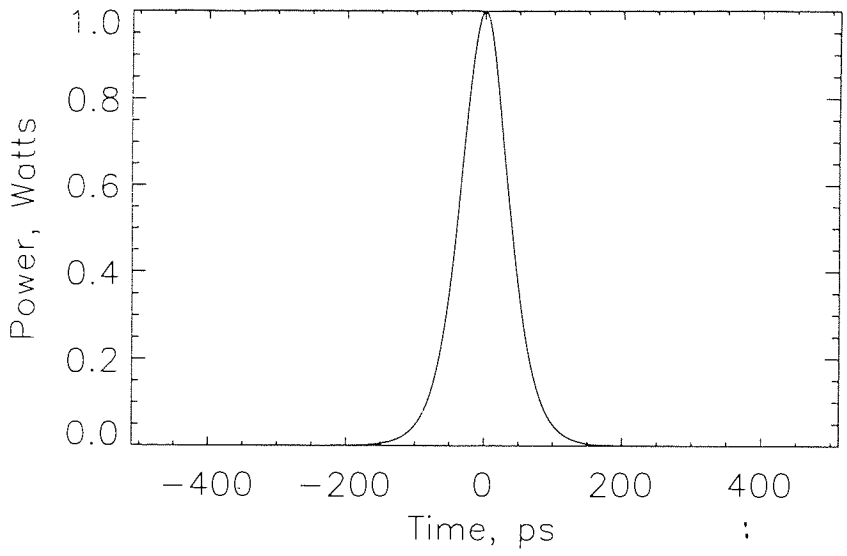

Figure 1.7: The temporal profile of a fundamental bright soliton.

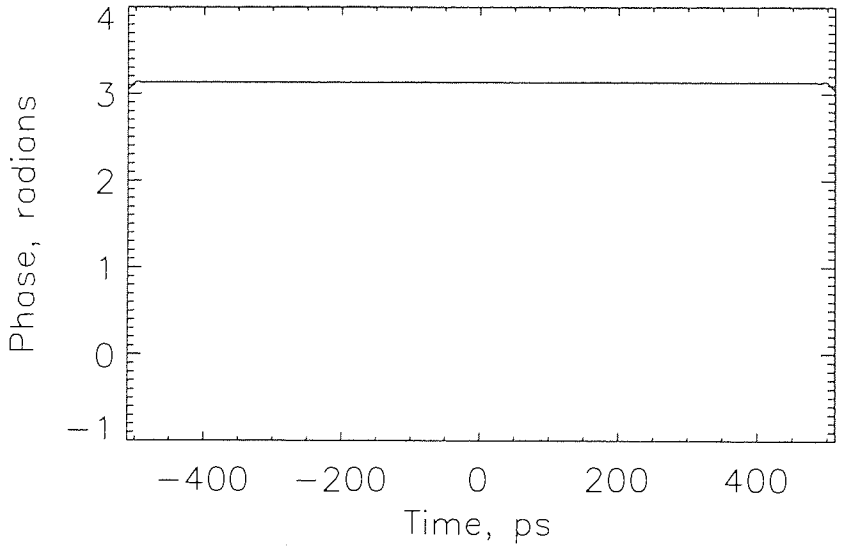

Figure 1.8: The phase profile of a fundamental bright soliton.

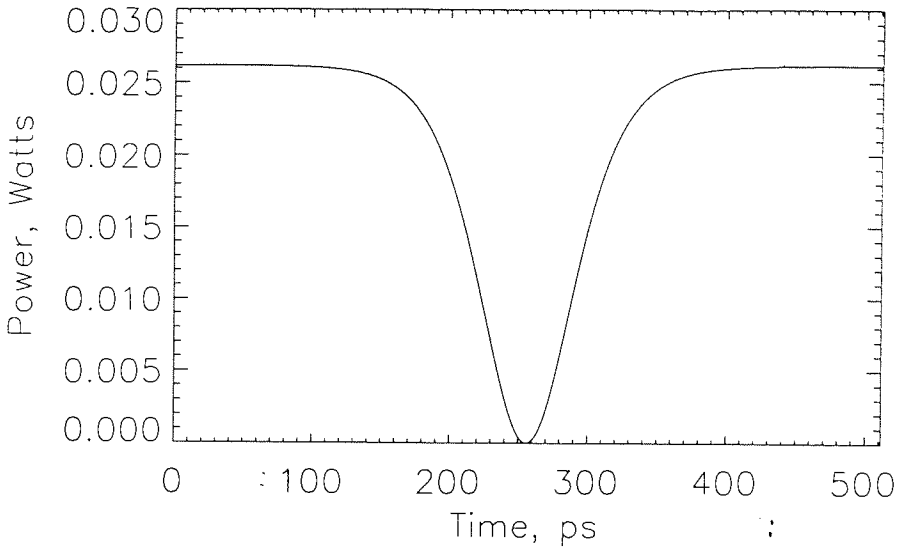

Figure 1.9: The temporal profile of a fundamental dark soliton.

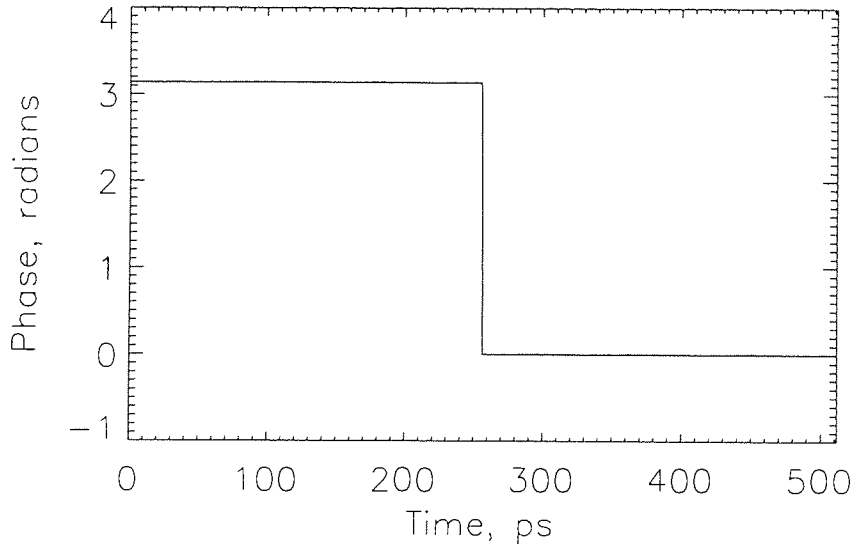

Figure 1.10: The phase profile of a fundamental dark soliton.

In the normal dispersion regime, with $\beta_2 > 0$, the NLS becomes

$$i\frac{\partial U}{\partial \xi} = \frac{1}{2}\frac{\partial^2 U}{\partial \tau^2} - N^2|U|^2U \tag{1.35}$$

and the fundamental soliton solution to this form of the nonlinear Schroedinger equation is the dark soliton, described mathematically by equation 1.36 and with amplitude and phase profiles shown in figures 1.9 and 1.10. The asymmetric phase profile is of particular interest, this feature of dark solitons being possibly of far more importance in comparison with bright solitons than their obvious differences in shape.

$$u(\xi, t) = \tanh(\tau)\exp(i\xi) \tag{1.36}$$

The early work on solitons made no distinction between bright and dark solitons in terms of how much study each merited, and it was only with the experimental success with bright solitons beginning in the early 80's [16] that the main focus shifted towards the bright solution.

The soliton period.

Observing the propagation of higher order bright solitons it is possible to identify a periodicity in both the spectral and temporal domains. This feature of bright soliton propagation has been used to define a characteristic length scale, known as the soliton period. In normalised units, the soliton period is defined as:

$$z_0 = L_D\pi/2 \tag{1.37}$$

Over this distance the bright soliton phase rotates by $\pi/4$. Although the distance over which the phase makes a complete cycle might be considered a more

satisfactory characteristic length scale, the obvious periodicity exhibited by higher order bright solitons over the shorter distance has meant that the former definition has been retained. Figure 1.12 shows the evolution of a third order bright soliton over two soliton periods.

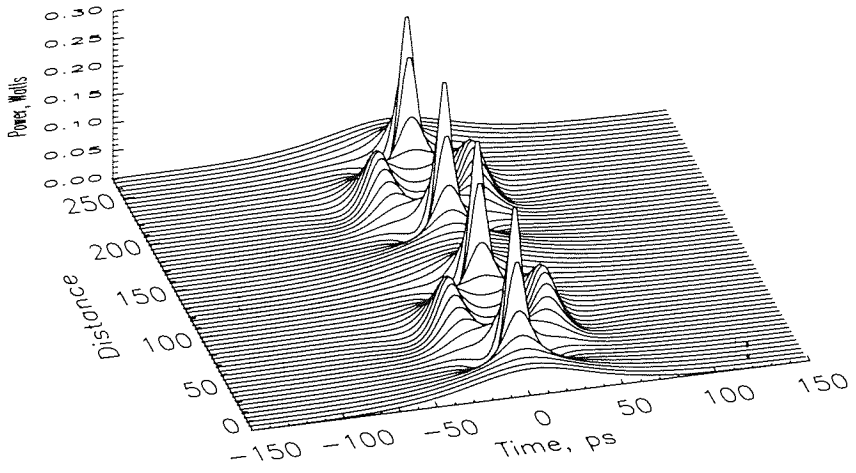

Figure 1.11: The temporal evolution of a third order bright soliton.

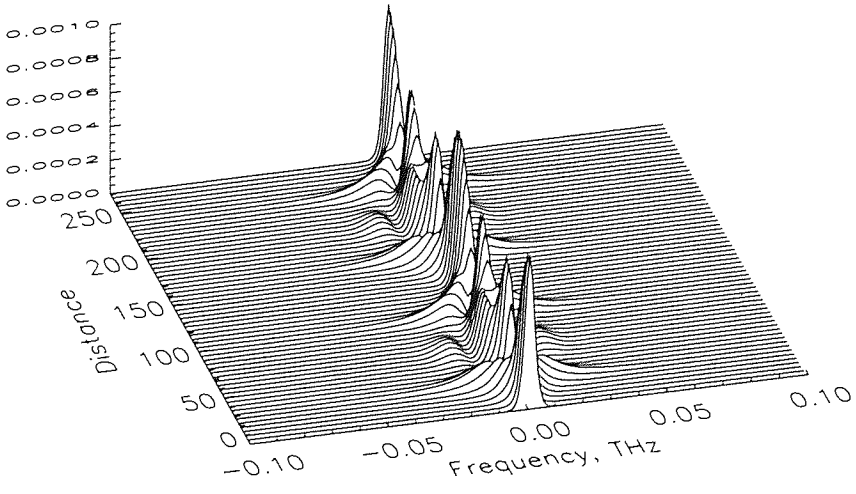

Figure 1.12: The spectral evolution of a third order bright soliton.

The distance z_0 is generally used to permit dimensionless comparisons of behaviour at different propagation distances in different systems.

Comparing equations 1.34 and 1.36 it can be seen that the period associated with the dark soliton as defined in this manner is one half of the bright soliton period for the same dispersion and pulse width. Since higher order dark solitons do not undergo periodic reshaping but divide into a number of grey solitons, the concept of a period per se has no meaning, but for the purposes of comparison the dark soliton period in this work is taken to be the distance over which the background phase rotates by $\pi/4$.

The dark soliton solution will be discussed extensively elsewhere in this work, but it is worth first reviewing some features of bright solitons, to allow comparisons between their more familiar form and responses in different circumstances, and the behaviour of dark solitons.

1.4.2 Bright Soliton Characteristics

Solitons have many potentially useful applications in telecommunications, both in terms of data transmission and data processing, an area of increasing importance as networks become more intelligent. Their ability to reform after perturbation, the ease with which they can be generated, and their particle-like response to many situations has led to them being described a 'natural data bits'.

To understand the ease of generation, it is useful to consider the propagation of a pulse with slightly higher power than would be appropriate for a bright soliton of that width. The extra power will mean the pulse sees a larger nonlinear change in refractive index, producing spectral broadening. Dispersive effects will then compress this chirped pulse, as the different frequency spectral components have different velocities with respect to the central frequency. The pulse will narrow, and ultimately, by a combination of reshaping and energy shedding, form a soliton. This means that any laser producing arbitrary pulses of approximately

the right form may be used as a source of bright solitons. It also means that bright solitons are very stable with respect to small perturbations, for example noise and loss.

The effects of loss can be included in the inverse scattering solution of the NLS by treating it as a weak perturbation. For low losses, the pulse width increases as the peak power drops, maintaining a constant width*height product and the evolution is described as adiabatic. However, this assumption only holds for as long as the soliton period (which increases with increasing pulse width) is substantially shorter than the loss length. As this assumption becomes invalid, the evolution ceases to be adiabatic and the soliton is destroyed. With the advent of optical amplifiers (see section 1.2.2) the periodic amplification of solitons has become a practical possibility, and the response of solitons to such variation in power has been studied in some detail.

Average Soliton Model

The soliton's ability to reform following loss and amplification depends to some extent on the distance over which such adaptation takes place. For amplifier spacings very much less than the soliton period z_0, it is possible to replace the balance between linear and nonlinear effects at each stage of propagation by a balance between the average phase changes induced by each type of behaviour. The pulses are launched with higher power than is required for the the fundamental soliton and sees an excess of self-phase modulation during the first part of propagation, until fibre losses reduce the power levels to the point where GVD dominates. If the distance between amplifiers is sufficiently short, the phase shifts induced by each mechanism will be small enough to be balanced approximately. The approximation becomes invalid as the amplifier separation increases, the standard 'safe' distance is taken to be $8z_0/10$.

The situation has been analysed by several different groups, see for examples references [17] and [18]. It is possible to calculate what launch power is required to ensure that the average power over a span is sufficient to balance the average linear phase change over the distance. This is given by Blow and Doran[17] as:

$$A = \left[\frac{2\Gamma z_a}{1 - e^{-2\Gamma z_a}}\right]^{\frac{1}{2}} \tag{1.38}$$

where A is the initial amplitude of the soliton, Γ is the system loss and z_a is the distance between amplifiers normalised to the soliton period.

The equations hold for both bright and dark solitons. However, because the dark soliton period is half that for the equivalent bright soliton, to remain within the limitations of accuracy of the average soliton model a dark soliton system must have amplifiers spaced at half the distance required for a bright soliton transmission system. This is a serious disadvantage from the engineering point of view.

Bright Soliton Interactions

It is essential for accurate data transmission that the bits are independent, that is that the presence or absence of neighbouring bits has no effect on pulse shape and position. A great deal of work has been done on interactions between bright solitons, of which a few key points will be summarised here.

It has been shown (see for example [19],[20]) that interactions between bright solitons depend not only upon separation but relative phase and amplitude. Solitons of the same phase, amplitude and which are less than three pulse widths apart will periodically collapse together and then separate again. This is clearly undesirable for communications. However, even a slight variation in relative phase or amplitude will reduce the attraction between the pulses, and can with careful design cause the pulses to repel one another instead.

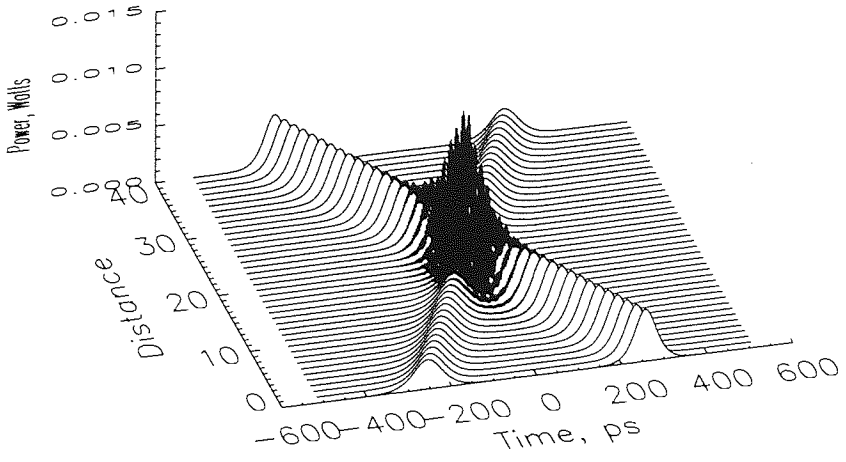

Figure 1.13: The collision of two bright solitons propagating at different wavelengths

If two bright pulses of different wavelength copropagate in a fibre, it is possible to observe soliton collisions. As mentioned earlier, in many cases solitons act as single entities and the collision of two bright solitons of different wavelength (and hence velocity) is an excellent example of this. as shown in figure 1.13 This figure shows the behaviour of two bright solitons moving with different speeds with respect to the background. As they approach the collision point, the two fields overlap, to form a single bright pulse. Beyond collision, they separate completely from each other and continue to propagate as before. There is no change in pulse shape, the only effect of the collision being to slightly change the position of each pulse in time. The ability of bright solitons of different wavelengths to copropagate without interference means that the data carrying capacity of optical fibres can be increased many-fold using the technique of wavelength division multiplexing.

The main constraints when designing a bright soliton transmission system are then to ensure the pulses are sufficiently far apart that they do not interact, and that the spacing between amplifiers is significantly less than the soliton period. There are other considerations which must be taken into account, such as noise induced timing jitter, but these will be discussed in later chapters.

1.5 Numerical simulation techniques.

Although scattering theory can provide a useful insight into pulse behaviour in systems which are not greatly perturbed, many realistic situations cannot be studied in this way and can be better approached by using numerical techniques to simulate different aspects of propagation. Various algorithms are available to allow detailed analysis of complex systems, each with different advantages and disadvantages. The simulations described in this study all use the Split-step Fourier Method as the basis for the models used, partly because as a well-tried and tested technique the results produced can be considered reliable from a numerical point of view, and partly because the the use of finite Fourier transforms, which can make very efficient use of machine resources, means that running the model is reasonably fast.

The basic split-step Fourier method makes use of the fact that, providing the steps taken are sufficiently small, propagation over a short distance can be described in terms of a separate linear and nonlinear component:

$$\frac{\partial A}{\partial z} = (\hat{D} + \hat{N})A \tag{1.39}$$

$\hat{D}$ is a differential operator which includes the effects of dispersion and absorption in a linear medium, and $\hat{N}$ describes the nonlinear responses of the medium.

Simulation takes place in two steps, over a short distance h. In the first step, the effects of the nonlinear operator are determined ignoring any linear effects. This exclusion means the resulting equation may be solved very simply in the time domain. In the second step, only linear effects are considered, transforming the field into the Fourier domain to allow for fast calculation of the various partial derivatives involved. Again, the exclusion allows the remaining terms to be dealt with very efficiently, once the transformation into the frequency domain

has been made.

The algorithm used for the model in this work shows increased accuracy compared to the simple method described above, by including the effects of nonlinearity midway through the propagation step, and by using multiple small steps within the given interval.

The step size required to ensure that observed behaviour is real and not a numerical artifact may be precalculated for straightforwards bright soliton propagation. For more complicated initial conditions, or for dark soliton propagations a suitable step size was determined by convergence tests for a given set of simulations. Too large a step size will result in effects such as artificial (numerical) generation of spectral sidebands.

The bulk of the additional code needed to perform the simulations described here was written as required, or adapted from other work. Important features will be discussed elsewhere, as appropriate.

Chapter 2

Dark Solitons

This chapter provides an introduction to the general properties of dark solitons, and in particular examines those features of their behaviour which affect their suitability for use as data carriers. It outlines their advantages, but also possible problems which must be solved satisfactorily before dark soliton communication systems could become commonplace.

Although the existence of dark optical solitons was discussed when bright solitons were first brought to general attention, the difficulty in generating them reliably and the automatic assumption that dark solitons will require excessively high powers compared to bright has meant that they have been neglected to some extent and are only now starting to arouse interest as a possible medium for communications (see for example [21], [22]).

Improvements in both analytical and experimental techniques have meant that the study of dark solitons is much more straightforward than was true previously, and recent results (for example [23],[24] and [25]) are starting to suggest that they may be more stable than bright solitons in several very important situations. Because of this improved stability, the mark-space ratio for dark

solitons does not need to be so high as in the dark soliton case, with a corresponding decrease in the power needed to support them. The criticism of excessive power requirements can thus be easily refuted, and section 2.5 in this chapter uses typical values for communication system requirements to illustrate this.

Many of the optical fibre systems currently installed around the world use fibre which has been designed for transmission in the normal dispersion regime. It is possible to convert these to create an 'average' anomalous dispersion, by inserting short lengths of fibre with very high anomalous dispersion at regular intervals in the transmission line, allowing bright solitons to be supported[26]. This could permit a large increase in transmission rate, and/or signal-to-noise ratio of the communications link, thanks to the stability of the soliton solution.

However, if reliable techniques can be found for generating, modulating and controlling dark solitons, implementing a dark soliton solution would be a much more satisfactory method for improving the data link. Figure 2.1 shows an example of a modulated 10Gbit/s train of dark solitons, containing a byte of data, plus an even parity bit.

A fourth reason for the increase in the attention being paid to dark solitons is the successful development of in-fibre amplifiers for signals below and around 1.3μm, the zero dispersion point in standard fibre. The benefits or otherwise of in-fibre amplification over detection and retransmission, especially with respect to solitons, were discussed briefly in section 1.2.2, and can be summarised as increasing the system flexibility with regard to data-rate and signal wavelengths, but requiring greater control of pulse shape and position. The development of the erbium-doped fibre amplifiers at 1.5μm was one of the key features in the rapid rise of bright solitons, and the existence of amplifiers suitable for dark soliton transmission systems is an additional reason to consider the soliton

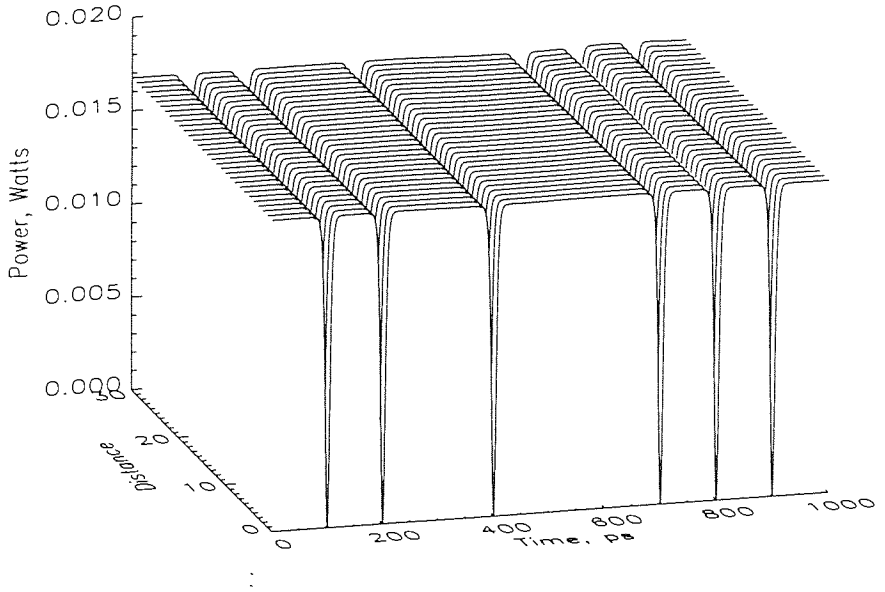

Figure 2.1: The data pattern 11010011, plus an even parity bit, imposed on a 10Gbit/s train of dark solitons.

solution in the normal dispersion regime more carefully.

2.1 Mathematical description of dark solitons.

The dark soliton is often described as an intensity dip in a bright background possessing, in addition to a $\tanh^2$ intensity profile, an asymmetric phase shift centred about the lowest point on the pulse. It is the soliton solution to the non-linear Schroedinger equation in optical fibres in the normal dispersion regime.

The equation for the black or fundamental dark soliton given in section 1.4 can be written more intuitively by switching to the notation of Tomlinson *et al* and then takes the form:

$$u(z,t) = A_0 \tanh\left(\frac{|A_0|t}{t_0}\right) \exp\left(\frac{-i\pi|A_0|^2 z}{2z_0}\right) \tag{2.1}$$

The parameter t_0 is the (arbitrary) time normalisation and z_0 a normalising length scale given by

$$z_0 = L_D \pi / 4 \tag{2.2}$$

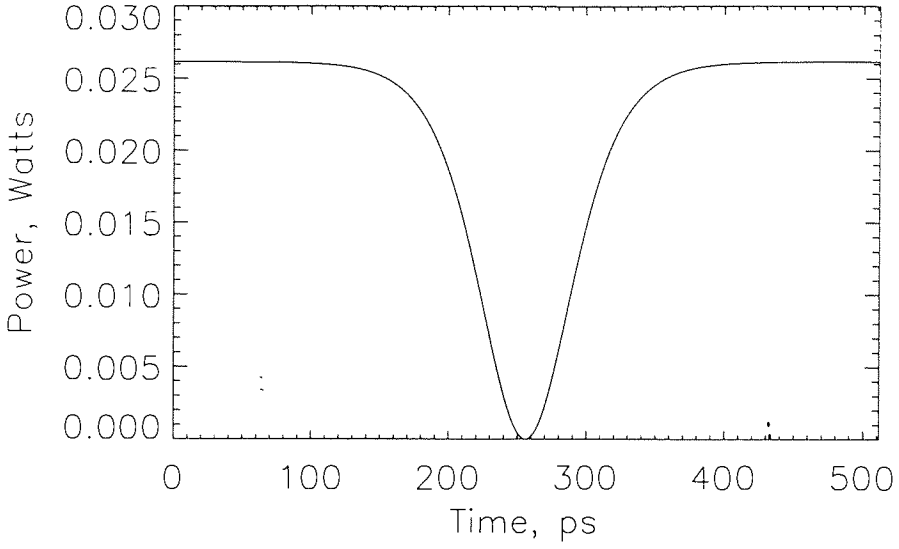

Figure 2.2: The temporal profile of a fundamental dark soliton.

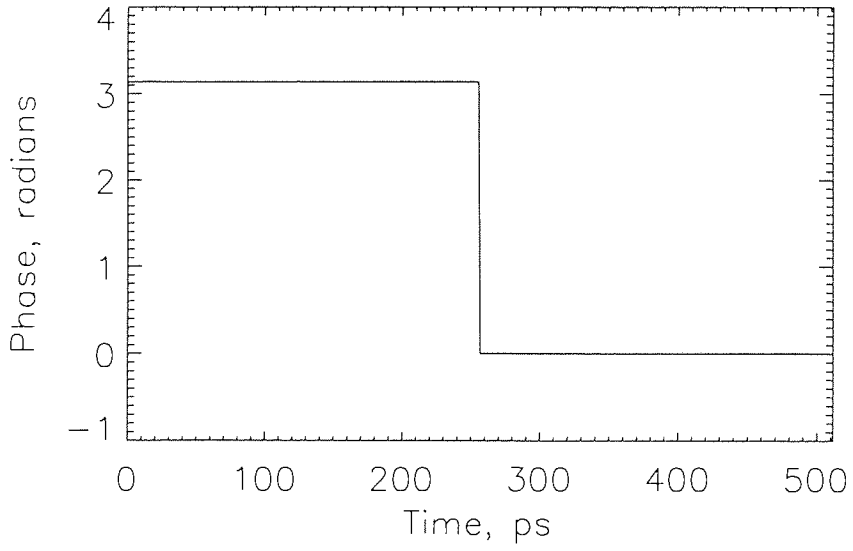

Figure 2.3: The phase profile of a fundamental dark soliton.

(Note that this definition of z_0 gives a length which is half that produced by the definition of the bright soliton period, given in section 1.4. It corresponds to the distance over which the overall phase of the dark soliton rotates by $\pi/4$,

in the same way that z_0 is defined for bright solitons. This confusion in the literature, owing to the difference in the rate of phase rotation for bright and dark solitons is one of the reasons why most of the original work in this thesis uses absolute length scales for comparison purposes.)

An important feature to note from the equations is the phase profile of the black soliton which has an instantaneous switch of π radians at time $t = t_0$. This is in contrast to bright solitons, which have a uniform phase profile across the entire pulse. Figure 2.2 shows the temporal profile of an 80ps black soliton, and figure 2.3 the corresponding phase profile, showing the π phase shift at the centre of the pulse.

Unlike bright solitons, dark soliton solutions exist for pulses which have a depth less than unity; the grey solitons. The general grey soliton solution to the NLS is:

$$u(z,t') = \frac{A_0}{|B|}\left[1 - B^2\,\mathrm{sech}^2\left(\frac{|A_0|t'}{t_0}\right)\right]^{1/2} \exp\left\{i\phi\left(\frac{|A_0|t'}{t_0}\right) - i\frac{\pi|A_0|^2 z}{2B^2 z_0}\right\} \quad (2.3)$$

where

$$\begin{aligned} \phi(\xi) &\equiv \sin^{-1}\left[\frac{-B\tanh(\xi)}{(1-B^2\,\mathrm{sech}^2(\xi))^{1/2}}\right] \\ \frac{t'}{t_0} &\equiv \frac{t}{t_0} - \frac{\pi}{2}|A_0|\frac{(1-B^2)^{1/2}}{B}\frac{z}{z_0} \end{aligned} \quad (2.4)$$

where u is the complex amplitude envelope, z the distance of propagation and t' the retarded time travelling along with the pulse.

Equation 2.3 has been given in this form to draw attention to the amplitude and phase profile of the dark soliton, in particular in terms of the greyness parameter B. For the case where $|B| = 1$, equation 2.3 reduces to equation 2.1. For cases where $|B| < 1$ the contrast ratio of the soliton with respect to the background is determined by $|B|$. The relationship between the parameters A_0 and B can be seen in figure 2.4.

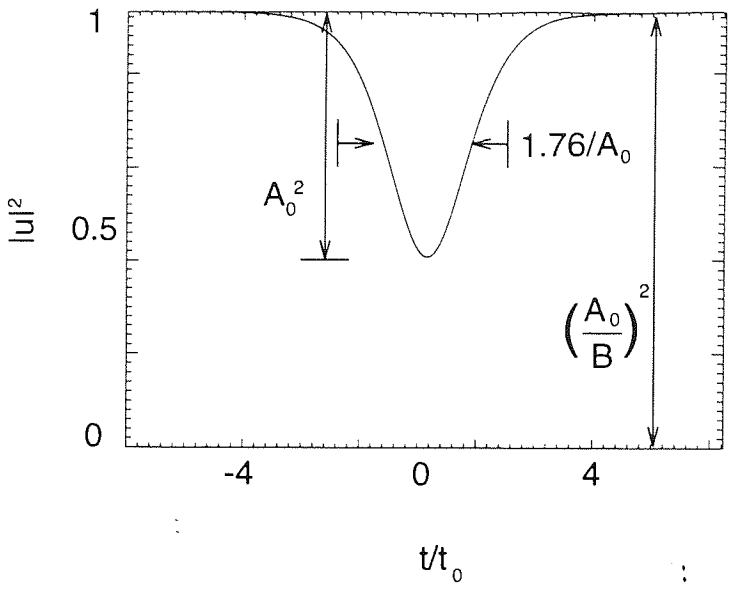

Figure 2.4: The relationship between the parameters A and B for grey solitons.

The continually changing phase across grey solitons means they have an effective frequency shift and therefore a velocity which is different to that of the supporting cw signal, and will either lag or advance with respect to the background, depending on the sign of B. Since to maintain phase continuity dark solitons must be formed in pairs with opposite phase shift, a train of grey solitons will in fact consist of pairs of pulses moving apart. In standard communication systems, receivers rely on finding pulses within a given time window and will treat the absence of a pulse as data in its own right. Grey solitons therefore present a special position control problem, which is discussed more completely in Chapter 6.

2.2 Fundamental, lower and higher order dark solitons.

One of the more important differences between bright and dark solitons is in the evolution of arbitrary input pulses with parameters corresponding to soliton number $N \neq 1$ (see section 1.4). Recall that for bright solitons, if the initial value for the soliton number N is less than $\pi/2$ times that required for a fundamental ($N = 1$) bright soliton the pulse will collapse. If the pulses are launched with sufficient energy that $N+\alpha$ where $|\alpha| < 1/2$ and N is an integer, the pulse will evolve into a nonlinear superposition of N solitons, which move together in an oscillatory manner, with an overall profile which repeats itself over each soliton period[27].

The behaviour of dark pulses is different in both cases to that of bright pulses, and, in addition to the situations when N is greater than or less than unity, the presence or otherwise of an appropriate phase profile will have an important effect on pulse evolution.

We consider first the case of an odd dark pulse (ie a pulse with an asymmetric phase profile) of arbitrary width. When launched into fibre it has been shown[23] that it will evolve non-adiabatically into a dark soliton having the same amplitude (depth) and speed as the input pulse, but a different pulse width. Excess energy is shed in the form of a number of secondary solitons, generated with smaller amplitude and larger pulse widths. For example, for an input pulse launched with initial power $N - \alpha$ where $0 \leq \alpha < 1$ is an arbitrary number, then in addition to the primary soliton, $2(N-1)$ secondary solitons will form, with increasing shallowness.

For the case of even dark pulses, it was shown in 1989 by Gredeskul et al [28], [29] that an arbitrary small dark pulse will evolve into a pair of grey solitons with

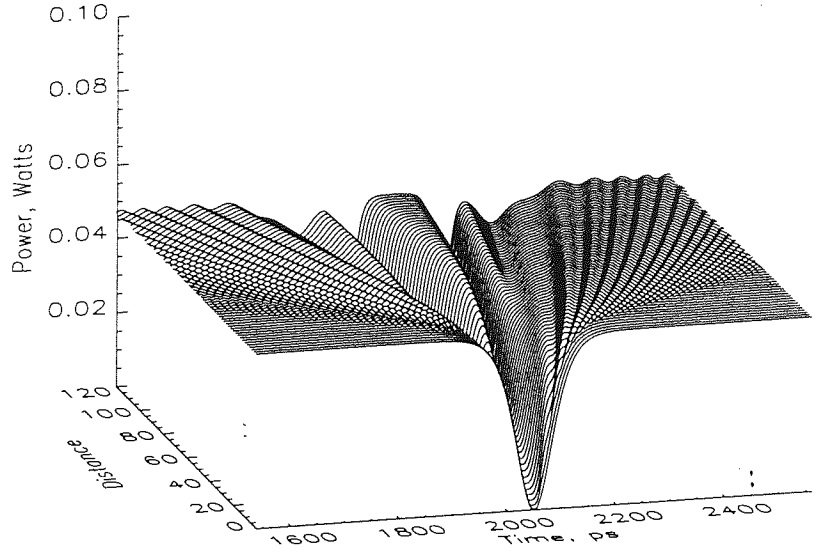

Figure 2.5: The temporal evolution of an even dark pulse, with the same amplitude profile as an N=3 dark soliton.

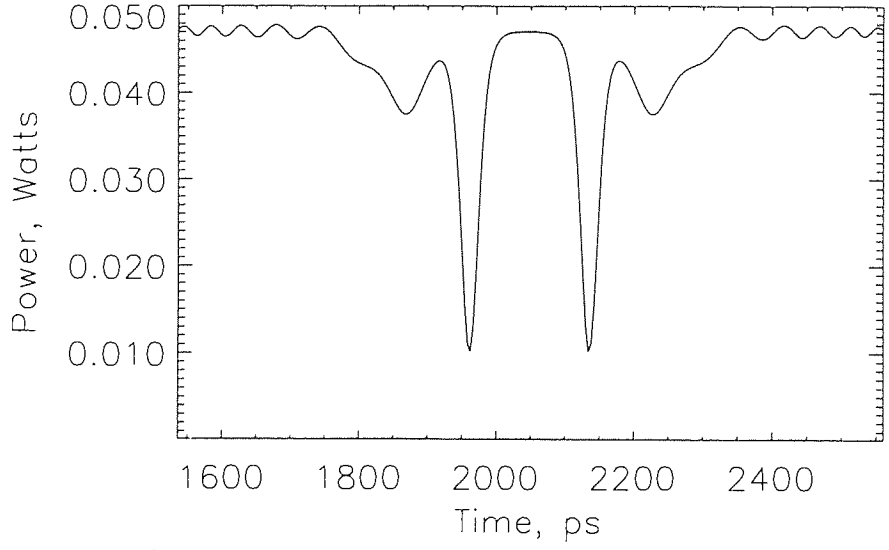

Figure 2.6: The profile following propagation.

equal amplitudes and opposite velocities (see for example figure 2.6) which shows the evolution of an even pulse with the same amplitude profile as the dark soliton shown in figure 2.8. The secondary pulses, despite not being true solitons in the mathematical sense, preserve soliton properties during propagation and interaction, as demonstrated by Diankov et al in 1995[30].

This is clearly different to the bright soliton case, where a pulse must have a normalised area within its envelope of greater than $\pi/2$ for a bright soliton to form. Bright soliton formation is then a threshold phenomena[31], whereas the creation of dark solitons is not.

It was shown in the same papers that for a box-like pulse described by:

$$u(t,0) = \begin{cases} u_0 e^{i\alpha} & |t| > T \\ u_0 e^{i\alpha} - u_1 \equiv \tilde{u} e^{i\alpha} & |t| < T \end{cases} \tag{2.5}$$

where u_1 is a complex constant $|u_1| \leq u_0$, then in a general case a number of dark soliton pairs will form with amplitudes $\sqrt{u_0^2 - \lambda_1^2}$, $\sqrt{u_0^2 - \lambda_2^2}$, ...and velocities $\pm 2\lambda_1$, $\pm 2\lambda_2$, ...where λ_1, λ_2, ...are real positive solutions to the system. In particular, for $|\tilde{u}| \ll u_0$ and $u_0 T \gg 1$ the number of dark soliton pairs can be estimated as $2u_0 T/\pi$.

This result was demonstrated in the same year by Zhao and Bourkhoff [23], who also showed that dark solitons were more stable than nonlinear bright pulses with respect to such effects as loss and noise. This was an important result, and will be returned to later (see section 2.5).

If a dark soliton is launched with power corresponding to $N > 1$ with N integer (see section 1.4.2) then instead of undergoing a periodic evolution in the time and frequency domains it will evolve to produce a black soliton plus pairs of grey solitons with equal amplitudes and equal and opposite velocities. Figure 2.8 shows the temporal and spectral evolution of a 'third order' dark soliton.

Comparing this with the bright soliton case (see figure 1.12) on page 43 the differences in behaviour, and the absence of any periodicity in the dark soliton evolution are very clear.

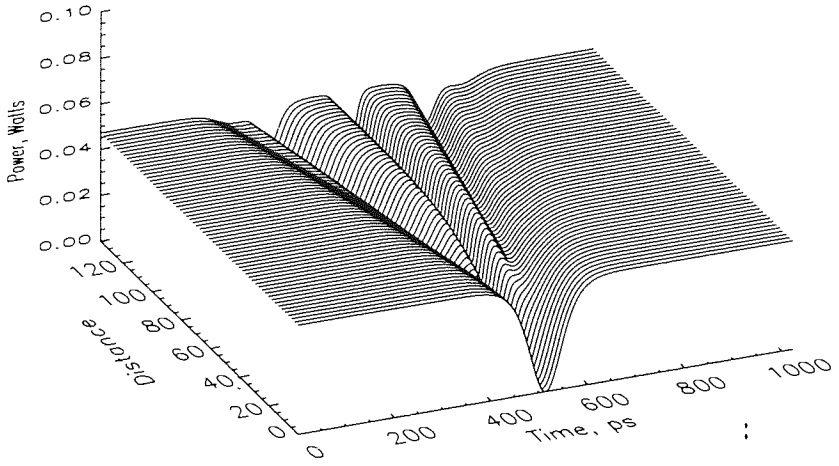

Figure 2.7: The temporal evolution of a third order dark soliton.

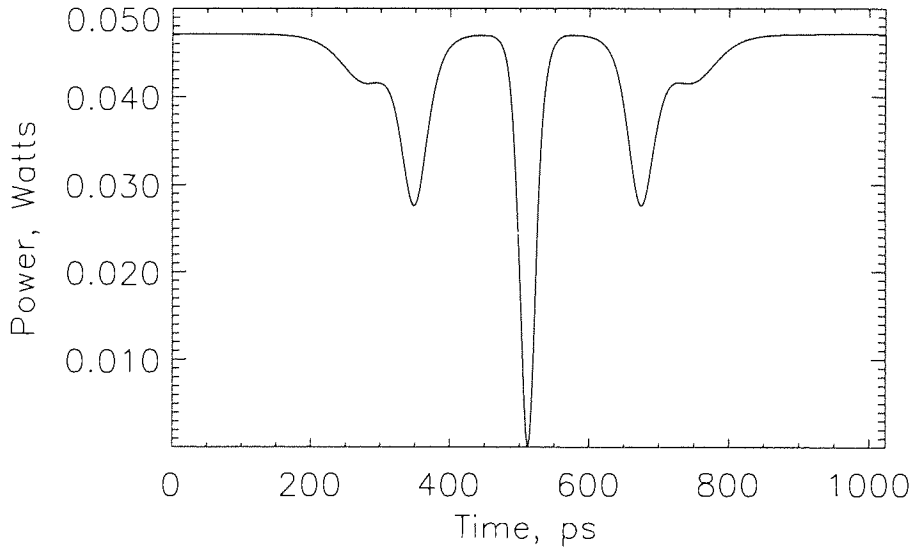

Figure 2.8: The profile following propagation.

As was shown by [32], and illustrated in figure 2.8, dark solitons do not form multiple bound states, and the interactions between them are therefore much simpler to understand than in the bright soliton case. However, this feature of high power propagation in the normal dispersion regime means that the gen-

eration of dark solitons is less straightforward, since any extra energy may be shed into the background not as noise but as shallow grey solitons. These move rapidly with respect to the black solitons and would cause timing errors during collisions with the data carrying pulses. Any successful generation technique would have to suppress the formation of grey solitons in some way, either by ensuring that no energy is shed, or by using some sort of amplitude sensitive modulation. An amplifier which saturated at power levels close to the background level, effectively removing any fluctuations, and which supressed the signal at low power levels would be preferred for this, simultaneously smoothing the background and ensuring that the black soliton remained black.

2.3 Propagation Properties

The dark soliton solution to the NLS requires that the background which supports the soliton is constant to infinity. Much of the mathematical analysis of the behaviour of dark solitons has been done assuming that this boundary condition is fulfilled, that is, that $u \rightarrow const$ as $t \rightarrow \infty$. The work done based on this assumption provides the basis for the current knowledge of their behaviour in many situations.

However, an infinite background cannot be realised physically, and is of questionable value in numerical simulations. It has been necessary then to determine to what extent the behaviours predicted in the ideal case will be observed for an odd dark pulse on a bright background pulse with a width of only perhaps ten times the dark pulse width, and this feature is discussed in this section in some detail.

The final important information about the propagation properties of dark solitons comes from studying the behaviour of two or more pulses, either of the

same depth and velocity or not, either black or grey. The work in this area is by no means complete, partly because of the tremendous complexity involved once the behaviour of more than two pulses is involved.

2.3.1 Adiabatic evolution

In the absence of any perturbations, a dark soliton will propagate unchanged indefinitely. In any real system, the presence of perturbations cannot be avoided, and the principle among these is attenuation, discussed at length in Chapter 1.2.1. In the presence of a gradual loss (or gain) the dark pulse will evolve to maintain its soliton structure[33]. A common feature of all solitons described by equation 2.3 is that they have normalised peak intensity (or depth) of $I_p = A^2$, and a pulse width at half maximum depth of $T_{FWHM} = 1.76/A$. Rearranging these relations gives $I_p T_{FWHM}^2 = 1.76^2$, ie the product of peak depth and the suqre of the full pulse width at half depth is a constant for all solitons.

This constancy can be used to give a clear indication of soliton-like behaviour, and was used by Tomlinson *et al* in 1989 to study the behaviour of dark solitons propagating on a finite-width background pulse[34]. Their simulations showed that the $I_p T_{FWHM}^2$ product does not remain constant in this case, but oscillates about the constant value of 1.76. This type of oscillatory behaviour has been observed for bright solitons propagating in the presence of a small non-soliton background and was assumed to be a result of interference with the background.

It was shown by Giannini in 1990[35] and by Lisak[33] in 1991, using different techniques, that the adiabatic broadening of dark solitons in the presence of gradual loss was at half the rate of that of the equivalent bright soliton. This may be explained physically by recalling that the background which supports the soliton will also be experiencing loss, and so the depth of the soliton will be reduced as a result of loss to the background, requiring less adaptation of pulse

width to maintain the product $I_p T_{FWHM}^2$ constant. A slower rate of spread is always beneficial for data transmission, and these results were extra proof that dark solitons had advantages compared to the bright solitons, so justifying further study.

2.3.2 The effect of stimulated Raman scattering on pulse stability.

Intra-pulse stimulated Raman scattering (ISRS) originates from the non-instantaneous, delayed response of the fibre nonlinearity[36]. Many theoretical studies have been carried out ignoring this effect, assuming an instantaneous nonlinearity, but any real systems with very short pulses (<1ps) will experience it to some extent. An early piece of experimental work[37] on the effect of ISRS on narrow dark solitons showed that it induced both a temporal and spectral shift on the dark soliton at a rate which is half that for equivalent bright solitons.

Prompted by these results, a series of simulations were carried out[38][22], confirming the factor of two in the shift rate. However, this temporal and spectral shift is far more destructive in the case of dark solitons, whose velocity and depth are inextricably linked, and the pulses become progressively shallower, eventually disappearing completely. These observations have now been explained analytically, also demonstrating the dependence of the effects on the sign of the soliton's velocity[39]. They showed that a dark grey soliton with initially negative velocity will become darker and pass through a point of zero intensity at the centre before becoming greyer and ultimately being destroyed. Grey solitons with positive velocity do not pass through this stage.

2.3.3 Interactions between dark solitons

The mutual attraction of neighbouring bright solitons is a limiting factor in the maximum data-rates which can be implemented in a soliton transmission system. It is caused by the effect of the nonlinearity which supports the soliton (see section 1.4.2 for more detail) and decreases exponentially with separation[40]). A 'safe' separation of ten pulse-widths was defined as the minimum required if interactions were to be avoided. The separation q (in units of pulse width) at any distance ξ was shown to be given by

$$\exp[2(q - q_0)] = 1/2\,\{1 + cos[4\xi \exp(-q_0)]\} \quad ; \tag{2.6}$$

It was shown by Zhao and Bourkoff[23] in 1989 that the interaction between neighbouring dark solitons is much less than that experienced by their bright counterparts. They used numerical techniques to deduce an empirical expression for the separation of two dark solitons as a function of initial separation q_0 and travelling distance ξ, thus:

$$\exp[2(q - q_0)] = 1/2\{1 + \exp[4\xi \exp(-2q_0)]\} \tag{2.7}$$

Comparing equation 2.7 with equation 2.6 there are several important differences. The interaction force between neighbouring dark solitons is always repulsive, and the separation between them increases monotonically, as opposed to the periodic variation in the separation of bright solitons. The force between the two solitons decreases with initial separation twice as fast as is the case with bright solitons, which has important implications for the minimum safe spacing between data bits. Zhao and Bourkoff conclude that an initial separation of only three times the pulse width would be sufficient to prevent excessive interaction between neighbouring pulses, a very significant decrease from the recommended

ten bright pulse widths. The importance of this result is discussed in section 2.5.

2.3.4 Collisions of dark solitons

One final response of dark solitons needs to be considered here, their behaviour during collision. The collision of bright solitons was discussed previously (see section 1.4.2), and cited as an example of the particle-like behaviour of solitons. In the bright soliton case it is possible to observe collisions by launching solitons at different wavelengths, the difference in group velocities of the two wavelength producing a difference in speed. To observe dark soliton collisions it is necessary instead to launch either two grey solitons of equal depth but opposite phase shift, or two solitons of different depth, and hence different velocity.

Figure 2.11 shows a collision between grey solitons. The two odd pulses approach each other, combine to form a single, even pulse and then separate again, each moving with the same velocity as it had prior to collision. (If two pulses of different amplitudes are used it can be seen that the pulses do pass through each other, and are not merely being reflected.)

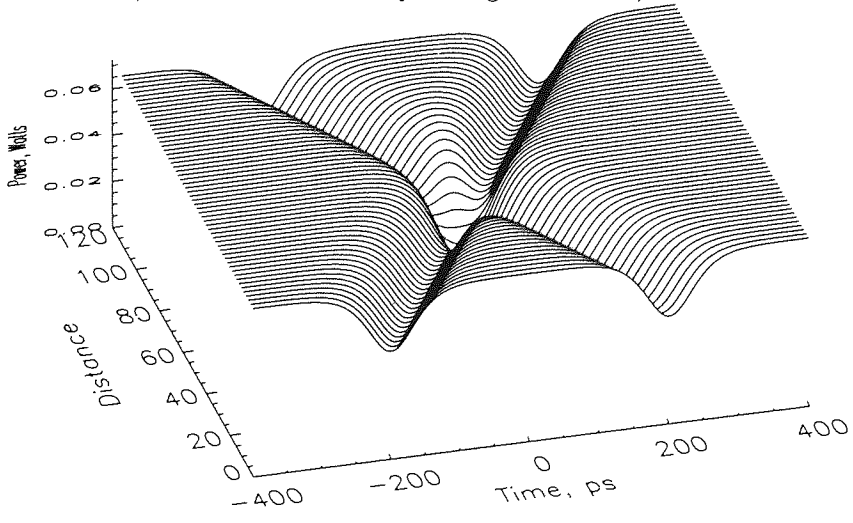

Figure 2.9: The collision of two 75% dark solitons.

When very dark ($\eta > 90\%$) solitons collide, as in figure 2.14 they cannot combine

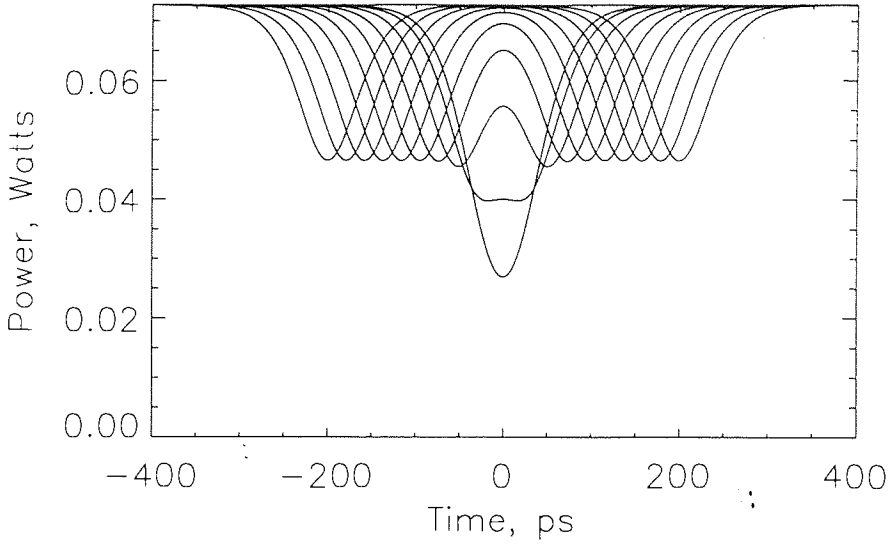

Figure 2.10: The profile of the two pulses at various points up up to collision.

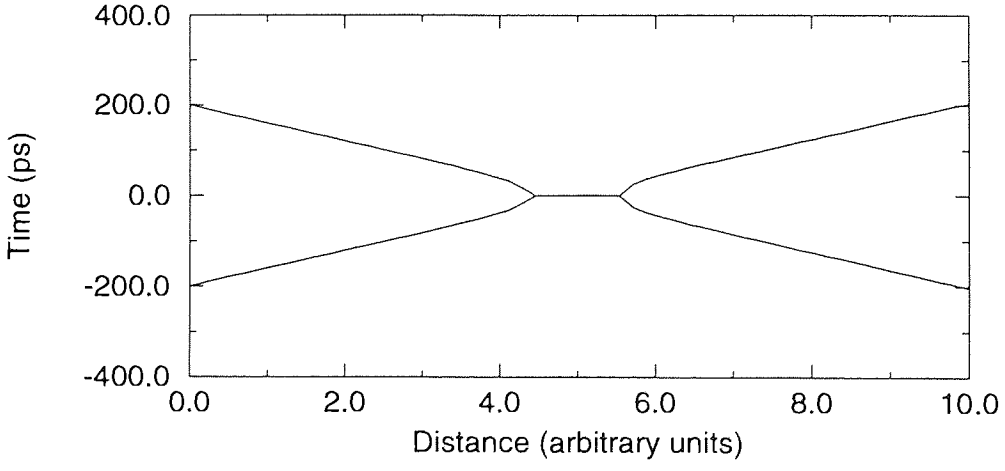

Figure 2.11: The position of the centre of the pulses during collision.

to form a single even pulse as above, but instead approach until each has a zero intensity minimum, and copropagate in this way. The phase profile continues to evolve, and for pulses of equal depth will flatten completely before reforming. Following this, the two dark solitons will begin to move apart again, having exchanged positions. Once again, the soliton with positive velocity with respect to the background will have been advanced slightly in time, while the soliton with negative velocity will have been retarded a little.

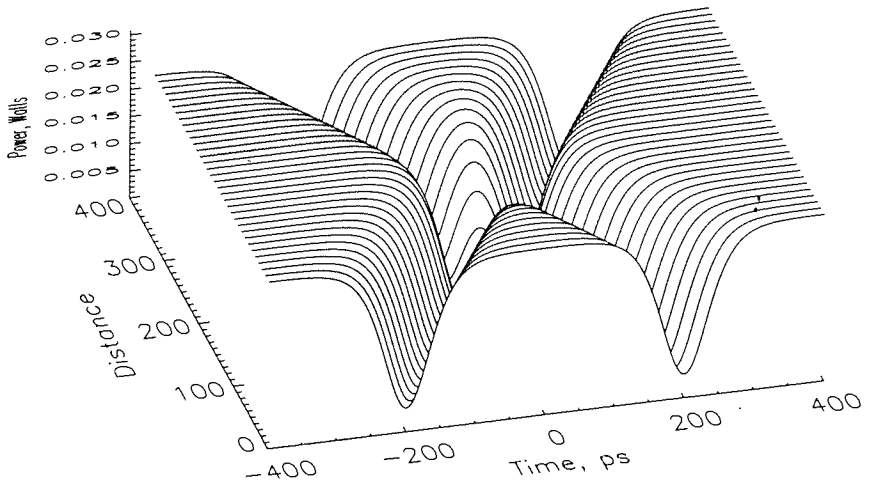

Figure 2.12: The collision of two 92.5% dark solitons.

The first work done on dark soliton collisions was a thorough study of the behaviour under a variety of different conditions, carried out by R. N. Thurston and A. M. Weiner in 1991[41]. They demonstrated analytically that in an ideal dark soliton collision the two solitons pass through each other unchanged except for a temporal shift, which causes the faster soliton to arrive earlier and the slower to arrive later than would have been expected had there been no collision. Numerical simulations were carried out to confirm this, and to allow detailed observation of the pulses during collision.

They developed the work to study the effects of propagation on a finite-width background, and in the presence of the Raman effect. The form of the background pulse meant that the parameters A and B which define the grey soliton

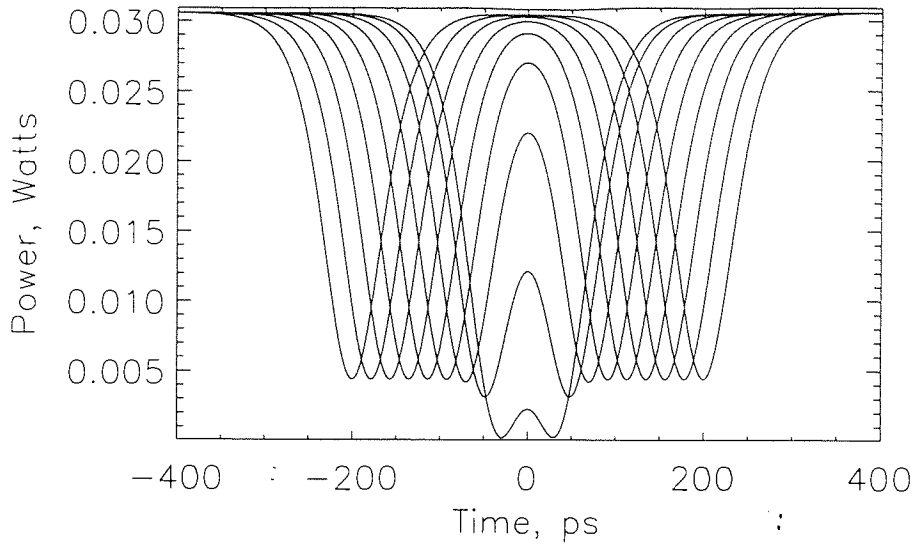

Figure 2.13: The profile of the two pulses at various points up to collision. Notice the double peaked structure at the centre of the collision.

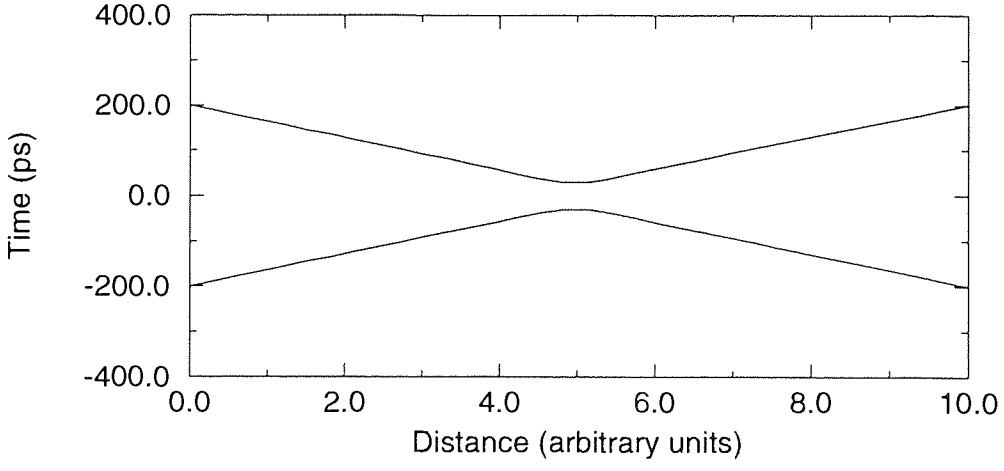

Figure 2.14: The position of the centre of the 92.5% dark solitons during collision.

could not be properly determined, and in conjunction with possible changes to A and B due to the broadening of the background pulse they found that the collision point could not be predicted from a knowledge of the ideal case. They found that the effect of Raman was to slow slightly the faster grey soliton, and slightly increase the speed of the slower. Their numerical results agreed very well with the earlier theoretical predictions of Kivshar[42].

2.4 Generation techniques.

The presence of the phase shift associated with dark solitons, and the general technical difficulty of creating dark pulses has meant that experimental techniques for the generation of dark solitons have been developed much more slowly than the equivalent bright soliton methods, being of necessity more complex. There are a variety of dark soliton generation techniques, which may be divided loosely into two groups, those which produce one or more solitons on a finite-width background pulse, and those which produce trains of dark solitons on what is effectively an infinite background.

Production of dark solitons on a finite background is more simple from an experimental point of view, and has been demonstrated successfully in a number of ways, but is of less use from a communications point of view, where there is a requirement for continuous data transmission.

2.4.1 Generation on bright pulse backgrounds.

Many of the early dark soliton generation techniques concentrated on manipulating the phase and amplitude profiles of bright pulses. In 1985, J. P. Heritage *et al*[43] showed that it was possible to manipulate the phase and amplitude

profiles of ultrashort (picosecond and sub-picosecond) bright pulses to produce any arbitrary pulse shape. Pulses from a suitable source were coupled into fibre and propagated, becoming chirped due to the effects of SPM and GVD (see chapter 1). The chirped pulse was compressed using a single pass grating pair [4] to produce a temporally short pulse with spectral components spread spatially in a fan shaped beam of about 7mm. A spectral window was used to remove surplus energy in the wings of the compressed pulse, which was then passed through a spatial amplitude and phase filter. The modulated signal was passed back through the grating pair, recompressing it prior to observation,

The amplitude mask used consisted of a periodic array of opaque strips. On its own, this resulted in a peaked structure, with the number of peaks related to the width of the spectral window. By placing a thin, optically transparent film in one half of the spectrum adjacent to the mask, and centering them with respect to the dispersed spectrum, they were able to produce a phase shift between each of the amplitude peaks, generating a sequence of regularly spaced odd pulses.

A second technique for producing odd dark pulses from bright pulses was demonstrated in 1987 by Emplit *et al*[44]. This method also used a plate with step variation in optical index to impose a phase shift on the bright pulse, spreading the pulse initially using a system of lenses. The phase modulated pulse was then reflected off a grating and focussed down onto a mirror, before being passed through a slit. The resulting odd dark pulse was propagated over a distance of 52m and the output profile observed at different initial power levels. For input powers close to those predicted for dark soliton formation, distortionless propagation was observed, but the total propagation distance was less than one soliton period and so this could not be taken as absolute confirmation of soliton generation.

Krokel et al [45] were the first group to claim to have generated dark solitons,

using amplitude modulation techniques to create an even hole in a bright pulse, which was then propagated for 10m before observing any reshaping effects. At low powers, the dark pulse broadened considerably and a ringing structure developed in the tails of the bright pulse. As the power was increased, the dark pulse was seen to split in two, with the regular modulation being forced out from the centre towards the wings. Comparisons with numerical results showed very good similarity, confirming the presence of dark solitons.

Other techniques exist, notably Weiner et al [46], Emplit et al [47], and Rothenberg et al [48], all bar the last using some form of imposed pulse shaping. The method used by Rothenberg is discussed in more detail in Chapter 3.

All the experiments described so far produce one or more odd dark pulses, on a finite width bright pulse. However, many of the results were considered questionable, since in the absence of an infinite background the pulses could not be properly classed as dark solitons. Tomlinson [34] et al showed by numerical simulation that the pulses formed exhibit very stable soliton behaviour even in the presence of a very rapidly changing background. An analytical proof of this result was provided by Kivshar and Yang in 1994 [49], showing that the combined effects of background decay and 'internal' soliton dynamics compensated each other to a large extent, resulting in behaviour comparable to that of a dark soliton propagating on an infinite background. Whether such pulses were of any practical use was a different question entirely.

2.4.2 Continuous Trains

Various schemes for producing the more useful continuous trains of dark solitons were proposed during the late 80's and early 90s, the first of these being Dianov *et al* in 1989 [50]. The method they proposed involved complex apparatus and experimental process to produce dark solitons via adiabatic amplification

of a periodically modulated signal. It has not, to the authors knowledge, been demonstrated in practice. A second proposal came from Zhao and Bourkoff [51] in 1990 who suggested using waveguide electro-optic modulators to simultaneously manipulate the phase and amplitude of a cw signal. A waveguide Mach-Zender interferometer is driven with square pulses, each of which produces a dark soliton at its leading and at its trailing edge.

One technique proposed by Kivshar in 1990 [52] was to generate dark solitons from phase steps imposed on a bright background. The mathematical analysis showed that in the presence of an appropriate phase profile a black or grey soliton would form, depending on the depth of the phase shift. However, simulations have shown that the radiation produced as a by-product of the dark soliton generation is likely to render the technique of limited use, unless some method can be found to control the bright background independently of the soliton.

Another proposed technique developed one of the finite background schemes, applying a spatial amplitude and phase mask to a spectrally dispersed train of bright pulses[53]. The source is chosen such that the maximum of its gain curve is located centrally between two of its longitudinal modes. Assuming the system design is such that the two modes are spatially separate in the Fourier plane, it is possible to filter them independently.

The first successful experimental generation of a CW train of dark solitons was demonstrated by Richardson et al[54] in 1994. The solitons were produced via nonlinear conversion of a high-intensity beat signal, generated by combining cw light from two single frequency lasers. The resulting periodically modulated signal was input to a length of fibre with slowly decreasing normal dispersion, producing at the output, when the signal power was sufficient, a train of high-frequency dark solitons. (This was similar to the scheme proposed in 1989 by

Dianov et al.) If a fibre with constant dispersion was substituted, the resulting pulse trains were not stable, but evolved and decayed periodically with propagation. The resulting pulses were propagated for two soliton periods and were shown to be stable over this length scale. However, the problem of modulating the train remained.

The first technique to provide a pseudo-random train of dark solitons, ie a continuous train of solitons upon which a data pattern of some form has been imposed has recently been developed and demonstrated experimentally by Nakazawa and Suzuki[55]. They have developed the method origianally proposed by Zhao and Bourkhoff, driving the MZ interferometer with a pseudo-random sequence of rising and trailing edges, generated by converting NRZ data to RZ data with a a duty cycle of 1/2. This produces a modulated train of dark solitons and is potentially a suitable source for optical communications. They also demonstrated propagation over 1.3 soliton periods, and coherent detection of the output pulse train[56].

2.5 Comparison of power requirements for bright and dark solitons.

A frequent criticism of dark solitons is that they require far higher powers per data bit than conventional bright pulse transmission systems, and would therefore not be economically viable. However, with the results above, it is possible to show quite trivially that the reduction in mark:space ratio for dark solitons compared to bright reduces the dark soliton power requirements to a workable level. The previously unpublished calculation which follows uses system parameters similar to those which would be expected in real systems to illustrate the point, using dispersion shifted fibre, with a dispersion of ± 0.25ps/nm.km at the

signal wavelength of 1.5μm, with a nonlinearity coefficient γ of 2W^{-1}km^{-1}.

Mark-space ratios were chosen of 1:7 for bright solitons and 1:4 for dark solitons, these being considered the minimum for bright solitons and a safe, though not extreme value for dark solitons.

For a data rate of 10Gbit/s, the pulse separation is 100ps, which implies a bright pulse width of 12.5ps and a dark pulse width of 20ps. The peak power required for either a bright of dark fundamental (N=1) soliton is:

$$P_0 = \frac{|\beta_2|}{\gamma\tau^2} = \frac{3.11|\beta_2|}{\gamma T_{FWHM}^2} \tag{2.8}$$

Substituting for the different systems parameters gives a bright soliton peak power of 0.8mW, and a dark soliton peak power (effectively the height of the supporting cw background) of 0.31mW

The average power in a train of bright solitons with peak power P_0 and FWHM 1.76τ is found by integrating over one bit period from -T/2 to T/2.

$$\begin{aligned} P_{av} &= \frac{1}{T}\int_{-\frac{T}{2}}^{\frac{T}{2}} P_0 \operatorname{sech}^2 \frac{t}{\tau} dt \\ &= \frac{P_0}{T}\left[\tau \tanh \frac{t}{\tau}\right]_{-\frac{T}{2}}^{\frac{T}{2}} \\ &= \frac{P_0\tau}{T}\left(\tanh \frac{T}{2\tau} - \tanh \frac{-T}{2\tau}\right) \\ &= \frac{P_0\tau}{T}\left(\tanh \frac{T}{2\tau} - \left(-tanh\frac{T}{2\tau}\right)\right) \\ &= \frac{2P_0}{T\tau} \tanh \frac{T}{2\tau} \end{aligned} \tag{2.9}$$

when $T \gg 2\tau$, $\tanh \frac{T}{2\tau} \rightarrow 1$, therefore:

$$P_{av}(brightsoliton) = \frac{P_0 2\tau}{T} = 0.2mW \tag{2.10}$$

which is the average power requirement for a train of bright solitons in the 10Gbit/s transmission system defined above.

The average power in a train of dark solitons with peak power P_0 and FWHM 1.76τ is also found by integrating over one bit period from -T/2 to T/2.

$$\begin{aligned} P_{av}(darksoliton) &= \frac{1}{T}\int_{-\frac{T}{2}}^{\frac{T}{2}} P_0 \tanh^2\frac{t}{\tau}dt \\ &= \frac{P_0}{T}\int_{-\frac{T}{2}}^{\frac{T}{2}}\left(1-\operatorname{sech}^2\frac{t}{\tau}\right)dt \\ &= P_0\left(1-\frac{2\tau}{T}\right) \end{aligned} \tag{2.11}$$

$$P_{av}(darksol.) = P_0\left(1-\frac{2\tau}{T}\right) = 0.188mW \tag{2.12}$$

In this particular case then, the power requirements for dark solitons are actually lower than for the equivalent bright solitons. Although specific details will vary from system to system it would be fair to say that were soliton-soliton interactions the only important effect then dark solitons would compare very favourably with bright simply on power budget terms.

There is a second important advantage of the dark solitons improved stability to interactions. Recall that the soliton period increases with the square of the pulse-width, and the dark soliton period is half the equivalent bright soliton period. This has serious consequences for dark solitons with those effects which are dependent on distance propagated relative to the soliton period, and increasing the soliton period is desirable.

For transmission at the same data rate, with the same soliton period, dark solitons must have a pulse width of 1.4142*T where T is the full-width at half maximum of the bright soliton. In the system described above, using a

bright soliton mark:space ratio of 1:7, the bright pulses had a FWHM of 12.5ps. A dark soliton with the same period would have a FWHM of 17.7ps, and a corresponding mark:space ratio of 1:5.6. This is well within the limits required for propagation without interaction.

These results suggest that the possibility of using dark solitons as information carriers merits serious investigation.

Chapter 3

Generation of Quasi-continuous trains of dark solitons.

Analytical and numerical demonstrations of the potential use or otherwise of dark solitons are of limited value in real terms if no reliable dark soliton generation technique exists. This chapter discusses original work done both in simulation and in the laboratory to produce trains of dark solitons on bright background pulses. It describes the numerical and experimental studies carried out and the results of attempting to expand the technique to produce true continuous trains[57], [58].

3.1 Previous generation techniques.

A simple method of generating trains of dark solitons was demonstrated in 1991[48], [59]. The work showed, both numerically and experimentally, that it was possible to produce pairs of trains of dark solitons on a finite background by the collision of two bright pulses.

The two bright pulses were launched into a fibre, with a controllable separation in time Δt. Propagating in standard fibre, the pulses experienced the linear and nonlinear broadening associated with propagation in the normal dispersion regime, developing a rectangular temporal profile with a varying frequency chirp across the pulse. This is due to a combination of GVD and SPM, which act together for positive GVD resulting in very rapid pulse shaping. At some distance determined by the initial separation the two pulses will have broadened to the point where they overlap and interfere with each other, resulting in a single bright pulse with sinusoidally modulated intensity and alternating phase (see figure 3.1a and b).

With further propagation the action of the nonlinearity causes the modulation to develop into pulses with characteristics which asymptotically approach those of fundamental dark solitons, as shown in figure 3.1c and d. As can be seen, this technique produced trains of dark solitons on a bright background, separated by a bright central region.

3.2 Numerical analysis of system.

The preliminary studies to be carried out on the generation technique outlined in section 3.1 were aimed at finding suitable parameters for dark soliton generation at longer wavelengths, where the fibre loss is lower and propagation may be observed over greater distances before the effects of loss need to be considered. Once appropriate values had been defined, it would be possible to generate trains of dark solitons in the laboratory, concluding the first stage of the work. The second stage is described in section 3.6.

The selection of suitable pulse powers and separations was done using numerical techniques to simulate propagation with a wide range of input parameters,

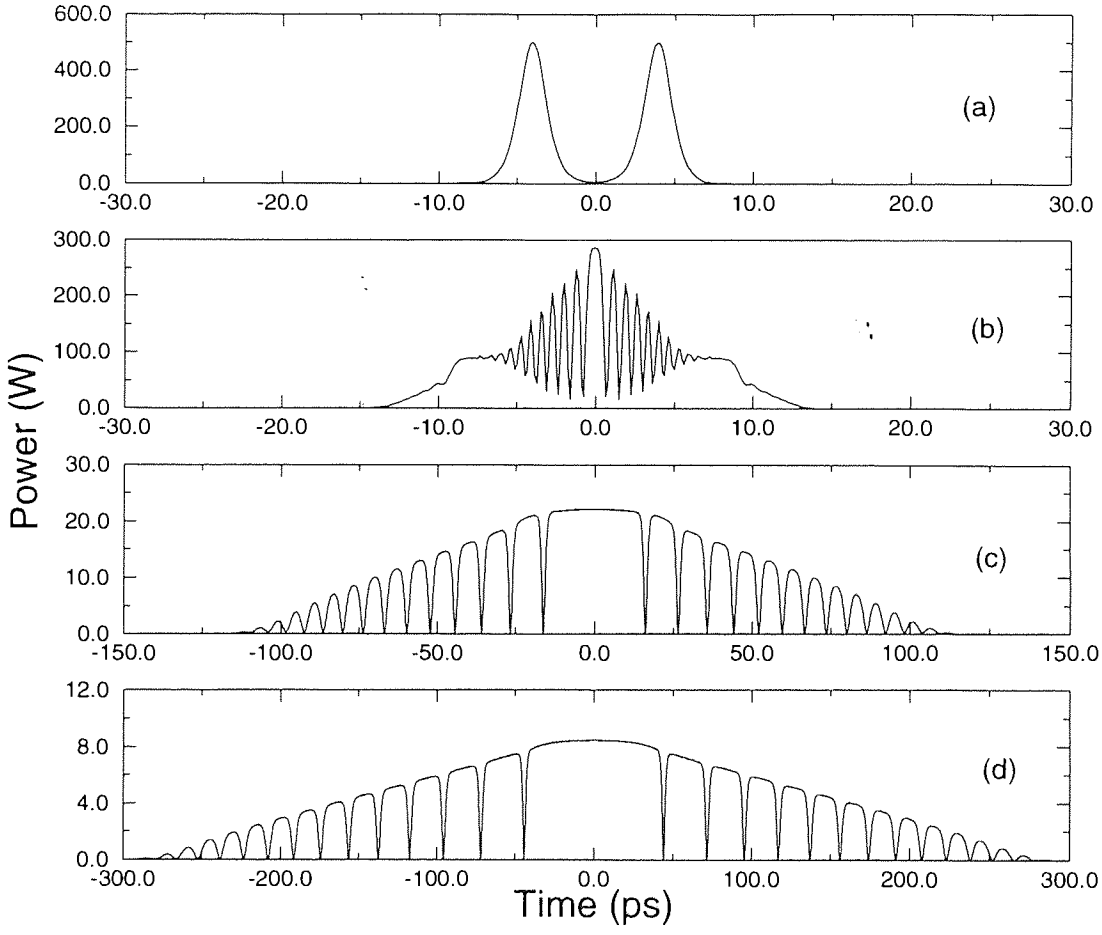

Figure 3.1: The interaction of two 2ps bright pulses, with an initial separation of 8ps, propagating for 0.5km, with propagation distances of (a) 0km (b) 0.006km (c) 0.2km (d) 0.5km *Note the change in scale on the time axis.*

starting from a pair of bright pulses with characteristics defined by the laser with which the lab experiments would be carried out, namely pulse widths of 3ps and peak powers of up to 1kW, at a wavelength of 900nm. It was necessary to determine how the resulting pulse profile varied with different initial conditions, and hence obtain values for suitable power levels and pulse separations to produce clear trains of dark solitons at high repetition rates.

From the initial numerical work it was possible to draw a number of interesting conclusions. For the same input power levels, varying the input pulse separation resulted in a variation in the number and density of dark pulses formed. Figure 3.2 shows the results for progressively greater pulse separations, to the point where it was possible to produce an apparently continuous train of dark solitons across the entire pulse, without the bright central region observed for smaller initial separations.

Examination of the frequency chirp on the pulses prior to collision for the different input conditions shows that for greater separations, and therefore longer propagation before collision, the chirp on each pulse is much more linear, and so the resulting modulation is more regular, and the dark pulses which evolve from the modulation more evenly spaced.

As the separation distance and hence the time before collision was increased, the distance remaining for soliton formation was decreased, and so the pulses formed with a separation of 30ps (figure 3.2d) do not after the total 2km propagation distance exhibit such a clear profile as the pulses formed by collision between two initially close bright pulses. Since experimental constraints meant that 2km was the maximum propagation distance physically realisable, limiting the nonlinear behaviour which could be observed. To overcome this, some other method was required to increase the effect of the nonlinearity, the most obvious being to increase the power in the system.

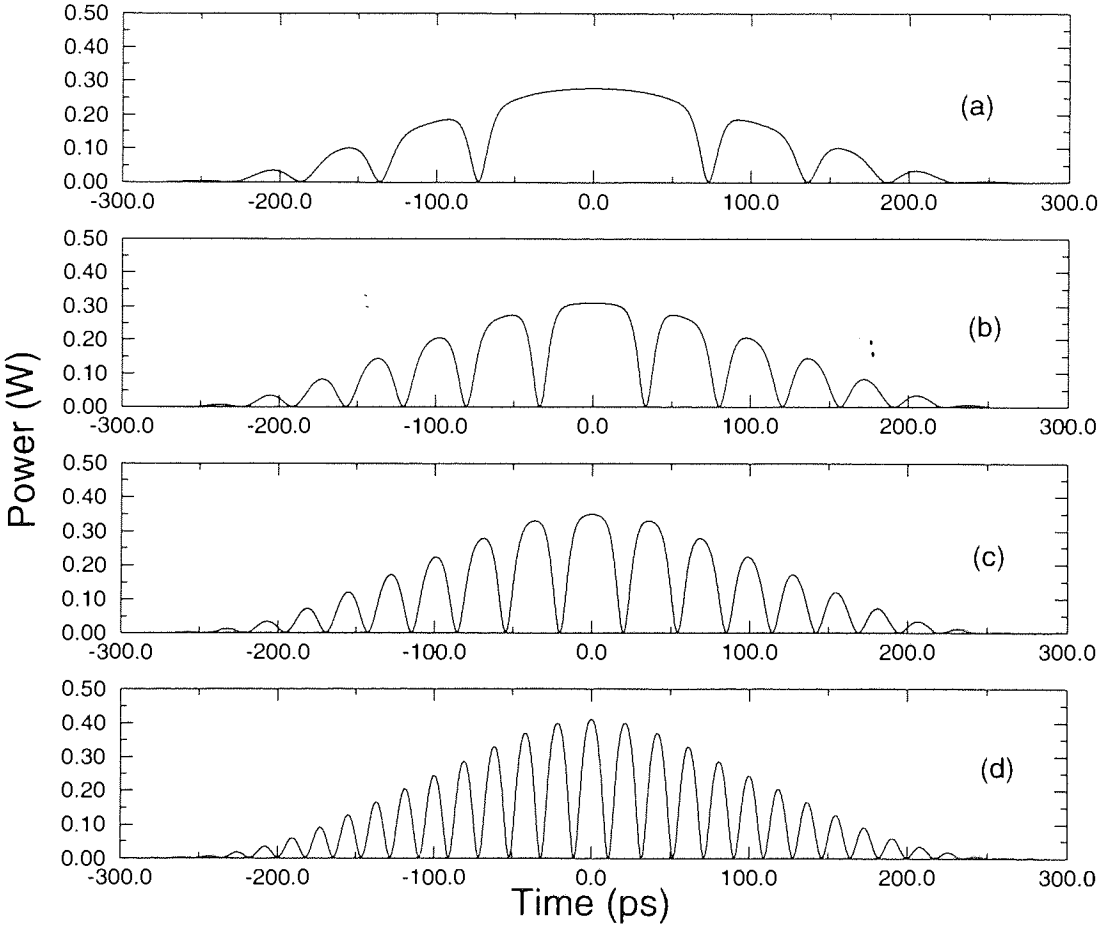

Figure 3.2: The effect of increasing the separation of the input bright pulses, with in each case a peak pulse power of 20W. The figures show the profiles after propagating for 2km, for initial pulse separations of (a) 10ps (b) 15ps (c) 20ps (d) 30ps

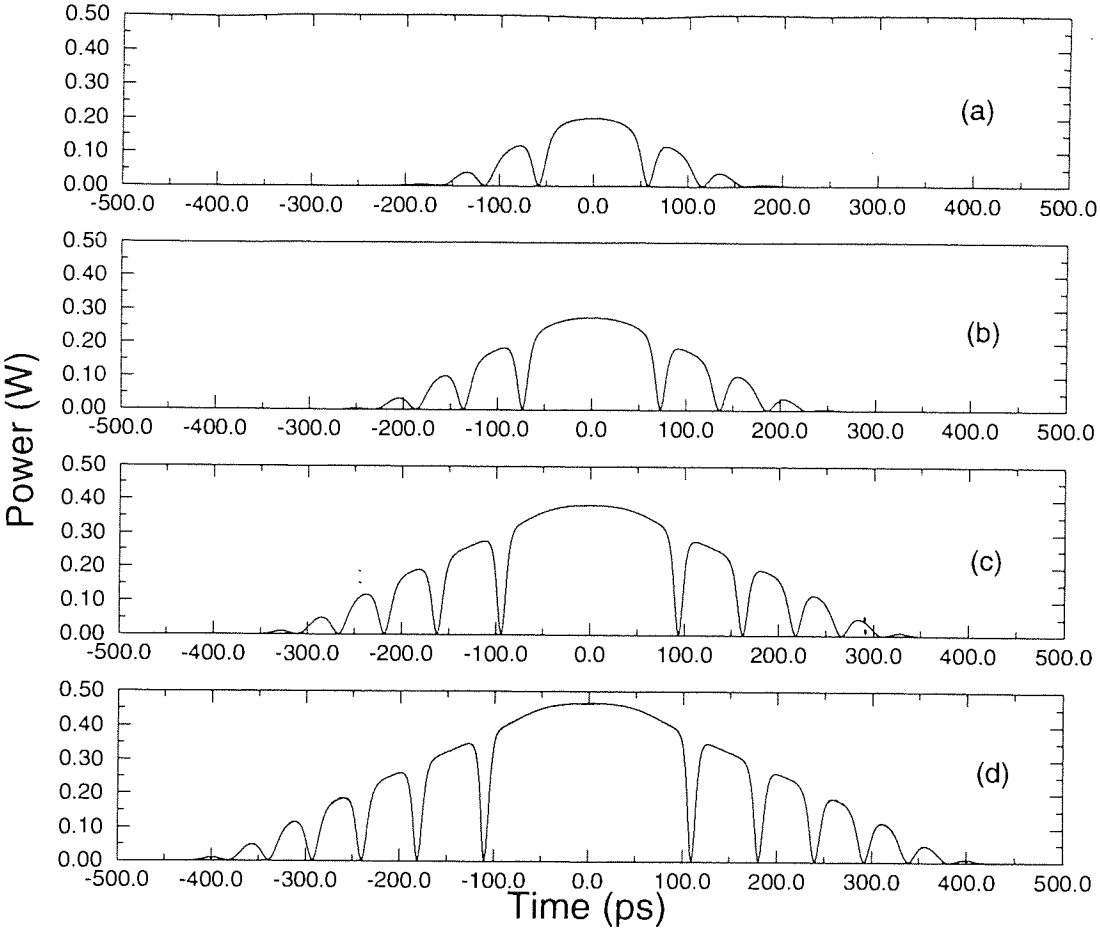

Figure 3.3: The effect of increasing the peak power of the input bright pulses. This figures show the profiles after propagating for 2km with an initial pulse separation of 10ps and pulse peak powers of (a) 10W (b) 20W (c) 40W (d) 60W.

Figure 3.3 shows that for the same pulse separation, an increase in power level would increase the number of dark pulses produced. This can be explained by considering the greater chirp across the bright pulses prior to collision, which results from the increase in the nonlinear contribution to the pulse broadening. Changing the input power did not affect the positioning of the two trains relative to the centre of the packet.

By manipulating the separation and peak power of the input pulses it was possible to simulate the generation of a satisfactorily continuous train of dark pulses. Figure 3.4 shows the output producing using bright pulses 20ps apart,

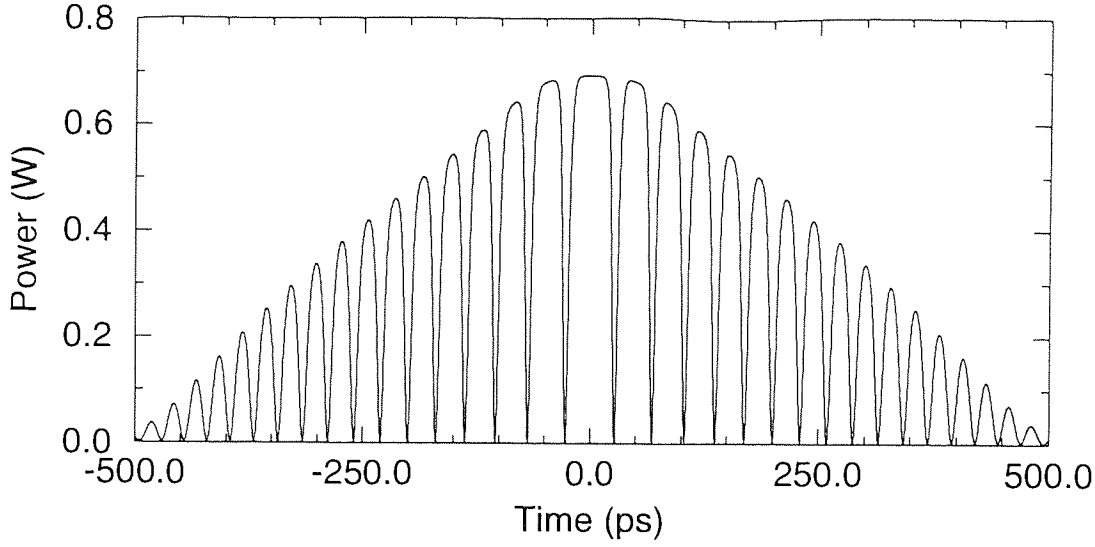

Figure 3.4: A train of quasi-continuous dark solitons.

with initial peak powers of 100W.

3.3 Verification of soliton-like behaviour of generated pulses.

The next stage of the simulation work was to confirm that the dark pulses produced were in fact solitons. It is possible to distinguish between dark pulses and dark solitons in a variety of ways, not least in terms of shape, phase profile and response to changes in background level. In numerical systems it is relatively straightforward to observe propagation, and examine the amplitude and phase profiles of simulated pulses in great detail, and so it was possible to demonstrate the properties of these dark pulses in some detail.

Firstly, it was confirmed that the pulses had the expected $tanh^2$ temporal profile corresponding to very dark grey solitons and a phase shift across the centre which deviated only slightly from the instantaneous π phase change of the black

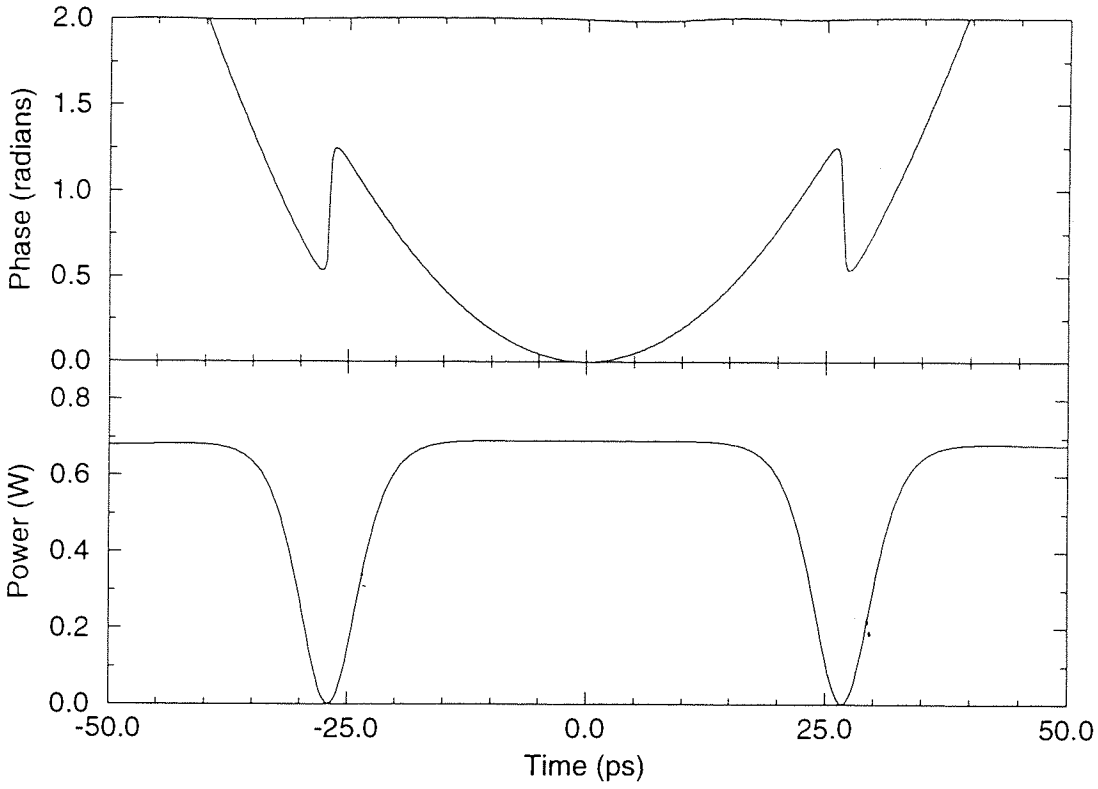

Figure 3.5: The amplitude and phase profiles of the dark solitons nearest the centre of the pulse. Note the superposition of the phase shift across the bright background, due to the chirp acquired due to propagation in the normal dispersion regime.

soliton, as shown in figure 3.5. The technique did not result in the generation of black, or 100% solitons. The bright background pulse showed a large linear chirp, and hence there was a large phase variation across the pulse, upon which the dark soliton phase profiles were superimposed (see figure 3.6). However, as was demonstrated by Tomlinson[34] and later proved analytically by Kivshar[24] the presence of such a large background chirp does not preclude the existence of dark solitons.

Secondly, the evolution of the pulse width and depth as the background pulse broadened could be studied. With increasing width, the bright pulse peak power fell, reducing the power supporting the dark pulses. Although the system's loss over the total distance was low (about 3.8dB) the dark pulses effectively

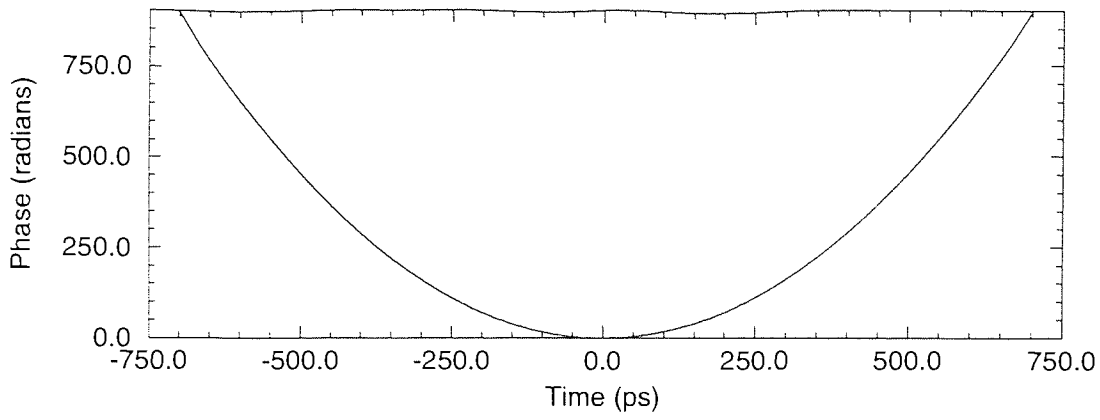

Figure 3.6: The phase profile of the bright background pulse supporting the solitons. This corresponds to a very large linear chirp.

experienced quite severe loss owing to this broadening, and so it was possible to get a clear description of their behaviour. It would be expected that the solitons would broaden adiabatically to maintain a constant width/depth product.

Software was written to allow the study of the evolution of the width/depth product during propagation. This showed that those pulses nearest the centre of the background pulse very rapidly approached an asymptotic dark soliton solution. Figure 3.7 shows the evolution of this product for four of the solitons shown in figure 3.4.

The pulses at the edges approach a constant value for this parameter much more slowly. A possible explanation may be found by considering the strength of the nonlinearity at different points across the background. Those pulses at the centre of the packet are supported by a larger background and so see greater nonlinearity than those at the edges, enabling more rapid evolution towards a stable soliton solution.

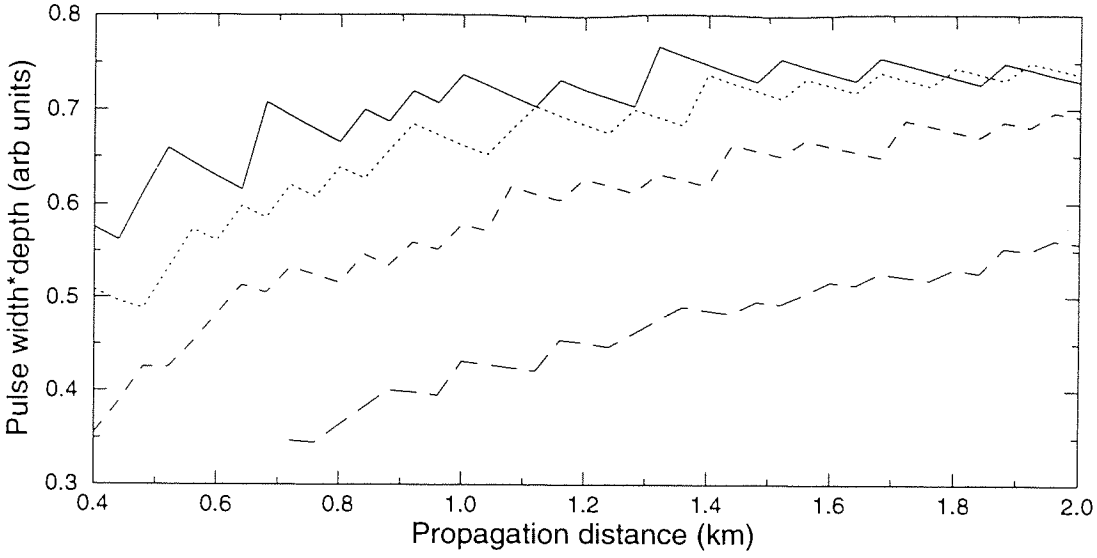

Figure 3.7: The evolution of the width/depth product for the first (solid line), sixth (dotted line), eleventh (dashed line) and sixteenth (long dashed line) pulses dark pulses being generated, counted out from the centre. (The discontinuities in the curve are due to numerical limitations in the software used to calculate pulse width and depth.)

3.4 Experimental confirmation of simulated results.

Having defined a suitable parameter range by numerical simulation, an appropriate experiment could be devised to test the predictions made, in the laboratory.

The experimental setup was as shown in figure 3.8. The pulse source used was a commercial titanium-sapphire laser operating at 900nm and producing transform limited sech^2 pulses with FWHM of 2.5ps. The incoming pulses from the laser were split and recombined, using a retro-reflector on a moving stage to vary the distance over which each signal travelled before recombination, and hence the temporal separation between the pulses could be varied for a range of about 40ps, or up to fifteen times the width of the initial pulses. The

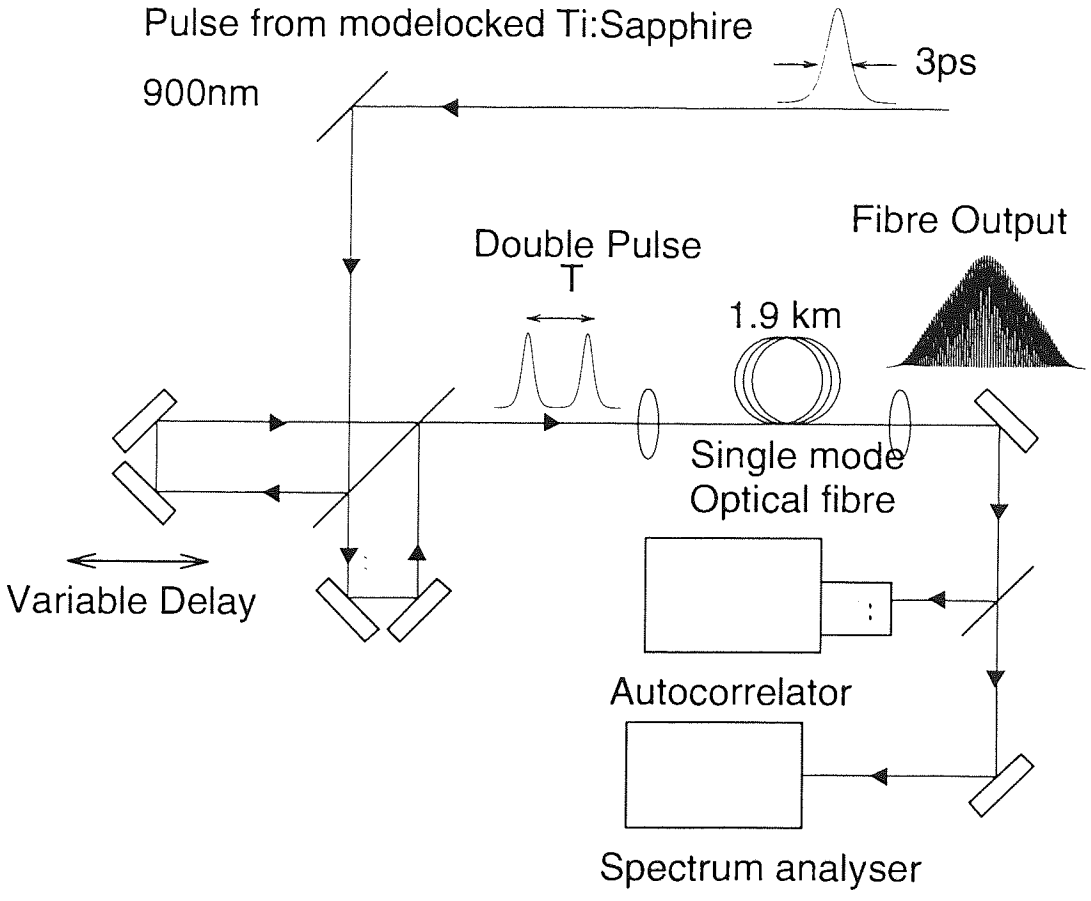

Figure 3.8: Schematic for the experimental generation of trains of dark solitons

pairs of pulses were then propagated through 1.9km fibre with a dispersion of 100ps/nm.km and the output viewed using autocorrelation techniques.

The fibre used in the experiment was designed to exhibit low loss at short infra-red wavelengths. The loss at 900nm was 1.9dB/km which corresponds to a loss length of 2.3km. The predicted pulse width for the narrowest solitons which could be generated with this equipment was 5ps, giving a soliton period of 0.294km. This is significantly less than the loss length. This experiment was the first to demonstrate dark soliton propagation over more than 2.5 soliton periods.

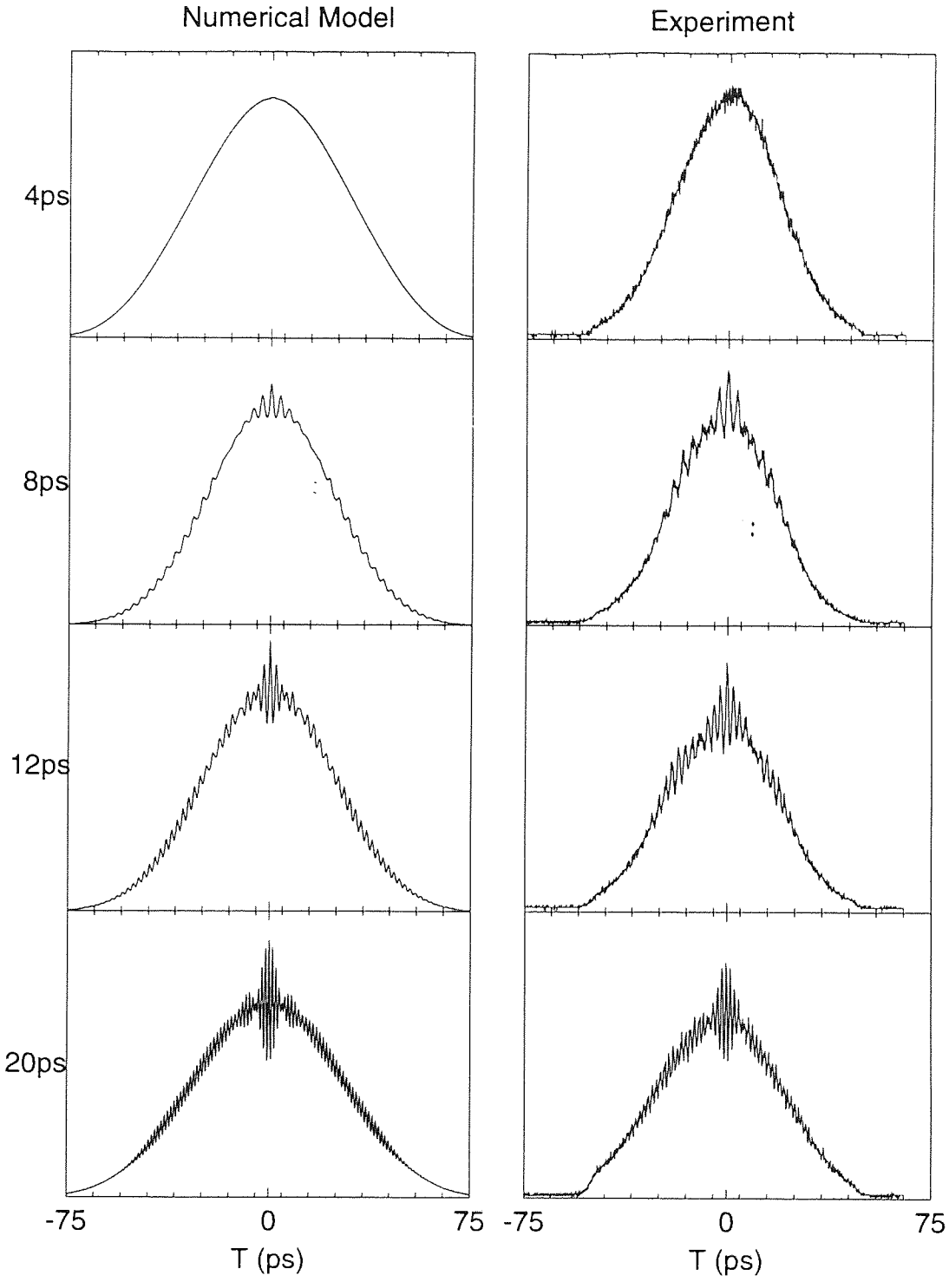

Figure 3.9: Predicted (left-hand column) and observed results for the autocorrelation of the output pulses, for a variety of initial pulse separations.

By comparing these results with those predicted by the model for autocorrelation of trains of dark solitons it was possible to be reasonably certain that the pulses were being generated as expected, and that the trends predicted for increasing power and pulse separation were being followed (see figure 3.9). However, because of the complexity of the pulse profiles it was not possible to obtain any detailed information regarding soliton depth and spacing.

More useful information on this point was available from the spectra of the output pulses for different powers and separations. In particular, because of the linear chirp across the bright background pulse, individual features representing solitons could be identified, and the increase and decrease in the number of dark pulses produced could be observed by changing the delay between the bright pulses.

3.5 Resolution of pulse profiles using a streak camera.

The limitations of autocorrelation as a means for studying the profile of dark solitons are clear from the above results, and a further series of experiments were carried out by John Williams at the Université Libre de Bruxelles in collaboration with Philippe Emplit. The purpose of these experiments was to observe the generated pulse profiles using a streak camera to give far more detailed information about pulse shape, providing a resolution of down to 10ps. The laser used in this case had an operating wavelength of 850nm, and so the pulses experienced a dispersion of 150ps/nm.km.

This work also produced results in excellent agreement with the numerical simulations, with appropriate changes to the system parameters. Trains of dark

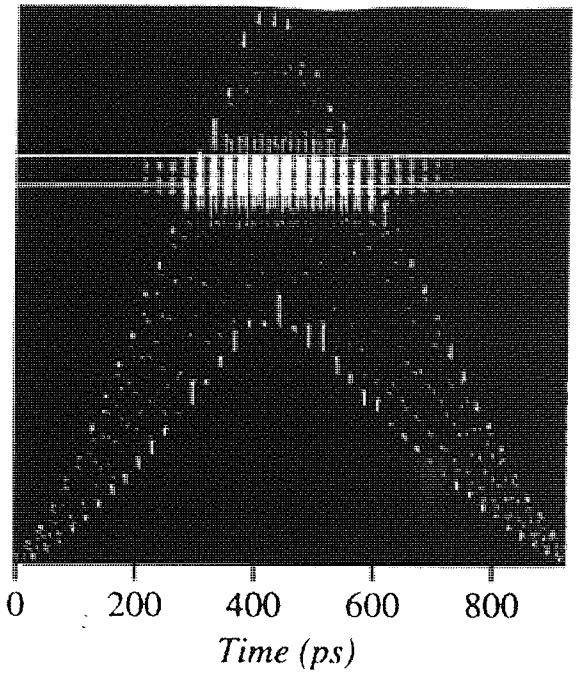

Figure 3.10: Streak camera image. Initial peak pulse power 64W, initial pulse separation 22ps.

solitons at rates up to 60GHz were observed in this manner, by varying input powers and pulse separations, confirming the predictions made regarding pulse shape and variation with input parameters.

Figure 3.10 shows a streak camera image of the pulse profiles with an initial pulse separation of 22ps. This compared very well with the numerical results when convolved with the predicted response of the streak camera to a delta function, suggesting that the dark solitons had a depth of at least 99%.

Figure 3.11 shows the variation in profile, and the corresponding spectra for a range of initial pulse separations.

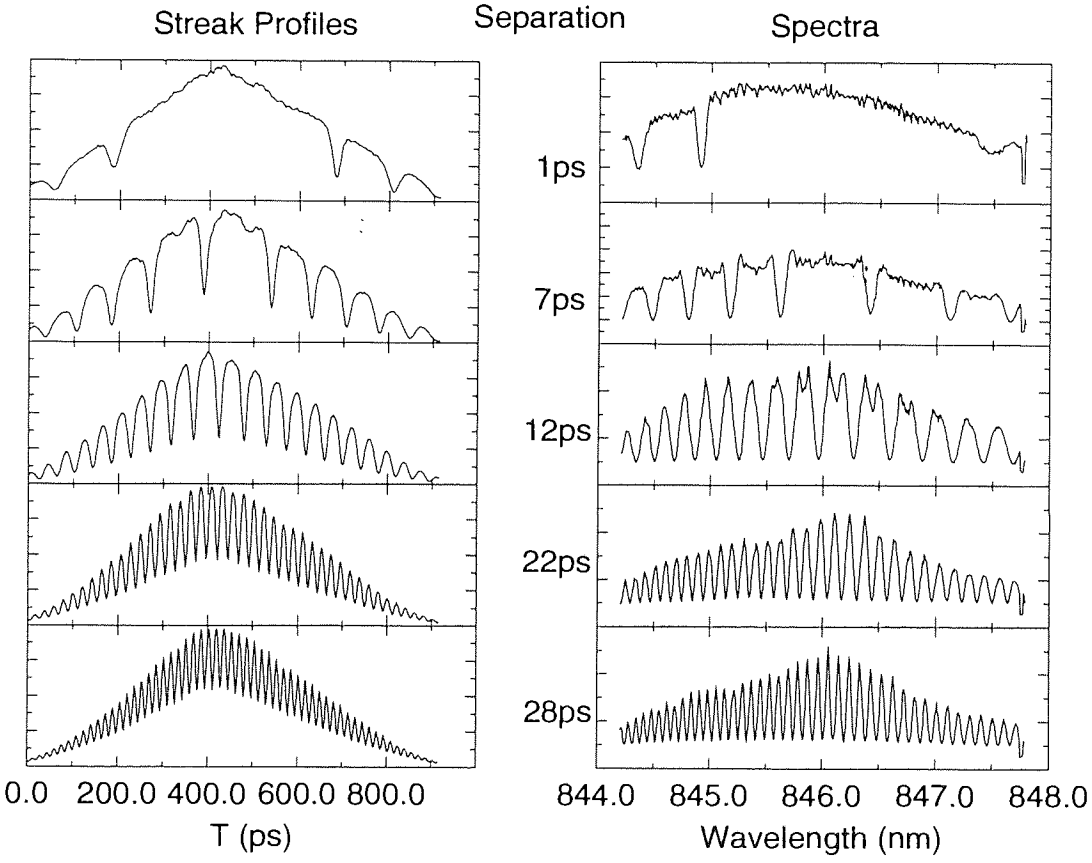

Figure 3.11: Typical sequence of streak camera profiles and corresponding spectra for varying initial pulse separations. Initial pulse peak power 64W.

3.6 Extension of technique to produce continuous trains.

From the results obtained it can be seen this technique provides a simple method for generating short trains of dark solitons. The experimental results also show that the model gives an accurate representation of the real system, and provides justification for the conclusions of the further numerical work done on this system, expanding the two-pulse interaction to three and more pulses.

3.6.1 Three Pulse Interactions

Figure 3.12 shows the profile of the background pulse supporting dark solitons before, during and after the propagation and collision of three bright pulses. As can be seen, not one but two sets of pulse trains are formed, each centred on the collision point between two of the three pulses.

It was found that, in general, increasing the number of bright pulses to n produces a bright background containing $n-1$ groups of dark solitons, with velocities determined by the chirp across their originating pulses prior to collision. The overall system at any point consisted of a large number of dark solitons, all with different starting points and velocities, continually colliding with solitons generated by the interaction between a different pair of neighbouring bright pulses.

This result meant that the technique could not be used to produce an infinite stream of evenly-spaced dark solitons, in the same way as an infinite number of light sources cannot be used to produce uniform illumination.

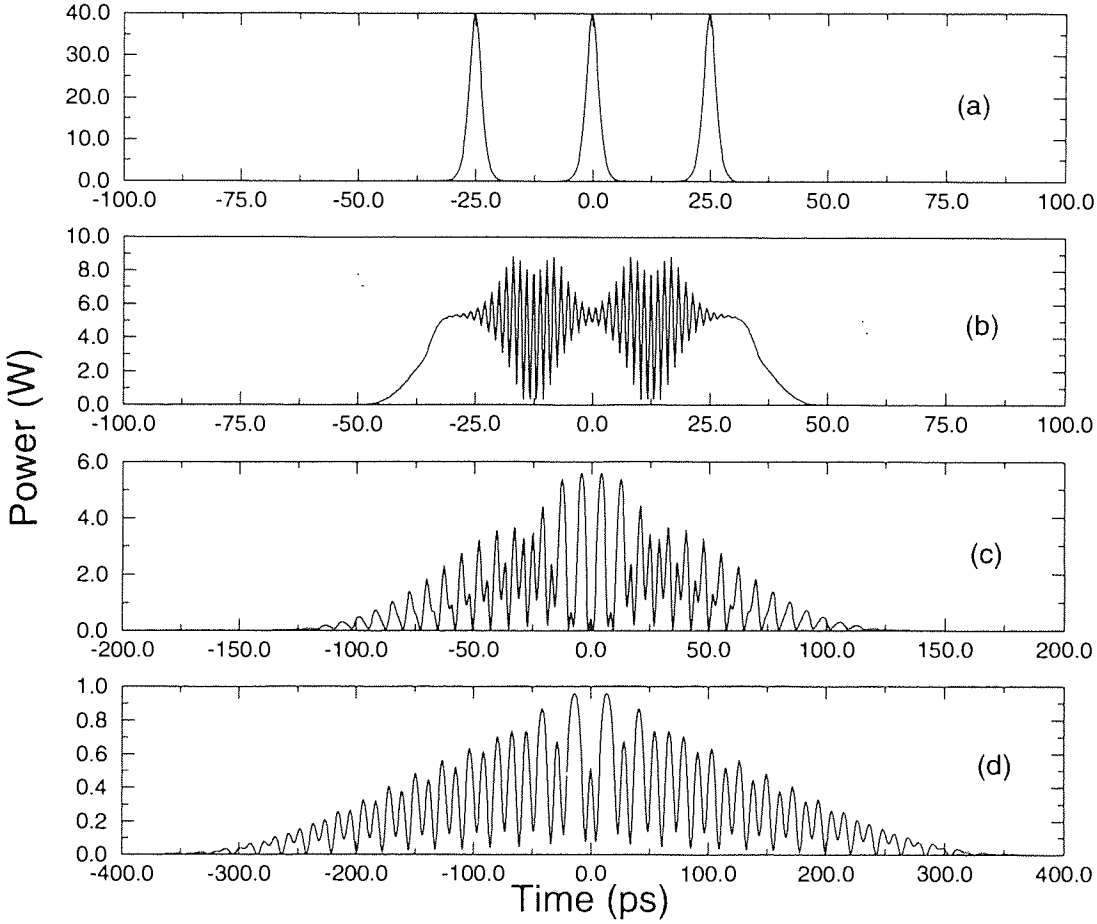

Figure 3.12: The interaction of three bright pulses. Note the change in scale on the x-axis. The figure shows the pulse profiles at propagation distances of (a) 0.0km (b) 0.14km (c) 0.68km (d) 2.0km.

3.6.2 Dark soliton collisions

The interaction of three pulses does however provide a useful vehicle for the observation of dark soliton collisions. These are of particular interest because as well as the normal properties of bright solitons during collision, that is that they pass through each other unchanged, but displaced by a calculable amount in time, (see section 1.4.2) the behaviour of very dark (as opposed to grey) solitons during collision is markedly different to what would be observed by inverting the system and observing bright solitons colliding. This was originally studied by Thurston and Weiner[41]), and their work is discussed in more detail in Chapter 2.3.4.

In the numerical simulations of the interaction of three bright pulses it was possible to observe a great number of dark soliton collisions, as the solitons produced between each pair of bright pulses radiated outwards. They are of particular interest as the solitons observed are typically of different depths and velocities. Figure 3.13 shows an example of a one such collision, and figure 3.14 the phase profiles at each point. For the case of non-identical dark solitons, there is no time during collision at which the phase variation across the window becomes zero. Instead, as each pulse reaches zero intensity at its centre the associated phase shift is reversed.

The collision of the pulses marked with long and short arrows in figures 3.13 and 3.14 is a particularly good example of this, with the two pulses being caught in the centre picture during the most interesting phase of collision, where one of the solitons has achieved zero intensity at the pulse centre, and its phase has reversed.

The observation of such collisions in simulation provided additional proof that the dark pulses generated were in fact solitons. However, in view of the fact that the method could never be used to produce anything other than groups of

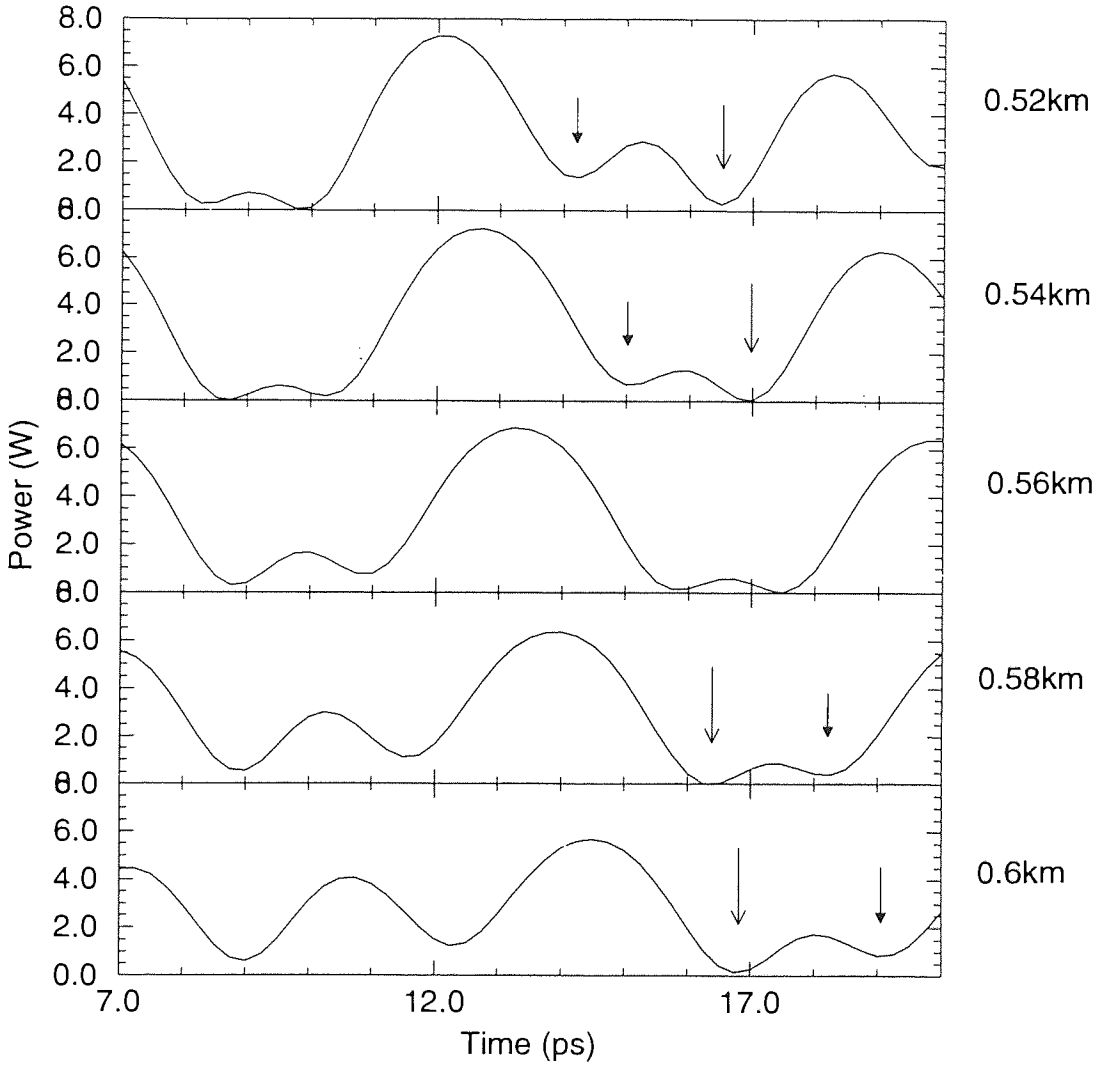

Figure 3.13: The collision of dark grey solitons generated by the interaction of three bright pulses. The arrows identify the two pulses discussed in detail in this section.

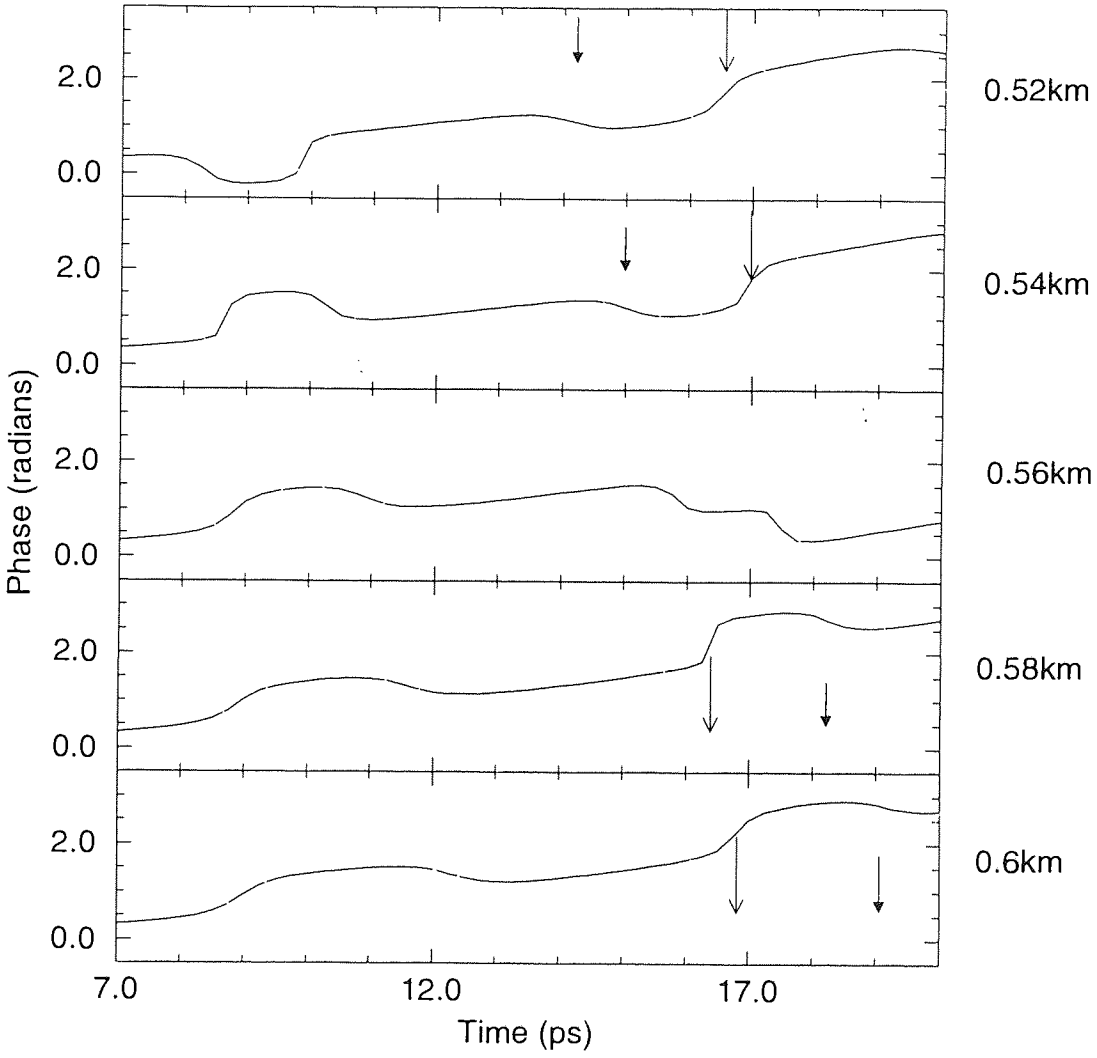

Figure 3.14: The associated phase profiles during the collisions shown in figure 3.13. The arrows identify the two pulses discussed in detail in this section. Note again the slope on the phase due to the chirp on the bright background pulse.

dark solitons on a finite-width background, in addition to the complexity of the equipment which would be required to interact three or more bright pulses, no attempt was made to observe this phenomenon experimentally.

3.7 Conclusions

Both numerical and experimental results showed that by interacting two bright pulses copropagating in fibre, it was possible to generate short trains of dark solitons. Using numerical simulations to optimise the pulse parameters prior to beginning the laboratory experiments it was possible to define a useful range of values to provide a convenient and stable source of packets of dark solitons. Use of numerically generated results also allowed an in-depth analysis of pulse shape, phase profile and spectral characteristics during propagation. This data was used to demonstrate the soliton-like nature of the dark pulses generated. (see section 1.5). The results were confirmed experimentally (see section 3.4) and streak camera images showed the production of trains of dark solitons at repetition rates up to 60GHz, with estimated pulse widths of 5ps for the central pulses (see section 3.5).

For use in standard communication systems, a source which provides a continuous stream of bits is preferable to a source of short bursts, and the second stage of the work described here had the aim of expanding the method to produce such a train. Again, the initial work was done using numerical simulations to examine the behaviour when three bright pulses were copropagated and allowed to collide (see section 3.6.1). Because the dark solitons form as a result of the interaction between the wings of two bright pulses, multi-pulse collisions produced multiple sources of dark solitons, each group having different velocities relative to the background. This was therefore not an appropriate method for

generating continuous trains of dark solitons.

The simulations of three pulse interactions did permit a study of dark soliton collisions, in particular the case of solitons of different depths and hence different velocities. This confirmed the soliton-like nature of the dark pulses generated, and provided a potential way to demonstrate this interesting type of behaviour.

Chapter 4

Experimental dark pulse generation.

This chapter describes work to produce a stable and continuous train of dark solitons in the laboratory using active optical mode-locking within a fibre laser cavity. The initial work was based upon results of Pataca *et al*[60], showing the generation of stable trains of dark pulses,. These results were repeated at longer wavelengths, and the laser thoroughly characterised. Experimental limitations meant that it was not possible to propagate the pulses as intended, but there were sufficient indications from the characterisation work to suggest the pulses were even pulses, rather than dark solitons. However, the source proved to be very stable with respect to a large number of perturbations, and could be of interest from the point of view of dark soliton generation if some external method of manipulating the phase profile could be identified.

4.1 Previous work.

It is possible to produce a source of mode-locking for optical pulses by making use of nonlinear effects such as cross-phase modulation (see section 1.3.2) to provide either phase or amplitude modulation within a laser cavity. Pataca *et al.* showed experimentally in 1995 that by controlling the sign of dispersion inside the fibre laser they were able to produce either bright or dark pulses. However, they were not able to show whether the dark pulses produced in this manner were odd or even pulses, that is whether or not they possessed the characteristic dark soliton asymmetric phase profile. A simple way of determining this would be to observe the propagation properties of the pulses formed over a distance of several soliton periods.

4.1.1 FM mode-locking.

Conventional FM mode-locked lasers use a sinusoidal signal to provide cross-phase modulation with the signal wavelength. There are two possible solutions to the equations for this system, one corresponding to each extreme of the phase modulation. The mode associated with the maximum of the imposed phase profile is referred to as the positive mode, the negative mode being associated with the minimum phase modulation. The two modes have opposite chirps, and so in the presence of a a fixed amount of dispersion only one will be stable, pulses of the other mode being broadened rather than compressed.

In the work described here, the modulation is not sinusoidal but in the form of pulses, which impose a positive phase window on the signal wavelength. In the normal dispersion regime this will stabilise as holes in a cw background, with a repetition rate equal to that of the modulating source.

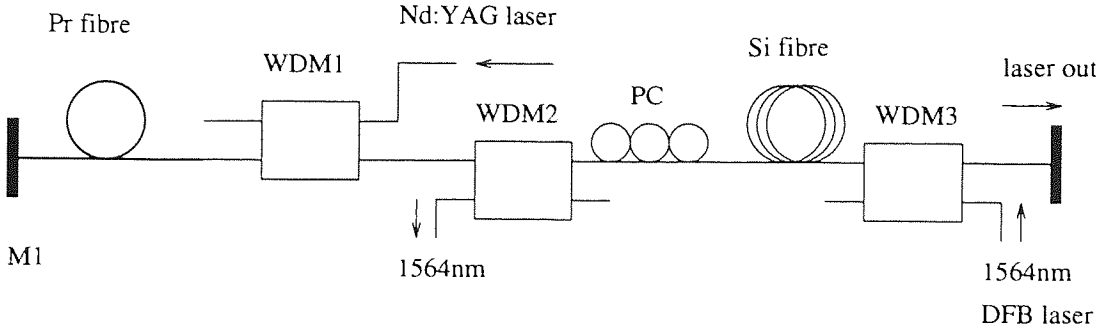

Figure 4.1: The experimental set-up used by Pataca et al to generate continuous streams of dark pulses.

4.1.2 Previous results.

The experimental configuration used is shown in figure 4.1. Amplification within the cavity was provided by a length of praseodymium(Pr^{3+})-doped fluoride fibre, a recent development in all-optical amplifier technology which has a working range centred about 1.3μm The amplifier was excited by a Nd:YAG laser operating at 1.064μm. Active optical mode-locking was achieved using a 1.564μ m DFB laser, whose pulses were amplified using erbium-doped fibre to a maximum mean power of 30mW. The output coupler M2 took a variety of forms, as an optically written fibre grating with bandwidth 2.4nm and reflectivity of approximately 70% and dispersion depending on orientation of $\pm$35ps/nm.

Depending on the orientation of the in-fibre grating, Pataca et al were able to produce trains of either bright or dark pulses, and with pulse widths of between 140 and 220ps obtained by varying the laser wavelength to alter the walk-off between signal and modulation source.

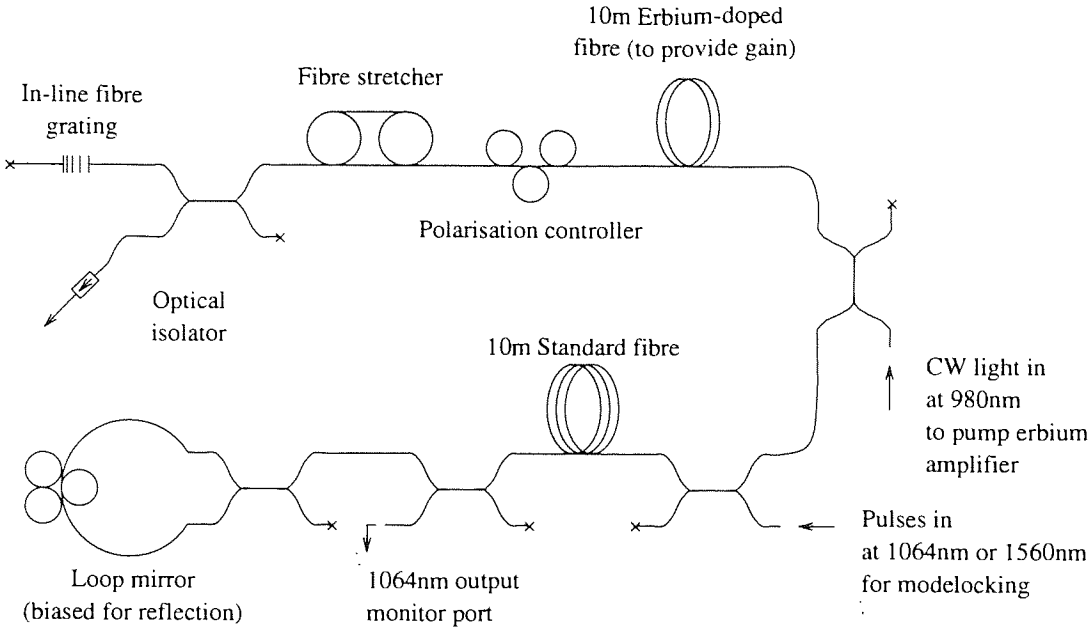

Figure 4.2: The basic cavity structure used in this series of experiments.

4.2 Experimental technique for dark pulse generation.

The experimental setup for this study used a variety of cavity structures and pulse sources to allow a thorough examination of the pulse generation technique.

Figure 4.2 shows the basic form of the laser. A range of reflectors were used at the ends of the cavity, to permit changes in system dispersion and operating wavelength. The reflector R1 was in each case an optically written chirped in-fibre grating, produced using the technique of dissimilar wavefronts, which allows for a continuous distribution of chirp across the grating, without steps, and so permits clear specification of bandwidth and dispersion. The reflector R2 was, in turn, a 100% mirror butted to the end of the mode-locker section of the cavity, a loop mirror whose reflectivity could be varied using polarisation controllers within the loop, and a narrow bandwidth, unchirped in-fibre grating used to constrain the laser to a single wavelength.

Amplification in the system was provided by an 8m length of erbium (Er^{3+})-doped silica fibre, pumped at 980nm by a commercial Titanium-sapphire laser operating as a source of continuous wave illumination. Total signal power could be varied by varying the pump power available using a simple polarising beam cube and half-wave plate arrangement.

The laser was FM-mode-locked initially using 100ps pulses at 1064nm from a commercial YAG laser with a repetition rate of 76MHz. This was copropagated with the cw light from the erbium amplifier in a length of standard fibre to produce modulation of the cw signal via cross-phase modulation. (see section 1.3.2)

In standard fibre the walk-off distance between signals at 1064nm and 1532nm is very long, over the experimental distances used of 40m and 10m there was no appreciable walk-off expected. However, because standard fibre is not single mode at 1064nm it was possible that there was distortion to the signal due to pulse break-up into higher-order fibre modes. Later experiments used a tunable source of pulses at around 1560nm with pulses of FWHM 10ps. Because of the constraints of the couplers used to combine and later separate the signal and modulating source it was not possible to tune the modulating source over a wide range. Hence the resulting pulse-width could not be optimised in terms of walk-off speeds between the two wavelengths, but again there was very little walk-off predicted over the distances involved, and so this was not seen as a limiting factor.

To allow the cavity length to be matched exactly with the repetition rate of the modulating source a rough approximation was made by inserting or removing fibre from a section between WDM4 and R2. The final adjustment was made using a fibre stretcher wound with 10m of standard fibre.

4.3 Experimental Aims

Initially, this experiment was planned to reproduce the previous results at a wavelength of 1.5μm, using erbium doped fibre to provide amplification, rather than the rare and expensive praseodymium doped fibre used in the previous work. The second part of the experiment was to propagate the resulting dark pulses over several soliton periods, to observe their behaviour in fibre as a means of determining the characteristics of the pulses as either odd or even, and hence as either soliton or non-soliton pulses. For this stage it would be necessary to produce pulses with a soliton period considerably shorter than the loss length of any fibre in which they were to be propagated, so that issues such as periodic amplification and spontaneous noise could be ignored.

The suitable fibres available for propagation were either 25km of dispersion shifted fibre with a dispersion of around 1ps/nm.km at 1550nm, or a 1km length of dispersion flattened fibre with a dispersion of 90ps/nm.km at all wavelengths around 1550nm. For the first fibre, this meant a maximum pulse width of less than 5ps would be necessary, and for the second fibre a maximum pulse width of less than 10ps. In each case, this would provide a propagation distance of 2.5 soliton periods.

If it proved impossible to achieve these pulse-widths, then alternative methods for determining the characteristics of the dark pulses would be explored. These would include varying the power, dispersion and wavelengths in the cavity, observing the effect on pulse formation of changes in each parameter.

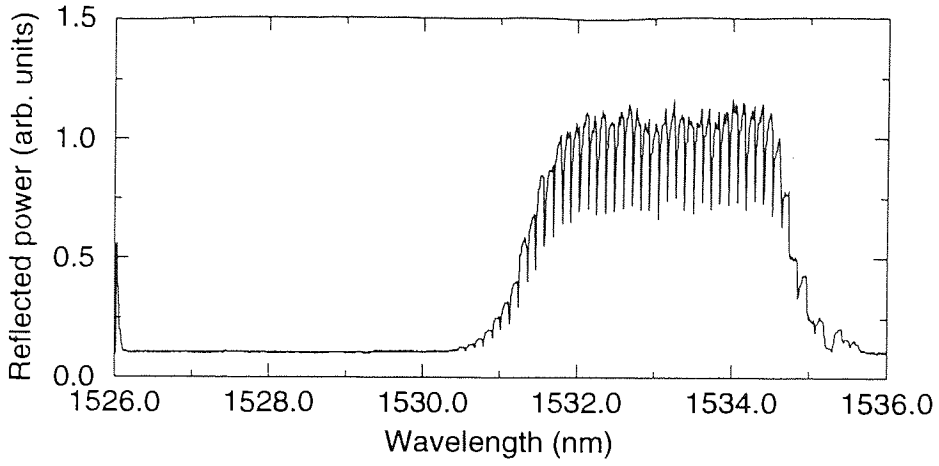

Figure 4.3: The reflection profile of the grating used in the preliminary experiments. (The fine structure in the profile is due to the measurement technique used, and is not a feature of the grating.)

4.4 Results

4.4.1 Preliminary characterisations.

The preliminary results were taken using 100ps pulses from the YAG to provide a mode-locking signal. The reflector R1 was an in-fibre grating with transmission and reflection profiles as shown in figures 4.3 and 4.4. This grating had a dispersion of approximately $\pm$20ps/nm, depending on orientation, with a peak wavelength centred around the peak of the erbium spectrum. Reflector R2 was a loop mirror (see section 1.3.2), using 40m of fibre in the first case. This was biased using polarisation controllers to reflect as much light as possible back into the cavity. The system as a whole proved to be remarkably stable with respect to polarisation effects, with very little adjustment being required to optimise the position of the various controllers.

As can be seen in figures 4.5 and 4.6 the preliminary results showed reasonable promise. The output of the laser was viewed using a sampling scope, initially using a signal from the YAG laser as a trigger. The pulses produced had a

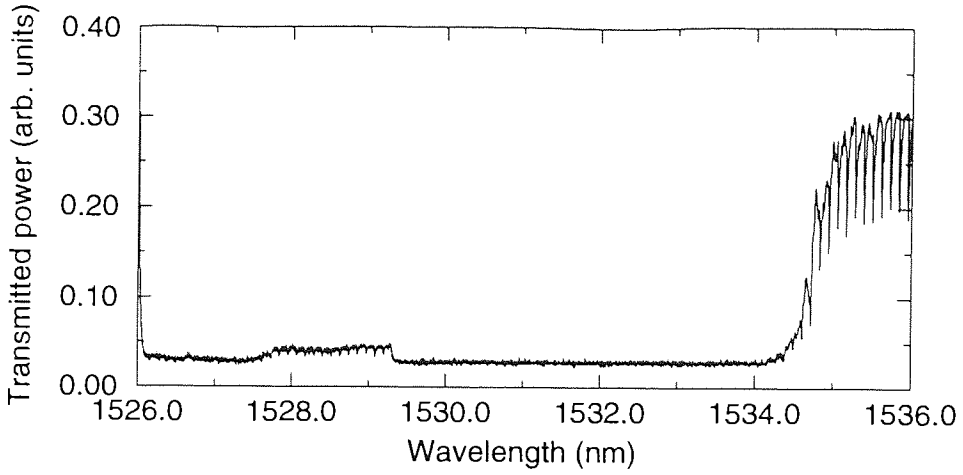

Figure 4.4: The transmission profile of the grating used in the preliminary experiments. The loss shown at short wavelengths was characteristic of the all the gratings used, but was not deemed a problem since only the reflected signal was of interest in this case.

contrast ratio of about 90%, and were of a good shape but with a full width at half the maximum depth of 250ps were too broad to be of any practical use. This pulse-width corresponds to a soliton period of approximately 25000km at a dispersion of 1ps/nm.km. Also, as figure 4.6 shows, extra pulses could be seen in between the main peaks. This would be undesirable in a source of pulses for communications.

The associated spectrum can be seen in figure 4.7. This is time averaged over ten readings and shows the laser hopping from one wavelength to another. The standard method for determining the cavity dispersion, by tuning through the full mode-locking range and observing the shift in signal wavelength could therefore not be used, and empirical methods had to be used to obtain an estimate for the dispersion. Given the very short lengths of fibre used in the cavity, the principle contribution to this came from the grating, with the standard fibre and erbium doped fibre adding less than 1ps/nm each to the total.

It was clear that using a 100ps pulse to provide cross-phase modulation for FM mode-locking would not result in dark pulses which had a pulse width of less

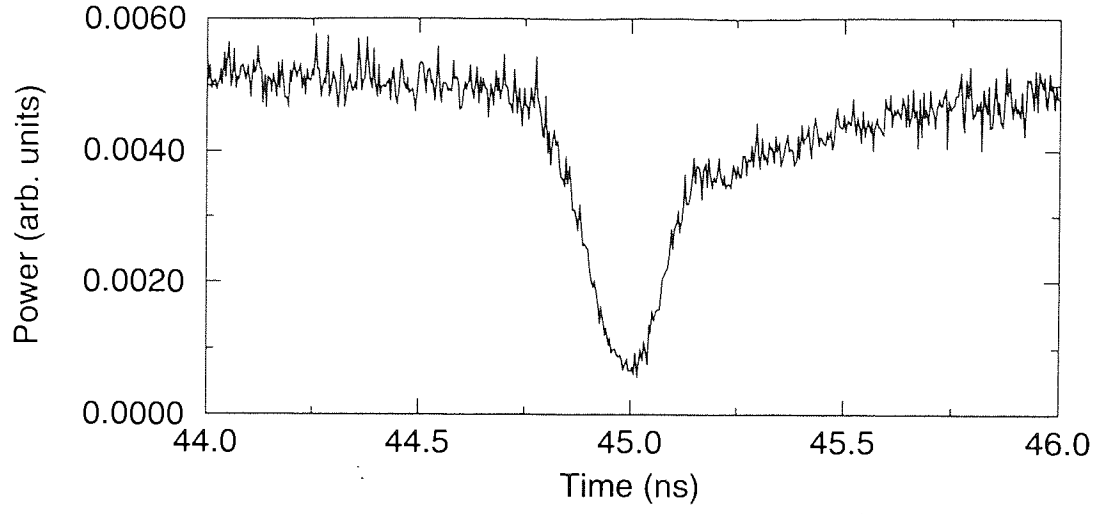

Figure 4.5: Preliminary results for dark pulse generation technique, showing main pulse only.

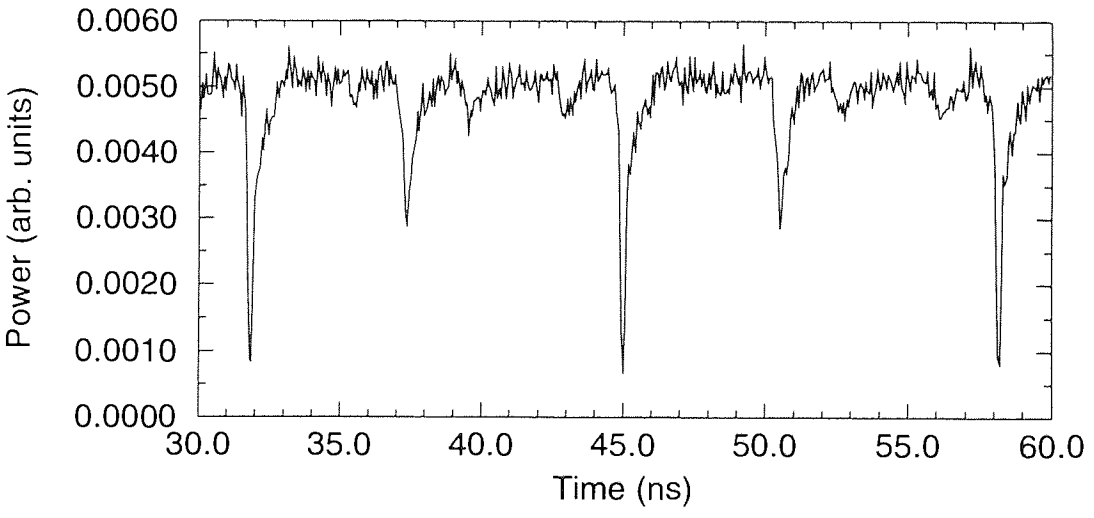

Figure 4.6: Preliminary results for dark pulse generation technique, showing two full mode-locking periods

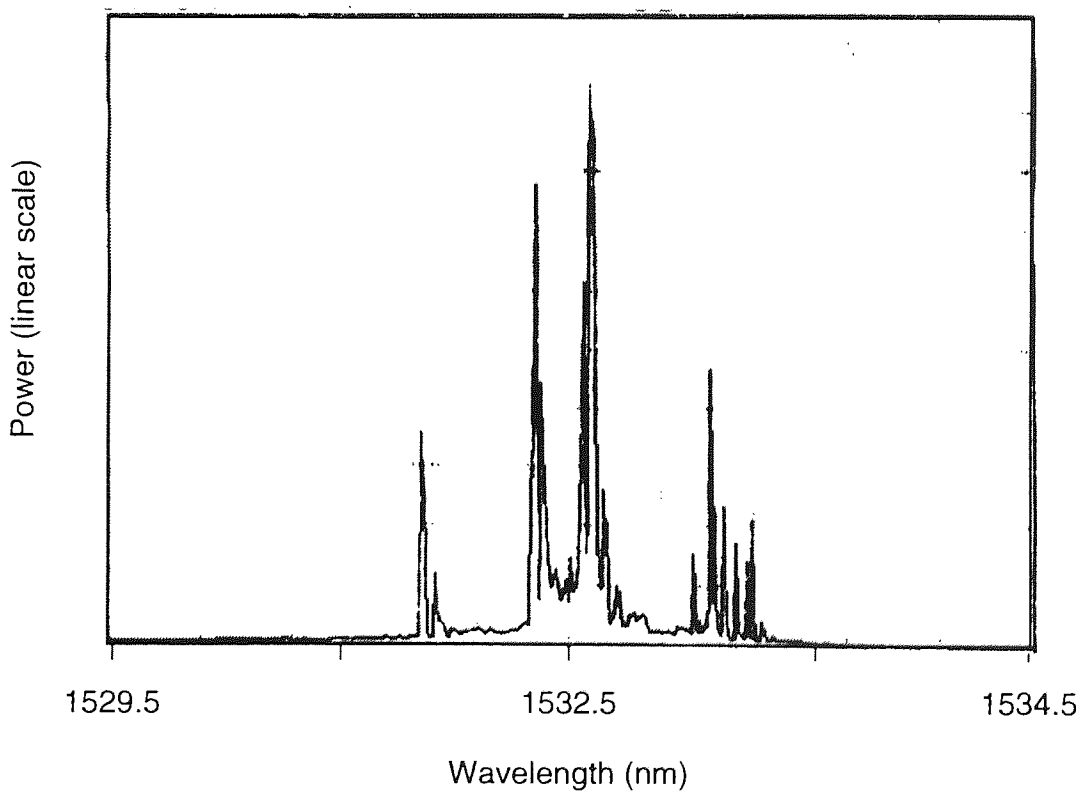

Figure 4.7: Optical spectrum associated with the pulses shown above, averaged over ten readings.

than 10ps. However, various other characteristics of the laser could be studied in this situation, with the advantage that direct measurement of the output pulse profile was possible. From the calculations above, the required pulse width for propagation would be approaching or less than the response time of the detectors available, making accurate characterisation difficult, and so it was decided to complete the first series of studies based on the YAG mode-locked system.

Recalling from section 1.3.2 that the phase shift induced on a signal at another wavelength by a pulse of the form $A(t) = U\,\mathrm{sech}(t)$ is

$$\phi(t) = U^2 \left[\frac{\tanh(t) - \tanh(t - \Delta\beta_1 L_i)}{\Delta\beta_1} \right] \qquad (4.1)$$

it can be seen that by varying the parameters U (the peak power of the mode-locking pulse) and L_i (the copropagation distance between the two signals) it should be possible to optimise the final pulse shape.

4.4.2 Changing power of mode-locking signal.

Figure 4.8 shows a series of pulse profiles taken with different strength mode-locking pulses. A low power signal will produce only a small amount of modulation (figure 4.8a), and increasing the power increases the depth of modulation. However, beyond a certain depth, no further increase is observed, and secondary modulation of the background develops. The pulses did not become significantly narrower for any modulator power.

Figure 4.9 shows the pulse profiles in a larger time window, showing the effect of varying the modulation on the depth of the subsidiary pulses. These may be observed at all powers, becoming deeper as the main pulses become deeper. They are not, then, a result of over-modulation.

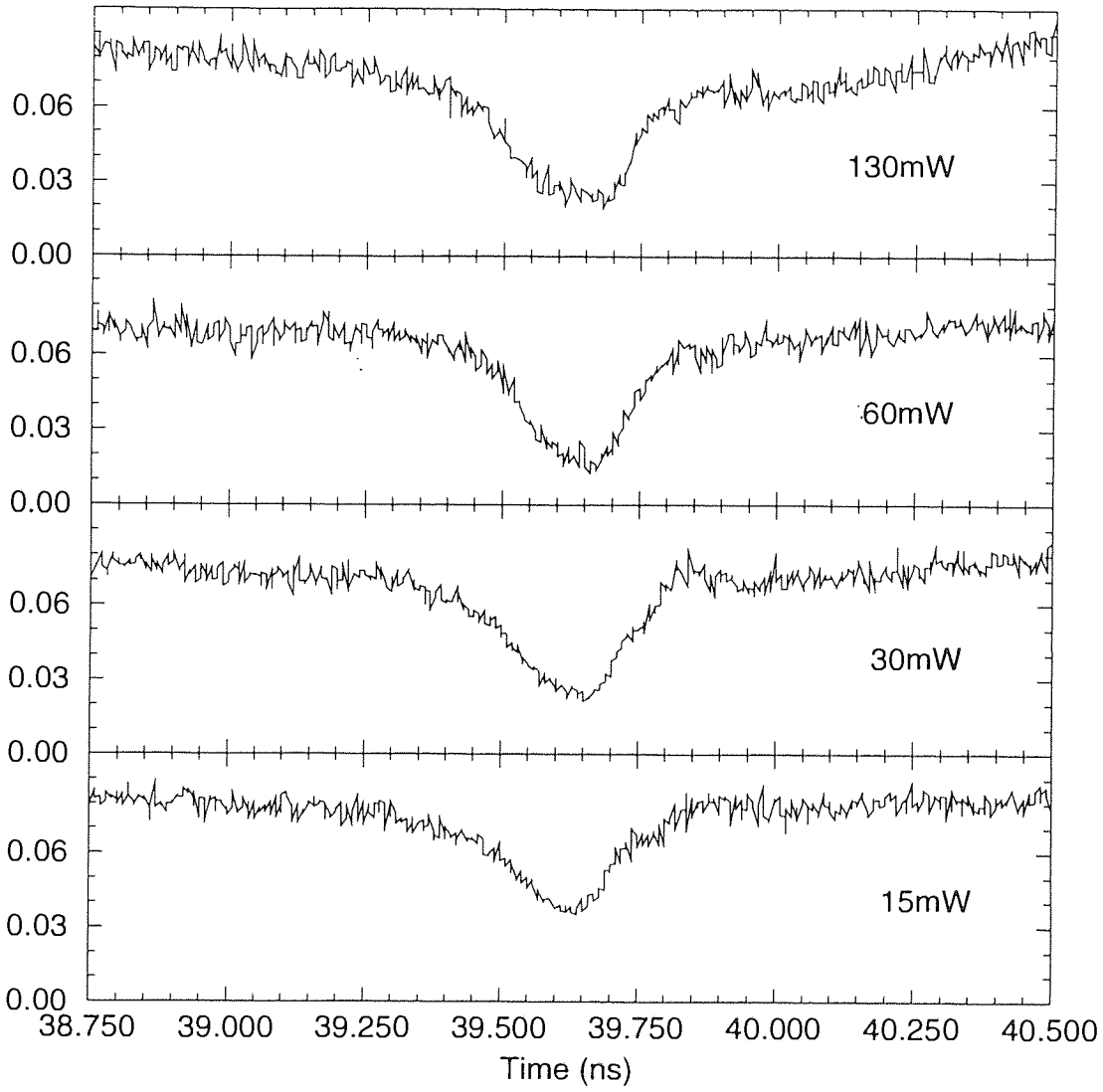

Figure 4.8: The effect of increasing the power in the mode-locking signal, showing main pulse only. The y-axis gives the power of the output signal in arbitrary units.

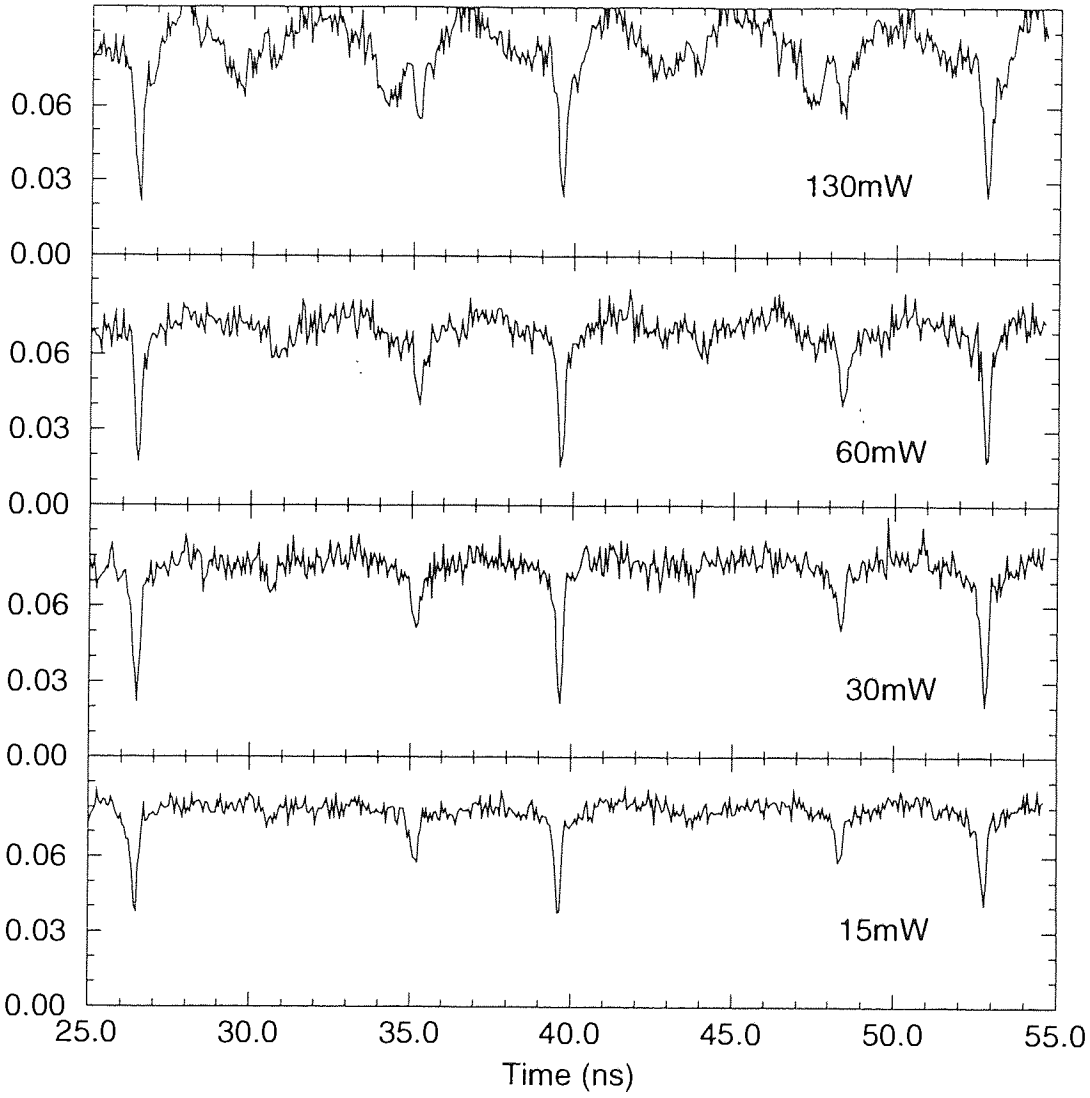

Figure 4.9: The effect of increasing the power in the mode-locking signal, showing two full modulation periods. Again, the y-axis gives the output signal power in arbitrary units.

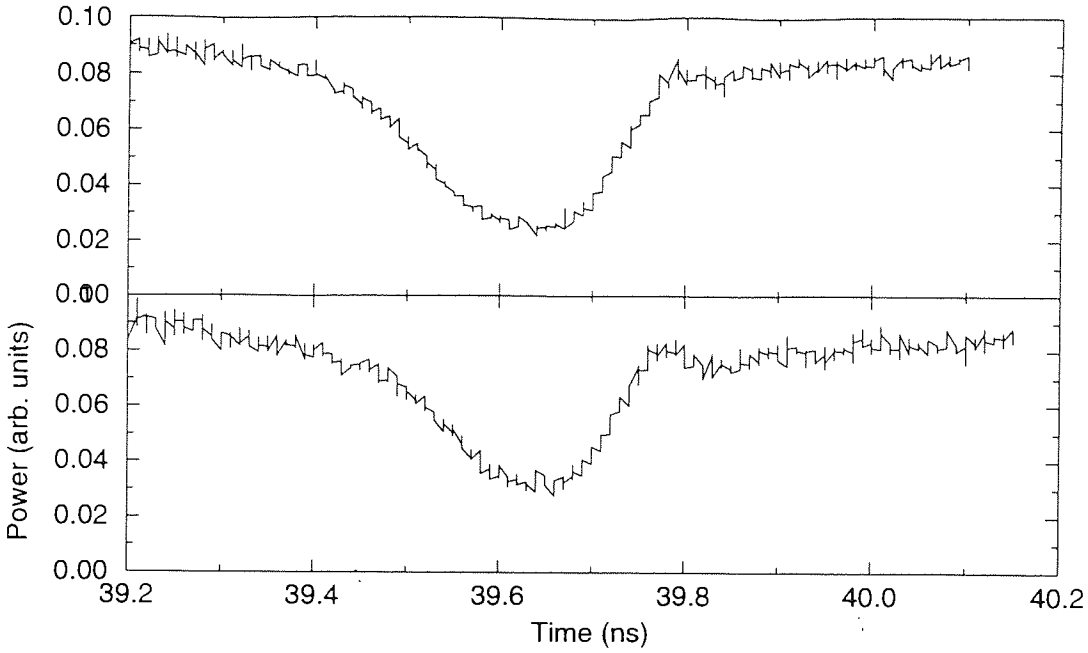

Figure 4.10: The pulse profiles produced with interaction lengths of 40m (upper trace) and 10m (lower trace).

4.4.3 Changing mode-locking distance.

A possible technique for narrowing the dark pulses produced would be to reduce the interaction length L_i, and providing an increase in peak pulse power to maintain the same total phase change. This should reduce the effects of any walk-off between the two copropagating signals. However, as mentioned earlier, the walk-off distance for signals propagating at the two wavelengths used here is reasonably large at 150m compared to the 10m and 40m of fibre used in the experiments and there was no significant decrease in pulse-width between interaction lengths of 40 and 10m (see figure 4.10).

This method might be expected to work better with a much smaller difference between the speeds of the two wavelengths, resulting in a walk-off distance several orders of magnitude larger than the co-propagation distance, guaranteeing that the pulse-shaping effects associated with walk-through were not involved.

This was a second motivation for switching to a different modulation source.

4.4.4 Changing cavity power.

Chapter 2.2 describes the propagation properties of odd dark pulses launched into fibre in the normal dispersion regime with a background power greater than that required to support a soliton of the same depth, and of appropriate width. Recall that this power is given by:

$$P_0 = \frac{|\beta_2|}{\gamma\tau^2} = \frac{3.11|\beta_2|}{\gamma T_{FWHM}^2} \tag{4.2}$$

Essentially, a number of secondary grey solitons will form symmetrically around the primary soliton, with the number determined by the difference between the power to support one soliton and the power available. The central pulse will narrow until the ratio between its width and depth corresponds to that of a soliton. Assuming the dark pulses observed were solitons, any variation in the cavity power should be reflected in a change in output pulse profile.

There were two methods available to change the power in the laser cavity. The overall power in the system could be increased by increasing the signal from the Titanium-sapphire laser pumping the erbium amplifier, or the output coupler could be replaced by one with a larger coupling ratio, thus increasing the intensity of light within the cavity itself, at the expense of output power. Since the output powers available were well in excess of what the the detection equipment could safely be exposed to, this was not a difficulty.

Figure 4.11 shows the form of the output pulses for a wide range of output powers (note the scales on the axes differ by an order of magnitude). There is no significant difference between the four traces, suggesting that the pulse is not affected by any self-induced nonlinear shaping.

Changing the output coupling ratio was similarly unconstructive, with little

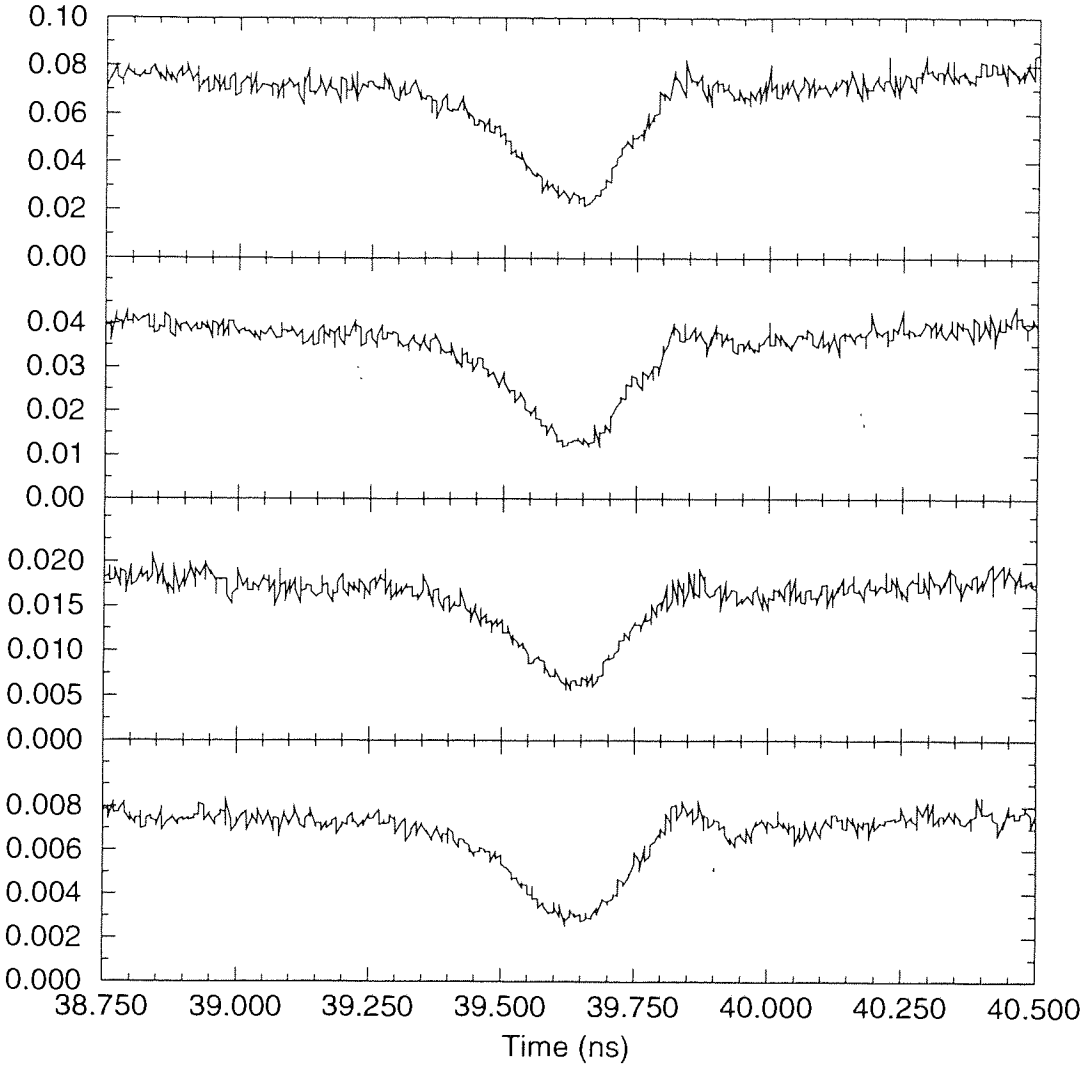

Figure 4.11: The pulse profiles observed with various pump powers. The scales on the y-axes give the relative powers, the value 0.1 corresponding to 8mW of signal power. There is very little change in pulse profile, for a range over powers extending for an order of magnitude.

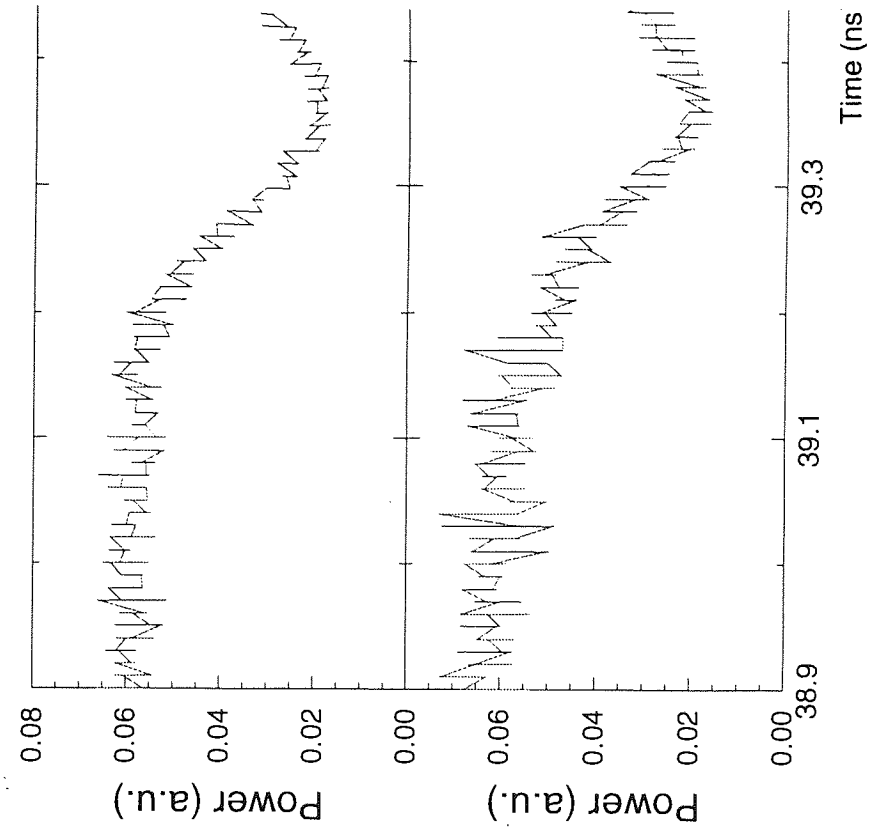

Figure 4.12: The pulse profiles with output coupler ratios of 90/10 (upper trace) and 80/20 (lower trace).

difference observable other than in total power output (see figure 4.12).

4.4.5 Laser stability over extended periods of time.

An advantage of fibre lasers over conventional bulk lasers is that the cavity is entirely enclosed, eliminating problems of dust and humidity, as well as the accidental misalignment of cavity components. working with the fibre laser discussed here over a period of months provided ample opportunity to observe the stability and reliability or otherwise of the cavity.

The only noticeably sensitive feature was the total cavity length (adjustable using the fibre stretcher located between the gain medium and the mode-locking section of the laser), which required very slight adjustments over the course of a day to maintain a symmetrical output pulse profile. This can be accounted for by the temperature sensitivity of the fibre, the total length change was never

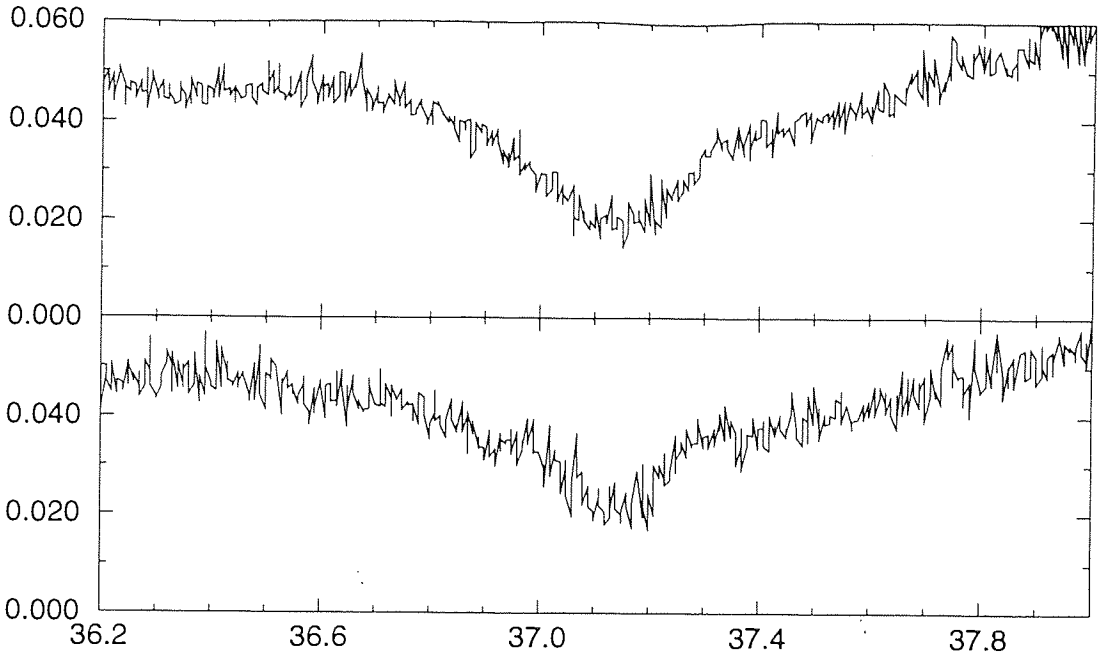

Figure 4.13: The pulse profiles observed with two different gratings (and hence different cavity dispersions) used as the end reflector R1.

greater than a few tens of micrometres.

4.4.6 Changing cavity dispersion.

The main contribution to cavity dispersion was due to the fibre grating, and so by changing the grating it was possible to study the cavity with a range of different total dispersions. The range over which the system remained mode-locked was too narrow to allow the cavity dispersion to be calculated directly, and so the total dispersion with any grating was assumed to be that of the grating. As discussed earlier the comparitive shortness of the cavity meant that the contributions to dispersion from the difference fibre elements were less than 1ps/nm in each case.

From equation 4.2 it can be seen that the power required to support a funda-

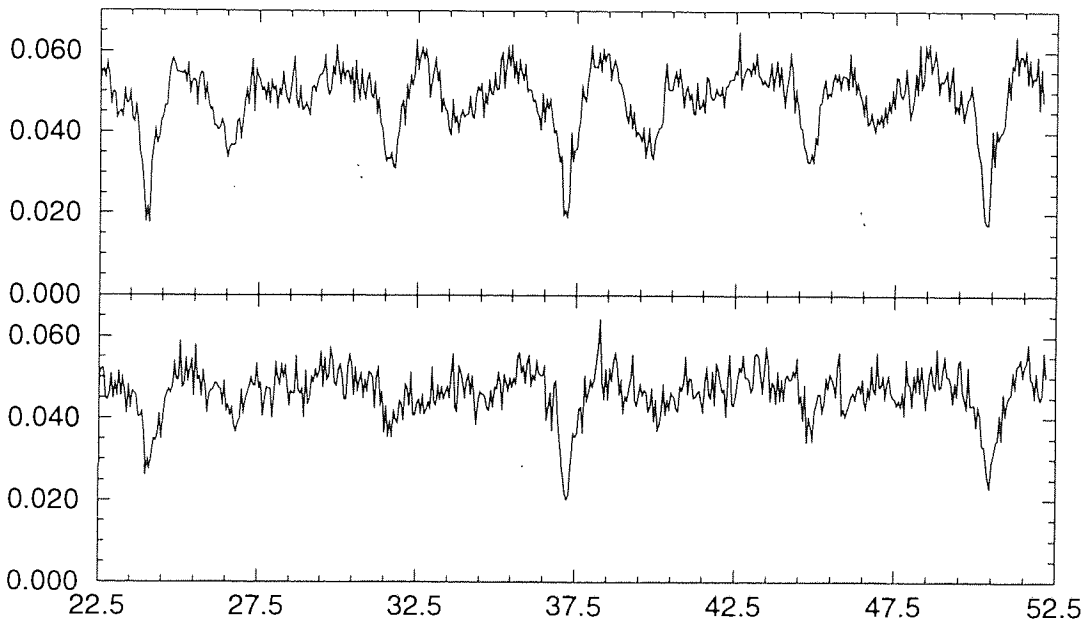

Figure 4.14: The pulse profiles as shown in figure 4.13 shown in a larger time window. Notice the position of the sub-pulses has not changed, despite significant changes to the cavity.

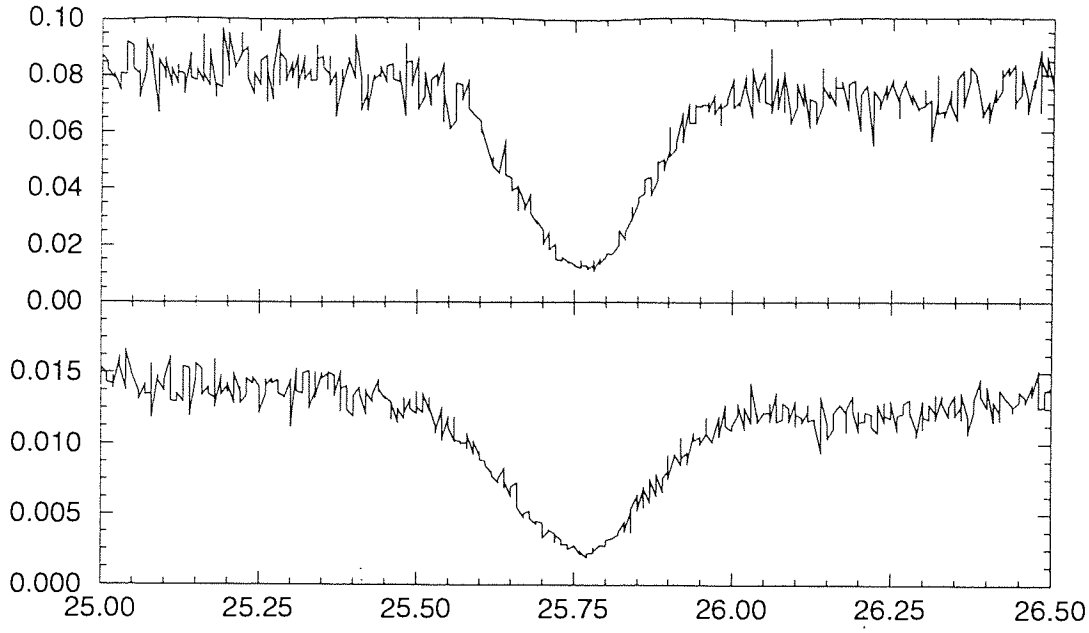

Figure 4.15: The pulse profiles observed with the output coupler placed before (upper trace) and after the grating(lower trace). Note the difference in scale on the power axis.

mental dark soliton is a function of system dispersion. It would therefore be expected that soliton formation within the cavity would be affected by a change in dispersion, with the pulses becoming broader or narrower accordingly. As the results in figures 4.13 and 4.14 show, this was not the case, once more casting doubts on the soliton-like nature of the generated pulses.

4.4.7 Changing position of output coupler

The original cavity structure placed the output coupler before the grating. Since the grating might reasonably be expected to have a significant effect on pulse shape, data was taken with the output coupler placed, instead, following the grating. Figures 4.15 and 4.16 show the pulse profiles with the output coupler positioned before and after the grating. Other than the difference in output

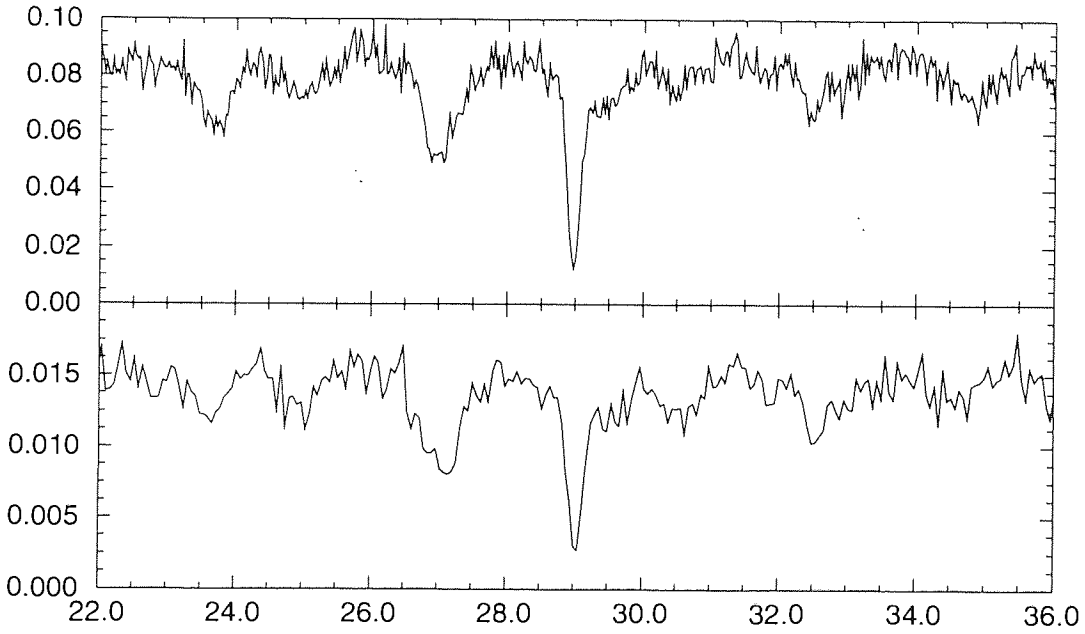

Figure 4.16: The pulse profiles as shown in figure 4.16 shown in a larger time window. The shapes are almost identical, and again, the position of the subpulses has not changed, despite significant changes to the cavity.

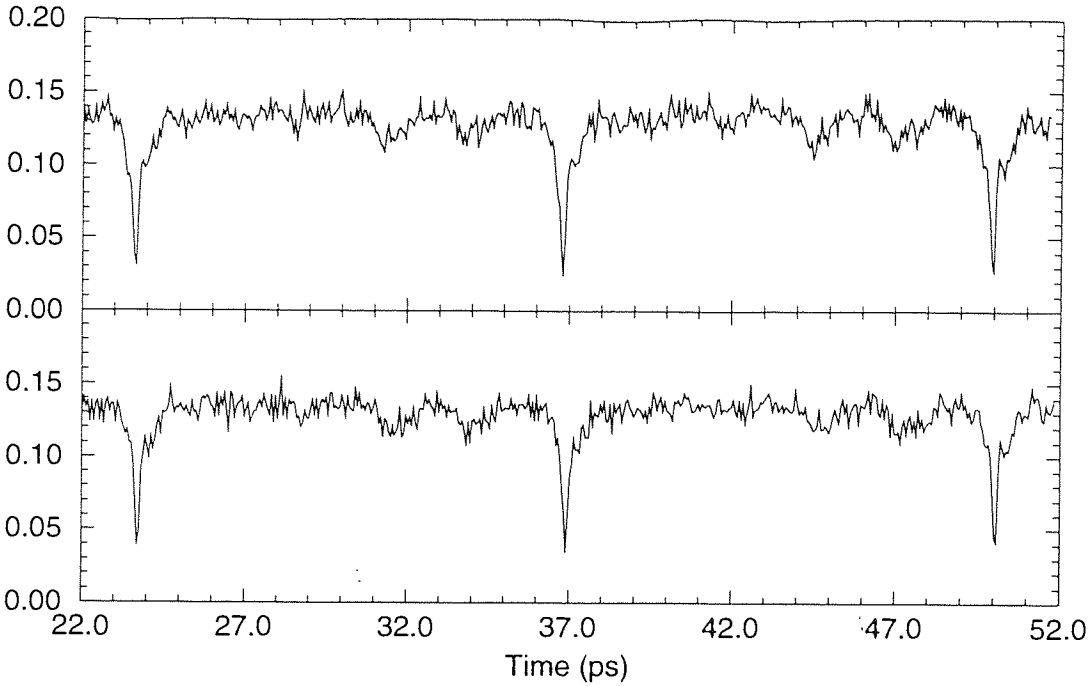

Figure 4.17: The pulse profiles before and after increases the cavity length by 5m. The position of the sub-pulses has not varied between the two systems.

power due to the orientation of the coupler, there was no obvious difference in the pulse profiles.

4.4.8 Changing large-scale cavity length

Identifying the source of the sub-pulses appearing between the main dark pulses proved to be a difficult task. There were observed to vary from day to day, but not as a result of changing the cavity power, the mode-locking power, the orientation of the gratings or the output coupler, the interaction length over which mode-locking occurred or due to the small changes in cavity when elements of the laser were removed and replaced, with the attendant changes in splices, cavity length etc. A final possibility was to change the large-scale cavity length, adding and extra 5m to the 30m of fibre which made up the laser.

Figure 4.17 shows the results of this experiment. There is no significant change in either the positions or the depths of the sub-pulses. It remained possible that the pulses were due to deformation of the mode-locking pulse signal, since the fibre in the cavity was not single-mode at the YAG wavelength. If this was the case, then switching to a different mode-locking signal should eliminate the problem.

4.4.9 Reducing modulating pulse-width.

There remained at this point only one possible technique for reducing the width of the dark pulses to a width more suitable for the propagation experiments planned, this being to reduce the width of the modulation window shaping the pulses. This window was created by cross-phase modulation with the bright pulse copropagating with the cw signal.

The modulation source was therefore changed from the 100ps pulse YAG laser operating at 1064nm to a colour centre laser (FCL) producing 8ps pulses at a wavelength of 1560nm. The choice of wavelength was determined by the availability of the wavelength selective couplers required to insert and remove the FCL pulses. These operated over a very narrow range, and so it was not possible to take advantage of the the large tuning range of the FCL to exploit the variation between walk-off rates at different wavelengths.

Figures 4.18and 4.19 show the pulse profiles obtained using 8ps pulses to provide a mode-locking signal. The width of the output pulses was reduced only to 100ps, which was still considerably longer than what would be required for any propagation experiments.

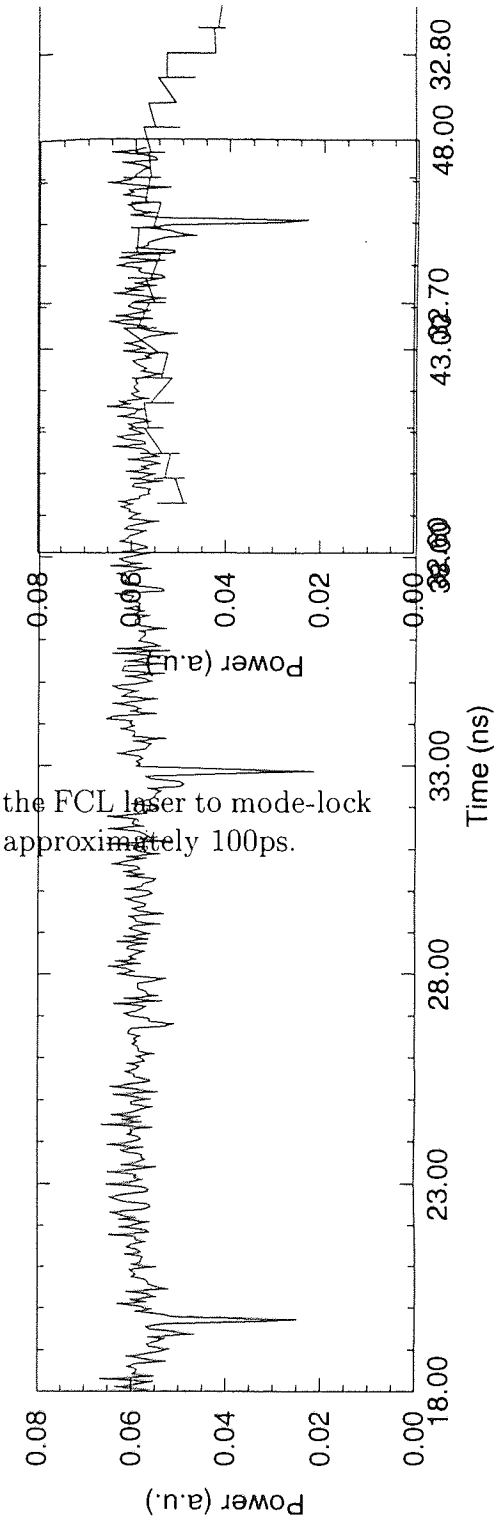

Figure 4.18: The pulse profiles using 8ps pulses from the FCL laser to mode-lock the cavity. The output pulse width at half depth is approximately 100ps.

Figure 4.19: The pulse profiles using 8ps pulses from the FCL laser to mode-lock the cavity, shown in a larger time window.

4.5 Conclusions.

Although it was not possible to study the behaviour of the dark pulses during propagation in fibre, there are several other indications in the work described above which suggest these pulses are not, in fact, dark solitons. One of the principle objections to this theory is that changing the background power by an order of magnitude does not produce any significant difference in either pulse width or number of dark pulses observed per round trip. As discussed in section 2.2, an odd dark pulse launched with greater background power than would be required for a dark soliton of that width will narrow, with the formation of symmetrically arranged grey solitons to each side. If the pulses were forming in the cavity as a result of nonlinear pulse shaping (other than via cross-phase modulation with the external pulse source) then it would be expected that changing the cavity power by a factor of ten would have a dramatic effect on the resulting pulse profiles.

In addition, changing the cavity dispersion would be expected to have a significant effect on any nonlinear pulse-shaping that was occurring, and none of the experimental work gave any indication that this was so.

However, the pulses produced by this configuration were remarkably stable in the face of large-scale changes to cavity dispersion, length, pump power and wavelength and pulse-width of the mode-locking signal. Fibre lasers are in general considered to be stable pulse sources, and this would appear to be particularly true in this case. Such a reliable source would lend itself well to dark soliton generation via the imposition of a suitable phase profile on a pregenerated dark pulse.

Chapter 5

Sideband formation in dark soliton systems.

Pulse propagation in real transmission lines is affected by many different mechanisms. In addition to the standard problems of loss and dispersion it is also important to consider the effect of any periodic perturbation the signal experiences during propagation. A prime example of this would be the disturbance caused by gradual loss followed by lumped gain in a transatlantic system, which contains many evenly spaced amplifiers.

This disturbance has been shown for both bright solitons and cw signals to cause the development of spectral sidebands, which gradually swamp the signal in the time domain. The phenomenon has also been observed in laser cavities, where the signal periodically experiences discrete loss at the output coupler followed by gain within the lasing medium.

This chapter discusses the effect on dark solitons of propagation in the presence of such periodic power variation, showing how it is essential to consider not only the response of the pulses but also the behaviour of the supporting background

when analysing the system[61].

5.1 The response of bright solitons to periodic perturbation.

Various studies, for example [62], have been made of the behaviour of bright solitons in a system which suffers periodic loss and amplification. This can either be in the form of gradual loss and lumped gain, such as would be experienced in a transmission line, or lumped loss and continuous gain in a laser cavity.

Taking the case of transmission lines with amplifiers at fixed intervals across the link, the problem arises because the amplification provided at the end of each stage is not adiabatic, that is, the pulse does not maintain a constant relationship between width and height. To propagate as a soliton, the amplified bright pulse must reform, becoming narrower and increasing in peak power. A combination of this plus the gradual loss experienced due to propagation in a fibre means that the soliton is continually reforming, shedding energy into low amplitude dispersive waves at all frequencies during every amplification period.

Those dispersive waves which are phase-matched to the soliton will interfere constructively with similar waves shed in earlier cycles, resulting in the development of sidebands which grow linearly with distance. Their separation $\Delta\omega$ from the main spectral peak was shown by Smith *et al.* [62] to be:

$$\Delta\omega = \pm\frac{1}{\tau}\sqrt{\left\{\frac{4m\pi}{z_a} - 1\right\}} \tag{5.1}$$

where the pulse has full width at half maximum intensity of 1.76τ, z_a is the amplifier spacing normalised to the soliton period and m is an integer.

The power transfered from the soliton to the sidebands becomes more significant as the spacing between amplifiers is increased. This then represents a limit on

the transmission system design in terms of amplifier spacing (or pulse width) for stable bright soliton propagation. Since the fibre parameters and amplifier spacings in a real system are rarely so uniform, the narrow bandwidth of the process may mean that the sidebands are washed out to some extent, and so this may not be a major problem for system designers. However, the same equations can be applied to a laser cavity, where the solitons experience periodic lumped gain and loss. In this case, the periodicity of the perturbation will be exactly uniform, and the effect is of some importance.

5.2 The response of a CW signal to periodic perturbation.

Matera *et al* demonstrated[63] that for both normal and anomalous dispersion, the periodic power variation of a cw signal can provide the phase matching required for a four-wave mixing process to occur (see section 1.3.3). This results in noise-seeded spectral sidebands which grow exponentially with distance.

It was shown that the positions of the spectral sidebands, relative to the central peak, are given by:

$$\Delta\Omega_p = \pm\sqrt{\left\{-\frac{2\pi p}{\beta_2 l} - \frac{2\gamma P_0 c_o}{\beta_2}\right\}} \tag{5.2}$$

where p is an integer, P_0c_0 is the average cw power and γ is the nonlinear coefficient defined by equation 1.13.

Although the bright soliton sidebands have the same origin in periodic perturbation, their nature is completely different, the key feature being that the soliton sidebands result from a resonant process, and increase linearly, whereas in the cw case the process is parametric. It should also be noted here that for large pulse widths, the bright soliton resonances have the same frequency as

the cw sidebands for even p. There are no soliton resonances at the frequencies defined by odd p.

5.3 The response of dark solitons to periodic perturbation.

The only previous studies of the amplification of dark solitons used stimulated Raman scattering to provide gain [23], [64]. This gain is a gradual process, and so might be expected to produce less disturbance. In [23] it was observed that increasing the amplification period beyond the dark soliton period resulted in unstable propagation, but the reasons for this were not investigated.

When considering the response of dark solitons to periodic perturbation it is necessary to consider the response of both the soliton and the bright background which supports it. The original analysis which follows shows how the four-wave mixing process described above for a cw signal affects the resonant sidebands produced by the perturbations to the dark soliton, and also the effect of the large cw signal on the phase of the dispersive radiation shed by the soliton.

We consider here the behaviour of the fundamental, or black soliton. The mechanisms involved in sideband generation are equally applicable to grey solitons, although the positions of the sidebands will be different.

A black soliton of FWHM 1.76τ can be seen from equation 1.36 to have phase ϕ varying with distance at twice the rate of the bright soliton phase, thus:

$$\phi = \frac{\mid \ddot{\beta} \mid Z}{\tau^2} \tag{5.3}$$

where Z is the distance in real units.

In a similar manner to bright solitons, periodic amplification and loss will pro-

duce a continuous source of frequency components outside the dark soliton spectrum. These are produced coherently with the soliton, but have different group velocities and so will experience different phase shifts over one amplifier spacing. During repeated cycles, particular frequencies will experience either constructive or destructive interference, depending on their group velocity (and hence phase rotation) relative to the amplifier spacing. It is the constructive interference which results in sideband formation, which will be observed at those wavelengths where the following phase-matching criterion is satisfied:

$$\psi(Z_A) - \phi(Z_A) = 2m\pi \tag{5.4}$$

where m is an integer and Z_A is the amplifier spacing in real units.

It is therefore necessary to determine $\psi(Z_A)$, the phase of an arbitrary low amplitude dispersive component after propagation over one amplification period. Such dispersive waves propagate in the presence of a large cw background and so will have a phase altered via cross phase modulation. Both components of the field must be taken into account when calculating the phase of the dispersive waves shed at any point.

We begin with the ansatz:

$$A = A_{cw}e^{i(\omega t - k_0 z)} + A_{ds}e^{iz\beta_2/\tau^2} \tag{5.5}$$

where A_{cw} and A_{ds} are the amplitudes of the cw and dark soliton parts of the total field, and k_0 is the wave vector associated with the cw field, for which we require a value in terms of β_2, ω and τ. To find this we substitute the ansatz into the Nonlinear Schroedinger Equation, to obtain an exact solution.

Recall that the NLS in the normal dispersion regime has the form:

$$i\frac{\partial A}{\partial z} = \beta_2 \frac{1}{2}\frac{\partial^2 A}{\partial t^2} - \gamma|A|^2 A \tag{5.6}$$

(See section 1.4.1 for more details.)

Let $a = (\omega t - k_o z)$ and let $b = z\beta_2/\tau^2$. Then we find the following variations of the field with propagation distance z and time t as:

$$\frac{\partial A}{\partial z} = -ik_o A_{cw} e^{ia} + \frac{i\beta_2}{\tau^2} A_{ds} e^{ib} \frac{\partial^2 A}{\partial t^2} = (i\omega)^2 A_{cw} e^{ia} \tag{5.7}$$

We assume A_{cw} is small, and so higher order terms may be neglected. This gives:

$$|A|^2 A = A_{cw} A_{ds}^2 e^{ia} + A_{cw} A_{ds}^2 (e^{ia} + e^{-ia} e^{i2b}) \tag{5.8}$$

The substitution is then straightforward.

$$k_0 A_{cw} e^{ia} - \frac{\beta_2}{\tau^2} A_{ds} e^{ib} = \frac{-\beta_2}{2} \omega^2 A_{cw} e^{ia} - 2\gamma A_{cw} e^{ia} A_{ds}^2 e^{ia} - \gamma A_{cw} A_{ds}^2 e^{-ia} e^{i2b} - \gamma A_{ds}^3 e^{ib} \tag{5.9}$$

Assuming the background field is sufficient to support a black, or fundamental dark soliton of pulse FWHM 1.76τ, that is that $P_0 = |\beta_2|/\gamma\tau^2$, we may make the substitution $A_{ds}^2 = |\beta_2|/\gamma\tau^2$. The remaining terms in A_{ds} cancel, and dividing through by A_{cw} gives:

$$k_0 e^{ia} = -\frac{\beta_2}{2} \omega^2 e^{ia} - 2\frac{\beta_2}{\tau^2} e^{ia} - \frac{\beta_2}{\tau^2} e^{-ia} e^{i2b} \tag{5.10}$$

To obtain the phase of the cw portion of the field, we retain those terms in e^{ia}, which produces the following expression for k_0:

$$k_0 = -\frac{\beta_2}{2} \omega^2 - 2\frac{\beta_2}{\tau^2} \tag{5.11}$$

The resulting phase of the dispersive wave with frequency offset $\Delta\omega$ at a distance Z will be:

$$\psi = \frac{\beta_2 \Delta\omega^2 Z}{2} + \frac{2 \mid \beta_2 \mid Z}{\tau^2} \tag{5.12}$$

The first term of equation 5.12 is the phase of the linear wave solution to the NLS in the absence of loss and nonlinearity. The second term includes the effect on the wave phase of cross phase modulation with the cw background supporting the black soliton.

Substituting (5.3) and (5.12) into (5.4) leads to the following expression for the sidebands' frequencies:

$$\omega = \sqrt{\frac{4m\pi}{|\beta_2| Z_A} - \frac{2}{\tau^2}} \tag{5.13}$$

For large τ this approximates to the same values expected for the equivalent bright soliton, despite the cross-phase modulation term. It could therefore be expected that the sidebands produced by bright and dark solitons would be the same.

However, as was discussed previously, the periodic amplifier structure can phase-match a four-wave mixing process with the cw background, providing parametric gain at certain frequencies.[63] Using the results of Matera *et al.*[63] for a cw signal of power P_0 and assuming that the background is supporting a black soliton as above, that is $P_0 = |\beta_2|/\gamma\tau^2$, we obtain the following expression for the frequencies of maximum gain due to this process:

$$\omega = \sqrt{\frac{2p\pi}{|\beta_2| Z_A} - \frac{2}{\tau^2}} \tag{5.14}$$

where p is an integer.

Comparison of equations 5.13 and 5.14 shows that the spectral positions of resonant loss from the solitons are a subset of those positions where parametric gain occurs. The dark soliton sidebands therefore grow exponentially, the linear growth of the resonant sidebands seeding the parametric gain. In addition,

sidebands will develop at the wavelengths for which p in equation 5.14 is odd, as a result of the large gain from the four-wave mixing process acting upon the dark soliton spectrum.

In the discussions which follow, the sidebands which occur at a point of resonance between the soliton and dispersive waves will be referred to as the resonant sidebands, while those which occur for odd p will be referred to as cw sidebands. This is for convenience only, since the names are an oversimplification of the mechanisms involved in each case.

5.4 Simulations of sideband formation.

To examine in more detail the behaviour predicted by the analytical description given above, a series of numerical simulations were performed, and the temporal and spectral responses of the solitons observed. The numerical demonstration of dark soliton sideband formation used the split-step Fourier method to describe pulse propagation (see section 1.5), initially ignoring the effects of amplifier noise, Raman terms, third order dispersion and shock. Once the behaviour of the simple system was understood, noise was added as the next most significant effect likely to alter propagation.

The simulations studied pairs of black solitons, to avoid boundary problems with the dark soliton phase shift. The initial background amplitude in each case was scaled to the power defined by the Average Soliton Model for optimum propagation of the fundamental soliton (see section 1.4.2). A distance of fifty amplifier spacings was arbitrarily decided upon, and the model run repeatedly with different values for amplifier spacing.

We observed exponential sideband growth at the frequencies predicted by both equations 5.13 and 5.14. Over amplifier spacings which were short compared

to the dark soliton period, no sidebands were observed and the dark solitons propagated without corruption for fifty amplification periods. As the amplifier spacing was increased, it became possible to locate sidebands in those positions where a region of parametric gain coincided with a dark soliton resonance point, ie at the frequencies given by equation 5.14 for even p. With further increases sidebands were also observed at those frequencies predicted by equation 5.14 for odd p.

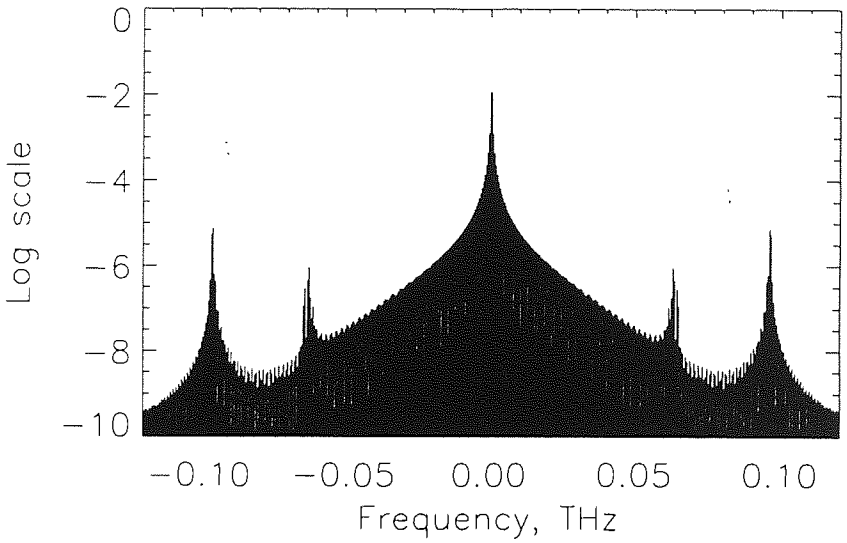

Figure 5.1: Spectrum of a pair of 10ps dark solitons after propagation over fifty amplifier spacings of 25km, with a system dispersion of -1ps/nm.km, central wavelength of 1.5μm, fibre loss of 0.2dB/km. The dark soliton period associated with these system parameters is 42.3km. Note the relative heights of the centre-most (cw) and second (resonant) sidebands.

This form of behaviour has been illustrated using a pair of 10ps FWHM black solitons, at a dispersion of -1ps/nm.km, central wavelength of 1.5μm, fibre loss of 0.2dB/km and amplifier spacing of 25km. The dark soliton period associated with these system parameters is 42.3km.

Figure 5.1 shows the spectrum following propagation over fifty amplification periods. Here both the first four-wave mixing sidebands and the first resonant sidebands can be seen, with the latter dominating. (The low frequency beating

in the spectrum is due to the presence of two pulses in the time window.)

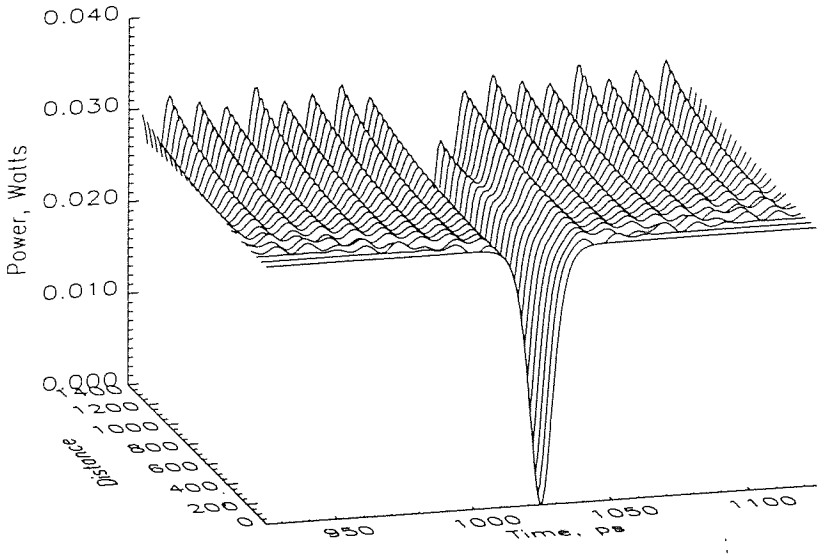

Figure 5.2: Evolution of the 10ps black soliton being re-amplified every 25km. Note the 10ps period of the modulation, corresponding to the first resonant sideband at 0.1THz, and the appearance of a secondary modulation towards the end of the propagation, due to the later development of the first cw sideband.

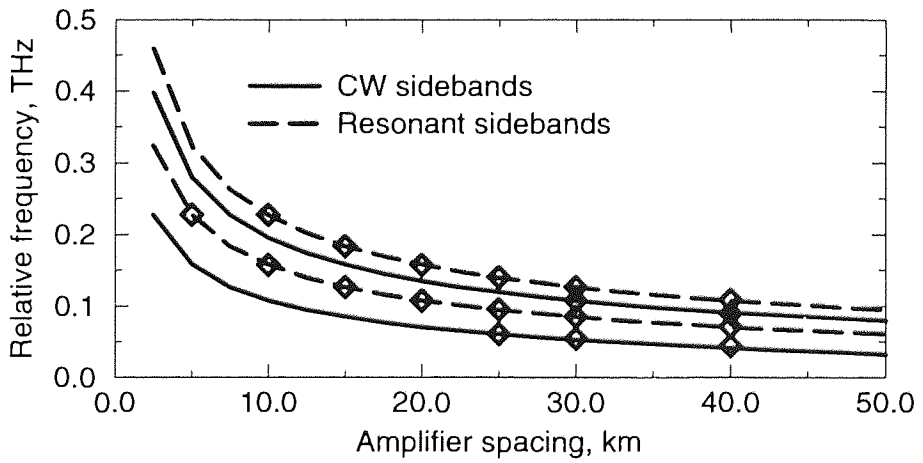

Figure 5.3: Position relative to the central frequency of any sidebands clearly distinguishable from background noise after propagation over fifty amplifier periods, for a variety of amplifier spacings. Numerical results shown with diamonds. The solid and dashed lines show the positions predicted by theory for the first four sidebands.

Figure 5.2 shows the effect of this sideband growth in the temporal domain. The growth of the sidebands at 0.1THz is clearly visible as a modulation with a

period of 10ps, with the increasing importance of the second spectral component appearing as additional modulation near the end of the propagation.

Figure 5.3 shows the agreement between predicted results and sideband positions observed in simulation, showing clearly the domination of the resonant dark soliton sidebands at short amplifier spacing. For each amplifier spacing, the resonant sidebands appear long before the noise-seeded cw sidebands. The solitons were in each case propagated over fifty amplification periods, at a pulse separation sufficient that the effects of soliton-soliton interaction over the system length could be ignored.

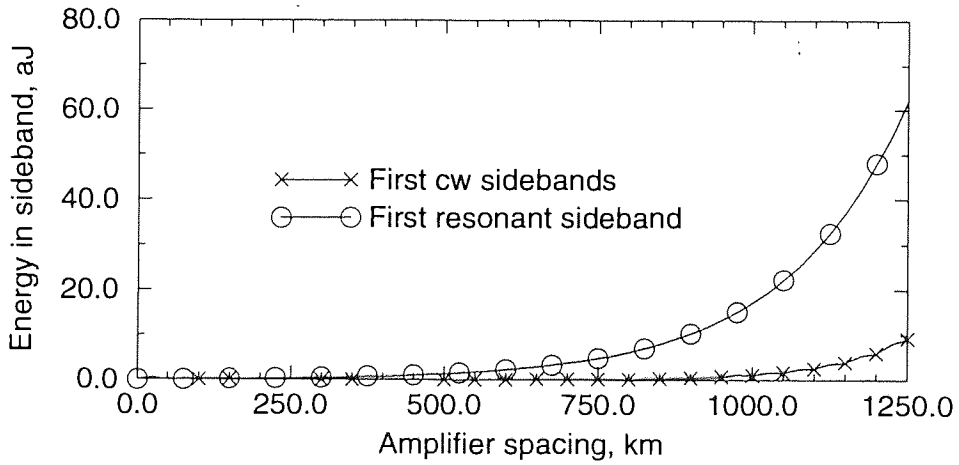

Figure 5.4: Energy transferred from the soliton spectrum into the first two sidebands, for the system defined in figure 4.1.

The width of the sidebands agreed well with the four-wave mixing gain bandwidth given by Matera *et al.*[63] for each frequency component. Using these values, it was possible to define a region within the spectral window around each sideband and observe the variation of energy at the predicted sideband position. Figure 5.4 shows the values obtained over a propagation distance of 50 amplifiers spaced at a separation of 25km for the first two sidebands, showing clearly both the domination of the first resonant sideband, and also the exponential growth exhibited by both.

5.5 Comparison with bright solitons.

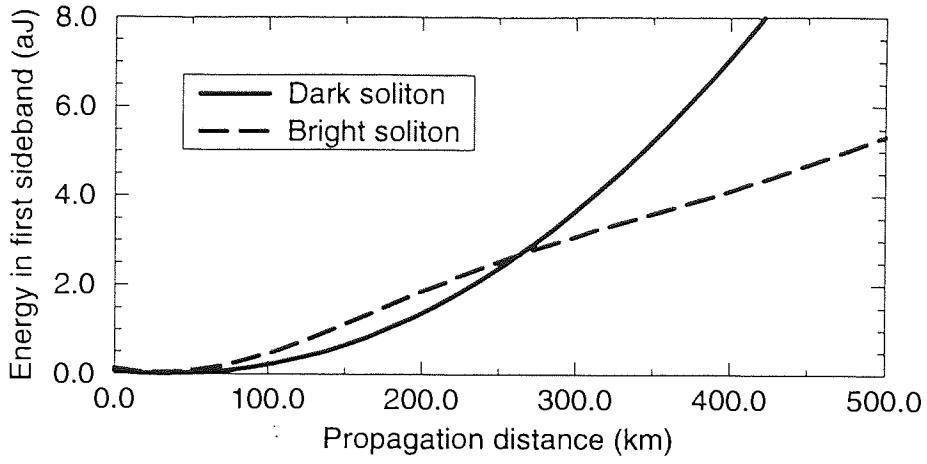

Figure 5.5: A comparison of the energy transferred into the first significant sideband for equivalent bright and dark solitons.

An interesting comparison may be made between bright and dark solitons when periodically amplified in this manner, by comparing the energy transferred into the sidebands of each pulse over systems with equal dispersion in the normal and anomalous dispersion regimes. Figure 5.5 shows how the energy transferred into the first significant sideband increases with distance in the case of fundamental bright and dark solitons of equal pulse width. The other sidebands associated with the bright and dark solitons were all less than 0.1% of the spectral intensity of the first sideband, and so have been neglected in this comparison.

Although the exponential growth of the dark soliton sidebands ultimately overtakes the linear growth of the bright soliton sidebands, the dark soliton system loses less energy from the soliton into sidebands over the first fifteen amplification periods. The precise location of the crossover point will of course vary with system parameters. In general it can be said that once the limits of the average soliton model are exceeded dark solitons are only more stable with respect to this perturbation over short amplifier chains.

The amplifier spacing was the same (15km) in each, a deliberate choice being made to use real units, rather than units normalised to the soliton period. It may be argued that this comparison is invalid, since the normalising length scale of the soliton period is different for bright and dark solitons of the same pulse-width and soliton number propagating in fibre with the same $|\beta_2|$. At this point, the reasons for making such comparisons must be considered, with likely possibilities being the cost in terms of equipment for bright and dark soliton systems. In this case, the system length must be in real units, and so the only results which are relevant are those which deal with kilometres, not soliton periods.

5.6 The effect of amplifier noise on sideband formation.

The initial simulations of sideband formation used the most basic system model available, with only the effects of dispersion, nonlinearity and loss included. However, because of the nature of the effect, an important consideration for real systems will be the effect of noise in modifying sideband formation.

Source and amplifier noise will both provide seeds for four-wave mixing with the cw background as described above. Thus significant sideband development may be observed much earlier in the propagation, and the presence of a second method of seeding the cw sidebands means that the seeding due to the soliton resonances may no longer be relevant.

The relative importance of seeding due to system noise compared to seeding via soliton resonances will depend on the noise parameters chosen. (The inclusion of noise in the numerical model is discussed in greater detail in Chap-

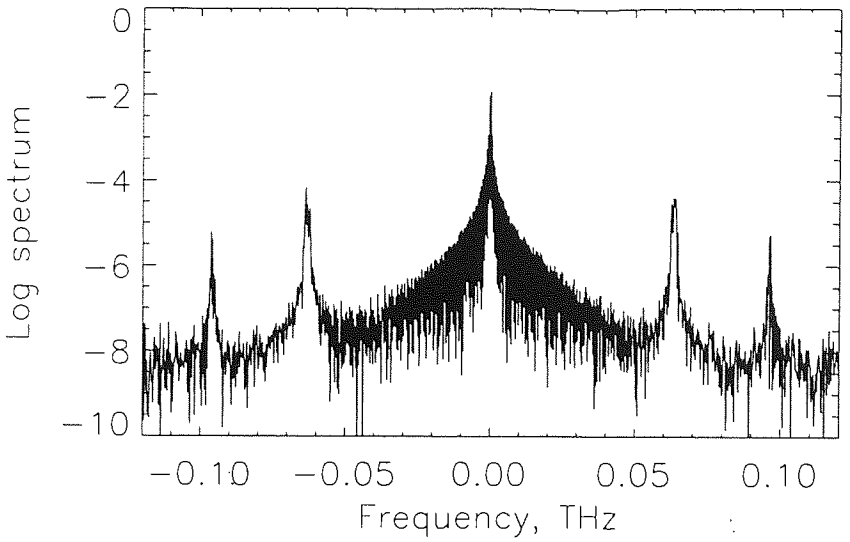

Figure 5.6: The spectrum of a pair of dark solitons experiencing periodic loss and gain in a system with noisy amplifiers. Other parameters are as defined in figure 4.1. Note the relative levels of the first two sidebands.

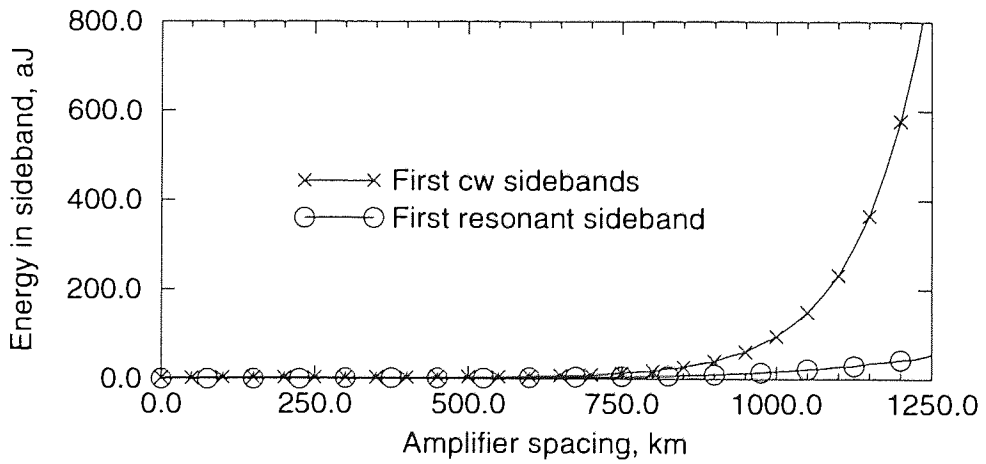

Figure 5.7: The energy transferred into the first two sidebands when noise is included in the system.

ter 6.3.1 Using the system described above and assuming a noise factor N_{sp} of 1.5, typical of non-ideal amplifiers, the central (cw) sidebands form after much fewer stages, and after fifty amplifiers are of far greater intensity than the first resonance-seeded sidebands. Figure 5.6 shows the spectral field at the output, and figure 5.7 the energy in the first and second sidebands. Compare this with the equivalent curves for a system with no noise (see figure 5.4, noting that the scales on the two curves differ by an order of magnitude). Although the energy in the resonant sideband is similar in each case, the cw sideband has been increased more than ten-fold.

5.7 Variation in amplifier spacing.

In long amplifier chains, the spacing between amplifiers is obviously more critical for dark solitons than for bright. Since dark solitons show reduced sensitivity to Gordon-Haus jitter compared to bright solitons[24] the main system limitation in terms of amplifier spacing may arise from the sideband instability discussed here, rather than jitter considerations.

However, it has been suggested [63] that in long-haul systems, such as the inter-continental optical links, non-uniformities in fibre parameters and amplification period will wash out the narrow bandwidth gain provided by the four-wave mixing process discussed for the cw background. Code was written to include such a variation in the simulated model.

Figure 5.8 shows the energy transfered into the spectral sidebands of the standard black soliton used in this work, propagating in a transmission line, with an average amplifier spacing of 25km, but with a small gaussian variation about this value. Figure 5.8a recalls the behaviour with no variation in amplification. Figure 5.8b shows the change with a variance of 0.2km in amplifier spacing, and

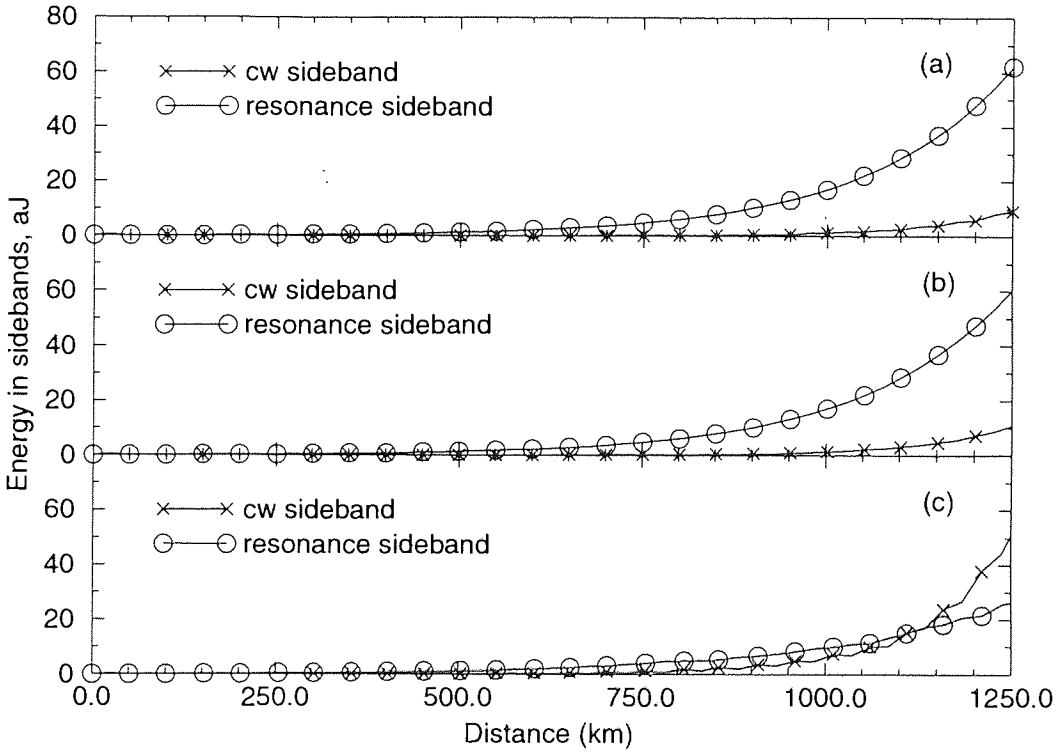

Figure 5.8: The effect on sideband growth of slight variations in amplifier spacing. (a) no variation, (b) 0.2km variation, (c) 1km variation.

figure 5.8c the results with a variance of 1km.

It can be seen that an average variation of ± 0.2km does not appear to make any significant difference to the energy transfer away from the soliton. Increasing the error to ± 1km produces a reduction in the energy in the second (resonance-seeded) sideband, but a large increase in the energy in the first (noise-seeded) sideband. A reasonable explanation for this would be that the variation results in a greater potential for seeding the parametric process, and so the sideband growth begins earlier in the propagation.

The interaction between the effects of including noise in the system, and varying the amplifier spacing from span to span has not been studied in any detail, owing to time constraints. It is not unreasonable to assume, a priori, that the sideband growth observed when noise is present will be reduced by some extent in systems with varied amplifier spacing. However, to quantify this reduction would require a more thorough analysis of all the factors involved than was possible in the time available.

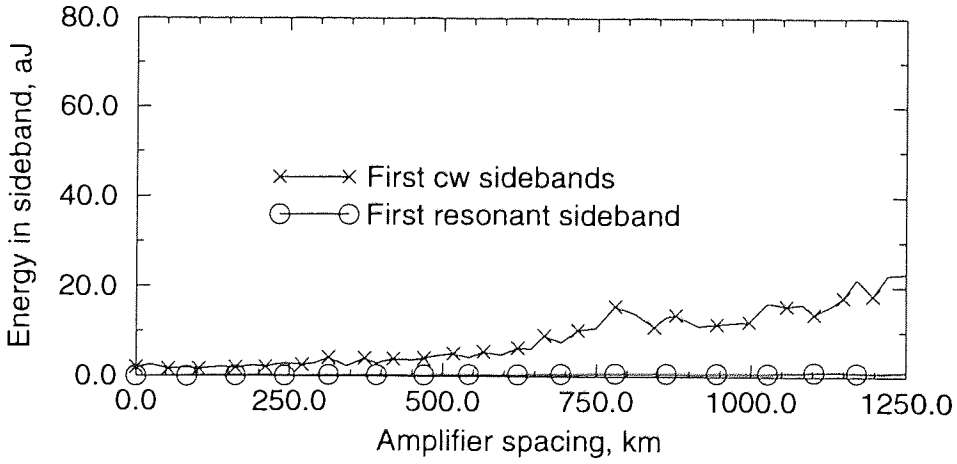

Figure 5.9: The sideband energy with a variation in amplifier spacing of 5km.

The value of 1km, (corresponding to a 4% error) was judged to be the largest reasonable variation in a transatlantic system, and produced only a minimal improvement in the final pulse profile. Obviously in land-based system there

will be a much greater variation than this, to accommodate natural and man-made features of the communications link, and simulations with a variance of 5km, corresponding to a 20% error, confirm this view (see figure 5.9). Including this information in the factors to be considered when designing new transmission systems would allow the problem of sideband growth to be virtually eliminated at the planning stage, by deliberately including a 20% variation in amplifier spacing.

5.8 Conclusions

The principle conclusion of this chapter is that in otherwise identical transmission systems, the growth of spectral sidebands due to the periodic nature of the loss and amplification cycle will result in greater deterioration of dark soliton signals than bright. This can be attributed in part to the shorter soliton period associated with dark solitons, but principally to the combination of the soliton response with that of the cw signal which supports the dark soliton to this type of periodic disturbance.

The exponential sideband growth predicted and observed in simulations of dark soliton propagation is in direct contrast with the linear sideband growth experienced by bright solitons. These results neatly illustrate the point that knowing the response of bright solitons to a given perturbation will not necessarily give any indication of the behaviour of dark solitons in the same situation. In this case, the presence of a large cw signal has a most dramatic effect on the final response, especially in noisy systems.

Including a large (20%) variation in the amplifier spacings across the transmission line has been shown to significantly reduce the energy transferred from the soliton into sidebands, and this may prove to be a convenient solution to the

problem. A more extensive study of the interplay of the effects of noise and varied amplifier spacing would be required before reaching a final conclusion on this issue. Chapter 6 looks at another possible solution, and analyses the benefits of spectral filtering to control sideband growth (see section 6.2).

The work described in this chapter has focussed mainly on the effects of gradual loss followed by lumped gain on the propagation of dark solitons, showing how the exponential sideband growth in the dark soliton spectrum can be explained by including in the calculations the effects of the cw field which supports the soliton. The results may be equally well applied to a system with distributed gain and lumped loss, for example in a fibre laser. Many observations have been made of sidebands in the outputs of bright soliton lasers[65], and the formation of sidebands with exponential growth may be an obstacle to dark soliton generation within long cavities, for example in fibre lasers which generally have a considerable cavity length compared with conventional solid state lasers.

Chapter 6

Dark soliton control techniques.

The problem of control of pulse position is of great importance in communication systems, and in this chapter the subject is studied from the point of view of dark solitons. The work described shows that their response to perturbations and control techniques is in many cases significantly different to that of bright solitons or other pulses.

Two of the standard bright soliton control techniques are to use spectral filtering and temporal phase modulation. Spectral filtering may be used to remove or severely limit unwanted energy in the wings of the soliton spectrum. This may for example be introduced by shot noise in the amplifiers, or as a result of periodic perturbations over distances comparable to the soliton period. Such filtering would then eliminate to a large extent such effects as Gordon-Haus jitter (see for example Mecozzi *et al.*[66] and Mollenauer *et al.*[67]).

Temporal phase modulation has also been successfully used to guide bright solitons, keeping them within a time slot defined by the shape of the modulation applied[68]. This technique could help solve the problem of timing jitter, and could also be used to constrain the motion of grey solitons, which have a different

velocities with respect to the background, depending for each on pulse depth and the sign of the associated phase shift.

6.1 The Response of Bright and Dark Solitons to Periodic Filtering

The response of both bright and dark solitons to periodic spectral filtering was examined numerically using the split-step Fourier technique to simulate propagation in a noiseless, loss-free system. The benefit of numerical analysis is that it allows the different contributions made to the total behaviour by such effects as loss, noise etc to be studied separately, to improve the understanding of combined effects. Here it was possible to ensure a comparison of like with like, changing only the sign of dispersion and the initial pulse conditions when considering the behaviour of dark and bright solitons.

Because solitons are formed as a balance between nonlinear and dispersive effects, it is possible for them to reform following spectral filtering with relatively narrow filters, providing the total energy lost to the system is restored following filtering.

In general, analytical and numerical studies of dark soliton propagation have been concerned only with the behaviour of the black, or fundamental soliton. Here we also consider the response of grey solitons, since initial work suggested there were some important difference, even between solitons of 100% and 99.99% darkness.

6.1.1 The response of bright solitons to periodic filtering.

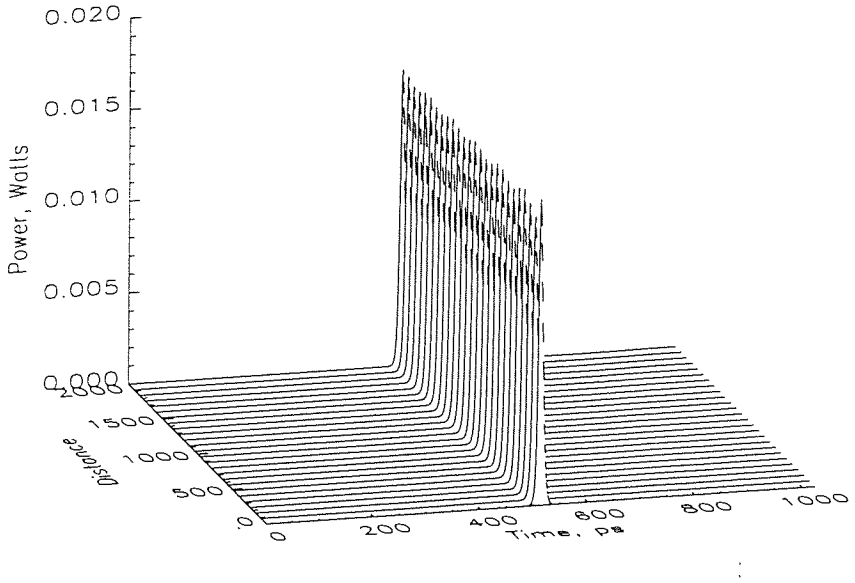

Figure 6.1: The propagation of a 10ps bright soliton, periodically filtered every 40km with a real Lorentzian filter of bandwidth 0.15THz, and experiencing a dispersion of 1ps/nm.km.

Figure 6.1 shows the temporal and spectral evolution of a 10ps bright soliton propagating in the absence of loss or noise, with a dispersion of 1ps/nm.km. This corresponds to a soliton period of 84.6km. The transmission line included filters every 40km, this distance being chosen to be close to the equivalent dark soliton period of 42.3km. (Recall that the phase of a dark soliton evolves at twice the rate of the bright soliton)

The filters used took the form:

$$H(f) = \frac{1}{\sqrt{1 + 2\left(\frac{f - f_0}{f_b}\right)}} \tag{6.1}$$

where f_0 is the filter central frequency, and f_b the filter bandwidth. This is the Real (as opposed to complex) part of a Lorentzian filter, a standard numerical approximation to the Fabry-Perot etalon which can be used to describe many practically realisable filters. Using the full form of the Lorentzian filter imparts a small temporal shift to the pulse at each stage, which complicates analysis

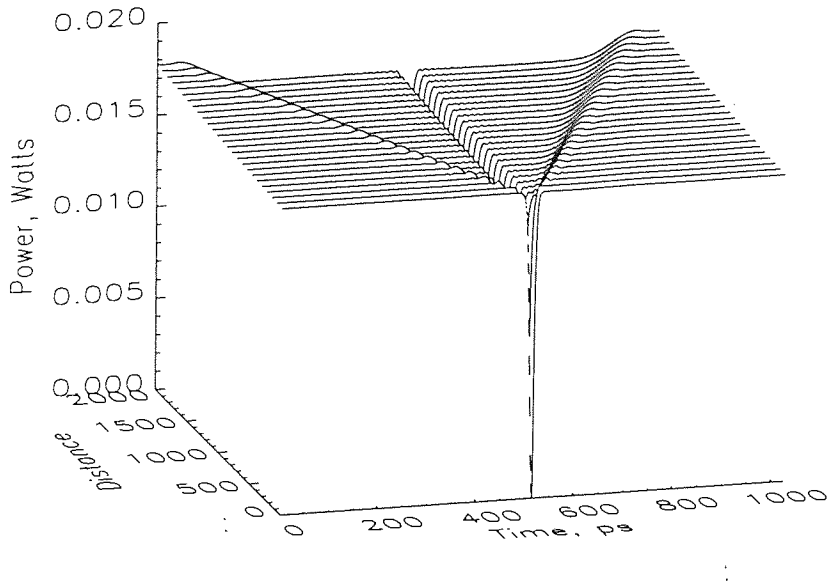

Figure 6.2: The propagation of a 10ps black soliton, periodically filtered every 40km with a real Lorentzian filter of bandwidth 0.15THz, and experiencing a dispersion of -1ps/nm.km.

and so the Real form was chosen for the initial work. The Real and complex filters have the same power spectrum, and are generally accepted to have the same effect on pulse behaviour, other than change in position produced by the complex filter.

The bright soliton reforms to accommodate the periodic filtering, and propagates without any significant loss of structural integrity, as would be expected. However, the response of the dark soliton is not so satisfactory.

6.1.2 The response of black solitons to periodic filtering.

Studying the propagation of a black soliton in the equivalent system to that described above for bright solitons, but in the normal dispersion regime (see figure 6.2), significant pulse reshaping can be seen occurring in the wings of the soliton. Figure 6.3 shows the temporal profile at the end of propagation.

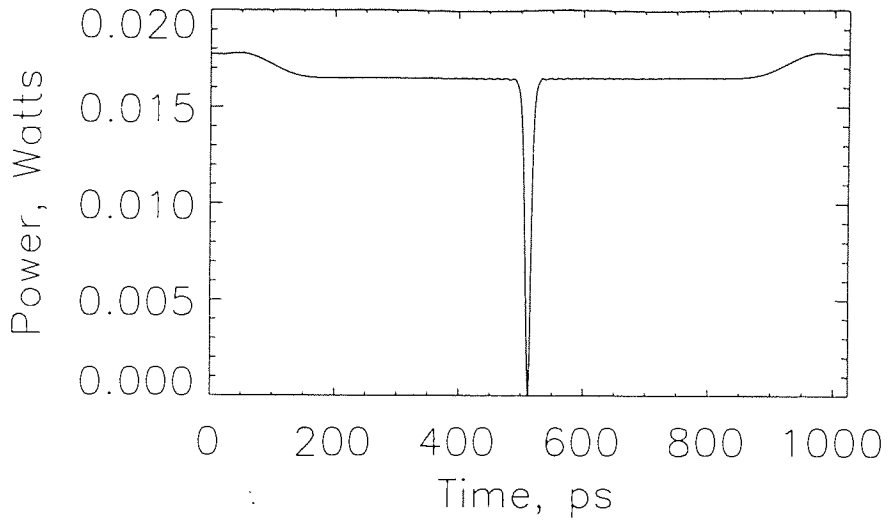

Figure 6.3: The final profile of a black soliton following propagation for 2500km filtered every 40km with an 0.15THz filter, with a dispersion of -1ps/nm.km

An inverted pedestal has developed across the soliton, becoming wider with increasing propagation distance.

One contributing factor in this comparison between bright and dark solitons is that in terms of the relative length scale of the soliton period, the dark soliton travels twice as far as the bright soliton between filters, and is therefore experiencing the equivalent of a much greater perturbation. Figure 6.4 shows the profile of a black soliton propagating in the same system, but with the dispersion halved to -0.5ps/nm.km, doubling the soliton period. The depth of the plateau has increased, and the width decreased, but the output is still clearly perturbed compared to the bright soliton propagation.

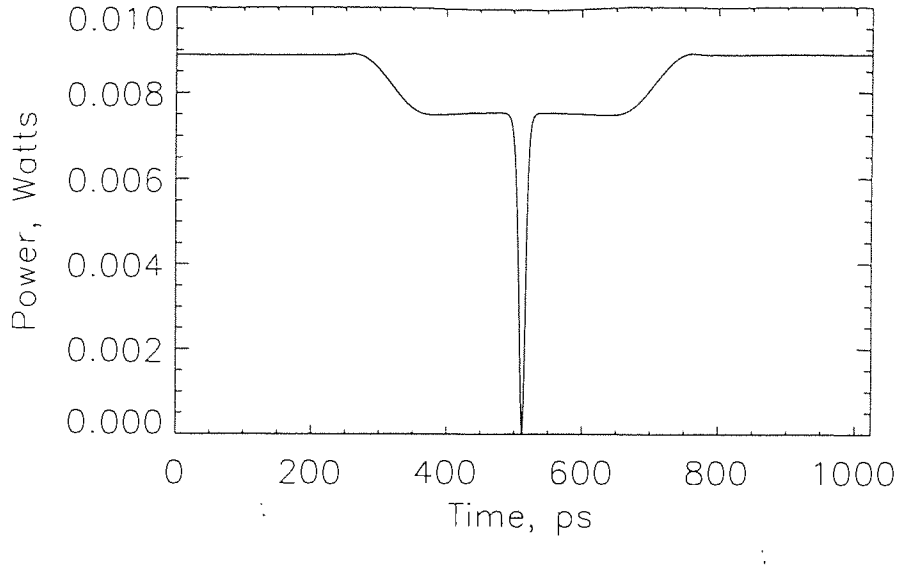

Figure 6.4: The profile of a black soliton following propagation for 2500km filtered every 40km with an 0.15THz filter, and a dispersion of -0.5ps/nm.km.

6.1.3 The response of grey solitons to periodic filtering.

In the case of a dark soliton with a greyness parameter of 0.99, a similar distortion is seen in the wings of the pulse (see figure 6.5). The combination of the natural movement of the grey soliton, and the modulation produced by periodic filtering produces an asymmetric profile.

There is, however, an important second effect of spectral filtering on grey solitons, the imposition of a change in velocity. To demonstrate this more clearly, the system parameters have been changed from those given above, to a system with a dispersion of -20ps/nm.km using solitons with pulse widths of 80ps. The filter spacing used was 12.5km, approximately one tenth of the soliton period.

Figure 6.6 shows the position in time during propagation of an unfiltered 99.99% grey soliton (solid line), and the variation in position when the soliton is filtered with a bandwidth of 0.1THz (dotted line) and 0.05THz (dashed line). There

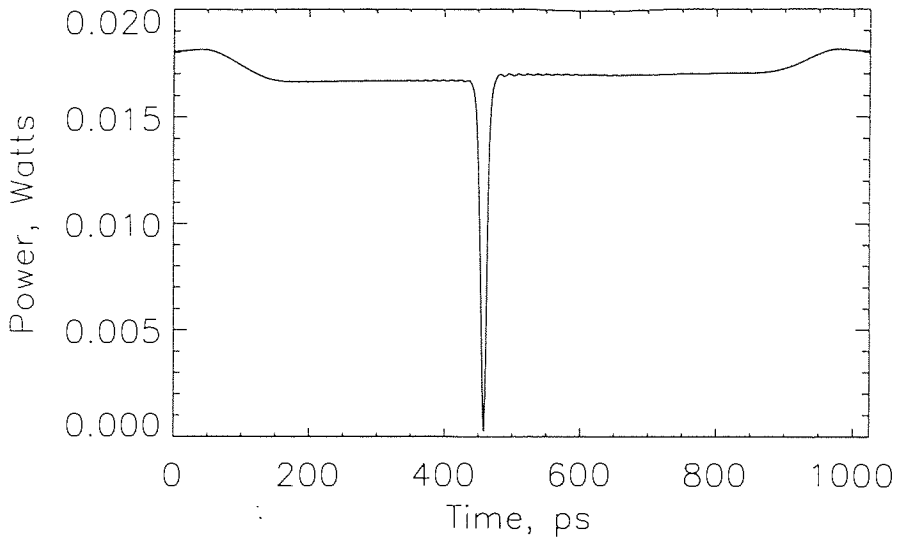

Figure 6.5: The profile of a 99.9% grey soliton following propagation for 2500km.

is clearly a contribution made by the filters to the timing of the pulses, the importance of which depends on the filter bandwidth. Instead of exhibiting a linear relationship between pulse position and propagation distance, the filtered grey soliton follows a curved path in time.

Implications of the effect of filtering on grey solitons.

This is an extremely important result from the point of view of systems design, since all real transmission systems contain some bandwidth limiting elements. Although the effects shown in figure 6.7 are a result of very severe filtering, such as is unlikely to be encountered in a typical system, the motion discussed above was caused by relatively weak filtering, on solitons which deviated from total blackness by only 0.01%, and is therefore potentially a much greater problem.

Some key features of the response may be identified, principally that the change in motion depends not only on the strength of the filter, but the greyness

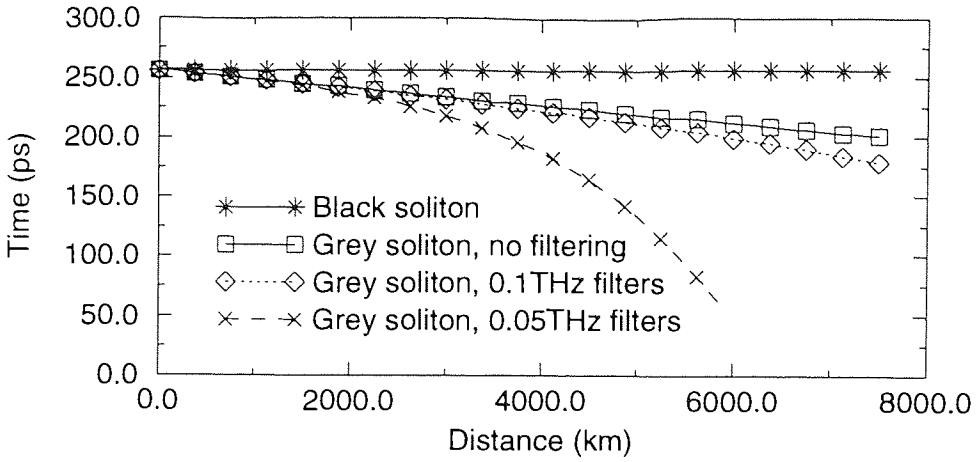

Figure 6.6: The temporal position of black and 99.9% grey solitons when periodically filtered with filters of varying bandwidths.

parameter B determining the depth of the soliton. This will be a crucial factor in the behaviour of dark solitons in noisy systems, where each pulse will have a slightly different depth, as a result of the reshaping which occurs when noise is superimposed upon the soliton profile. The small timing errors produced by this reshaping will be increased if the system contains any filtering elements, since each pulse will have its individual motion affected by a slightly different amount by the filters.

There has been only one experimental study of the propagation of data-carrying grey solitons[56] to date. The results of this work do not indicate a problem with timing of the grey solitons, but the propagation distance was only slightly greater than the soliton period, and so it is very possible that such effects would not have been observed.

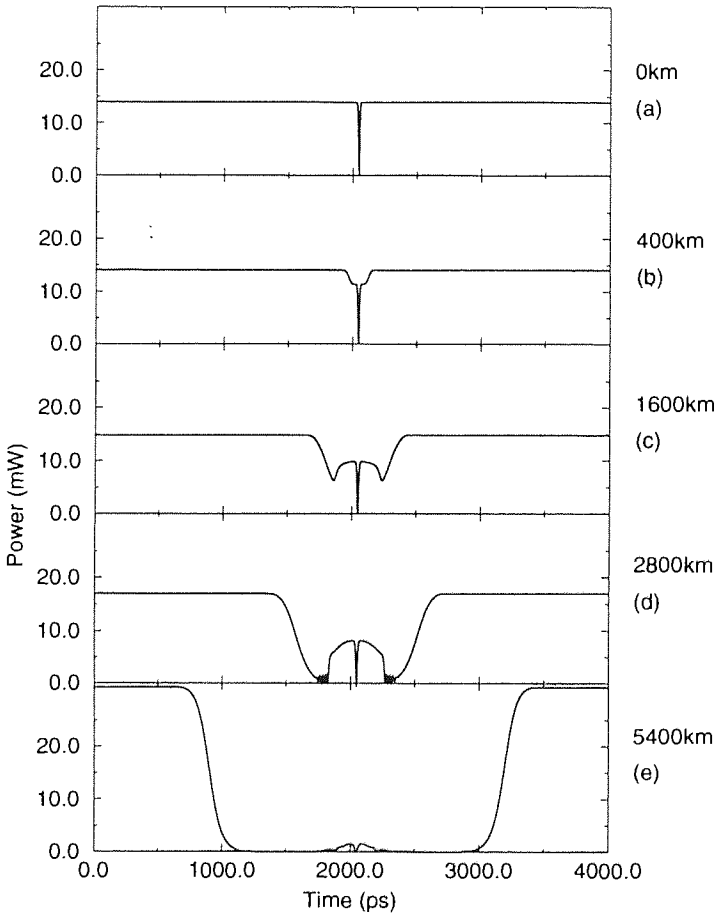

Figure 6.7: Various stages in the propagation of a strongly filtered black soliton, over many soliton periods.

6.1.4 The response of black solitons to extreme periodic filtering.

Increasing the severity of the perturbation, and propagating for extended distance allowed a more thorough study of the response of black solitons to be carried out. In more extreme simulations, such as those shown by figure 6.7, the formation of a dark pedestal across the black soliton (Figure 6.7b) was observed at an early stage. As propagation progressed, the edges of the pedestal became deeper (Figure 6.7c) with structure developing in the phase profile. The dark soliton was finally supported by a bright pulse of ever-decreasing intensity, becoming ever more isolated from the cw background (6.7d and e). This trend could be seen to continue until interference with neighbouring solitons became the most significant factor in the propagation. It is interesting to note that the soliton width, blackness and phase shift remained unchanged throughout, despite the large reduction in background level.

The 10ps black soliton used here was filtered every 10km with an 0.25THz filter, for a total distance of 5000km. A system like this is unlikely to be found in practice and so such an extreme response will be rare but the more minor pulse distortion shown in figure 6.3 could constitute a real problem for system design.

6.2 The effect of filtering on dark soliton sideband formation.

As shown in chapter 5, in a system with large amplifier spacing compared to the soliton period, the effect of periodic loss and amplification on dark solitons and on the background which supports the solitons combines to produce spectral sidebands which grow exponentially with propagation distance. In severe cases,

the signal is destroyed completely in a very few amplifier spans.

Sideband suppression by spectral filtering is an obvious method to consider, since it should in theory both reduce the noise which seeds the sidebands, and limit the growth of energy outside the soliton spectrum. Some additional amplification must be provided to restore the system energy, but in all the cases described below it was negligible compared to that required to compensate for loss over the previous span, and therefore assumed to have no effect on sideband growth.

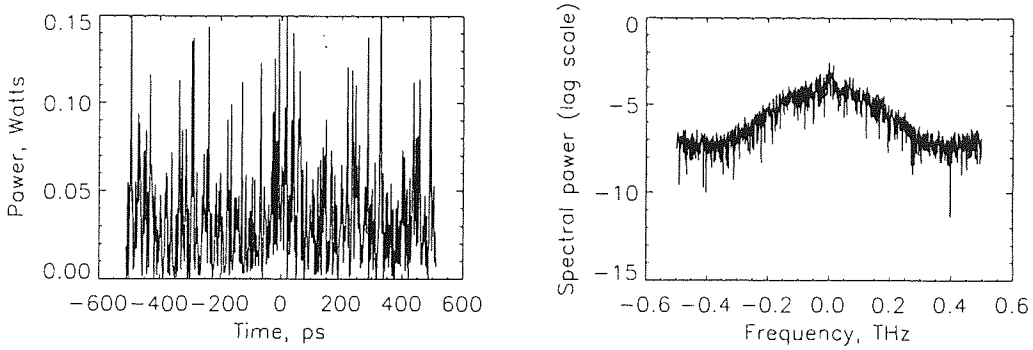

Figure 6.8: Pulse profile and associated spectrum after transmission for 60 amplifier spacings of 40km, with no filtering. The system used 10ps black solitons, and a dispersion of -1ps/nm.km, which corresponds to a soliton period of 42.3km.

Figure 6.8 shows the temporal and spectral profiles of a pair of 10ps black solitons following transmission over a distance of 2400km, with amplifier spacing of 40km, very close to the soliton period of 42.3km. Any information present at the start of transmission has been lost.

Figures 6.9 to 6.11 show the effects of filtering at each amplifier with progressively stronger filters. Beyond a certain strength of filter, the modulation observed in the ideal system propagations described above can be seen developing. There are clearly large benefits to be had from a certain amount of filtering, but these must be offset against the distortion produced by periodic filtering.

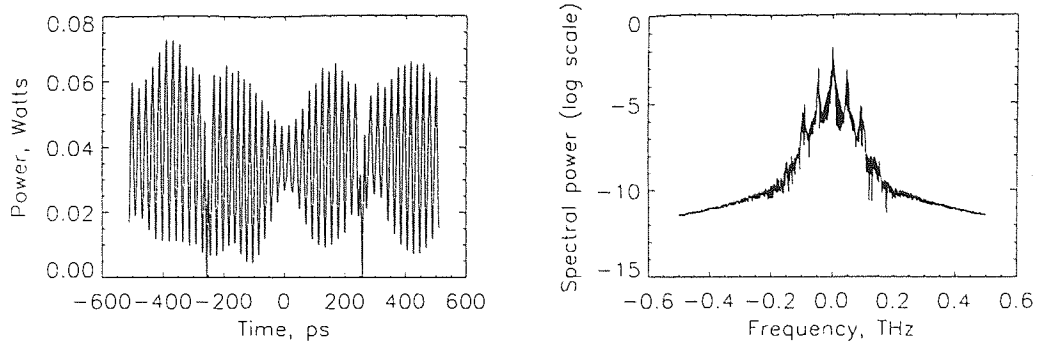

Figure 6.9: Pulse profile and associated spectrum, filtering every 40km with an 0.25Thz real Lorentzian filter, using the system parameters defined in figure 6.8

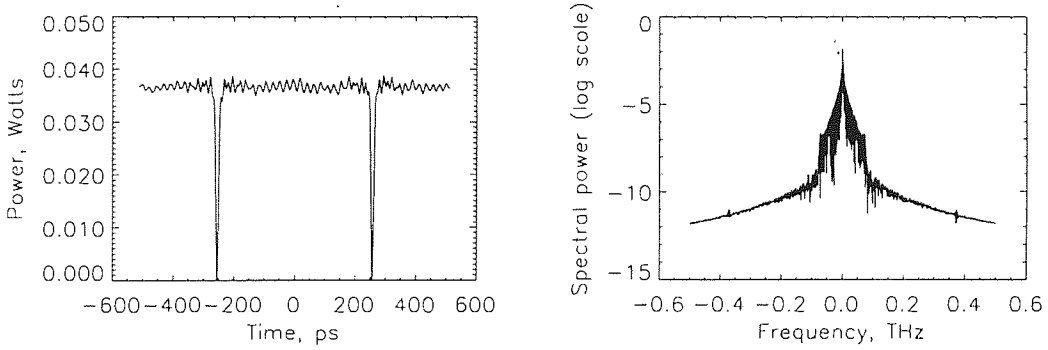

Figure 6.10: Pulse profile and associated spectrum, filtering every 40km with an 0.2THz real Lorentzian filter, using the system parameters defined in figure 6.8.

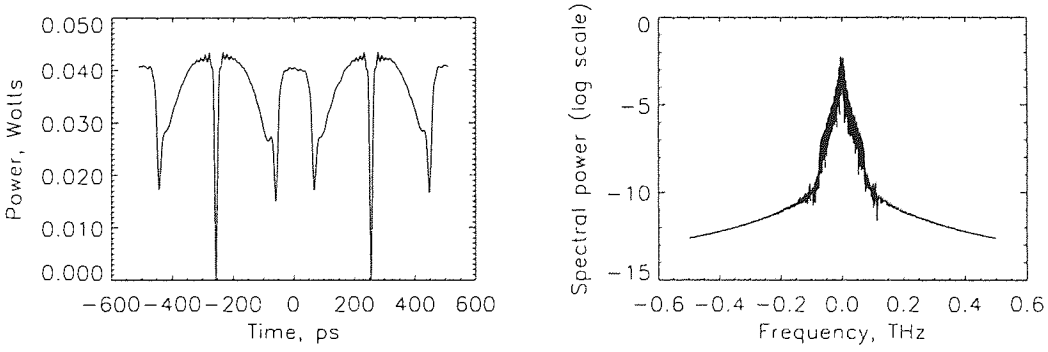

Figure 6.11: Pulse profile and associated spectrum, filtering every 40km with an 0.125THz real Lorentzian filter, using the system parameters defined in figure 6.8.

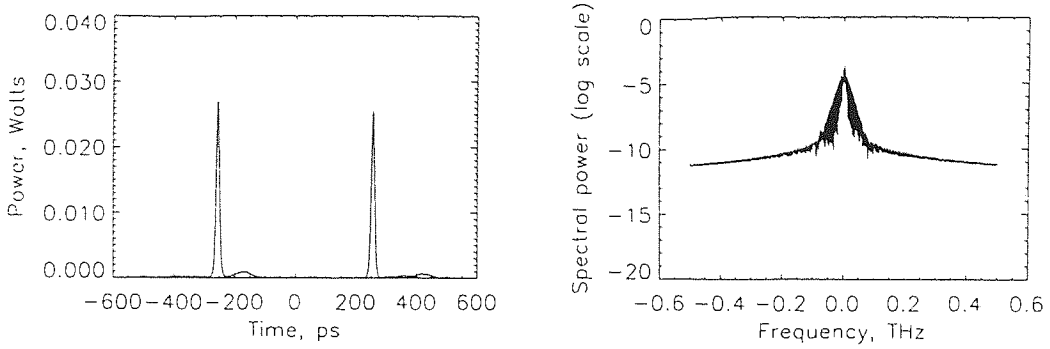

Figure 6.12: Bright soliton propagation in the same system, with 0.125THz filters

However, the results here show that spectral filtering can be very useful in suppressing sideband growth, and that the limits of the average soliton model may therefore be extended quite considerably without signal degeneration via this particular mechanism.

It is interesting to note that a bright soliton in the same system (with the sign of dispersion reversed) will propagate almost entirely unchanged (see figure 6.12). This suggests that the amount of distortion is in some way related to the amplifier spacing as a fraction of the soliton period, which for dark solitons is half that for bright.

6.3 The effect of filtering on Gordon-Haus jitter in dark solitons.

6.3.1 Gordon-Haus Jitter

A fundamental disadvantage of any amplification scheme over regeneration is the extra energy added to the system due to spontaneous-emission noise in the

amplifiers. This cannot be eliminated, although it may be reduced by good design. In the best case, the noise associated with an amplifier is white, that is it has an equal distribution across all orthogonal modes of the system, and has a mean energy of $(G-1)$ photons per mode, where G is the power gain. The quantum-limited white noise power of such an amplifier, with optical bandwidth $\Delta\nu$ is given by:

$$P_n = h\nu(G-1)\Delta\nu \tag{6.2}$$

where h is Planck's constant.

In nonlinear systems, this noise is not merely additive at each amplifier, a problem in itself, but by changing the power in the system may also affect the pulse's nonlinear behaviour.

It was shown by Gordon and Haus [69] that the incorporation of spontaneous emission noise in the field of a soliton results in a random velocity change due to a change in the soliton's carrier frequency. At the end of a transmission line of length L, with amplifier spacing L_{amp}, the standard deviation in pulse arrival time relative to its starting position may be calculated as:

$$\sigma = \left[\frac{1.763 N_{sp} N_2 D h (G-1) L^3}{9 t_s A_{eff} L_{amp} Q}\right]^{1/2} \tag{6.3}$$

where N_{sp} is the spontaneous emission factor associated with the amplifiers. The nonlinear constant N_2 of the fibre is taken to be $3.2x10^{-20}m^2/W$ in this work. D is the first order group velocity dispersion coefficient (measured in $ps/nm.km$) and h is Planck's constant. The factor Q is defined as:

$$Q = \frac{G\alpha L_{amp}}{G-1} \tag{6.4}$$

where $G = exp(\alpha L_{amp})$, and α is the power loss coefficient of the fibre. The factor Q is used to scale the input power from that required for a fundamental soliton to that defined by the average soliton model (see section 1.4.2). L_{amp} is the distance in kilometres between amplifiers, and L is the total system length.

In simplistic terms, adding random noise to a bright soliton spectrum will change its profile. To accommodate this change the spectrum will shift slightly as the soliton reforms, and the frequency shift produced will translate into a change in the soliton velocity. The central frequency of dark solitons is fixed as the frequency of the supporting cw background, and so it might be expected that the effect of noise would be somewhat different. The velocity of a dark soliton is linked, via its phase, to its amplitude. Small changes to phase or amplitude, such as those resulting from a superposition of noise on the soliton, will produce changes to the group velocity by increasing (or decreasing) the chirp on the soliton, changing the width and height of the power spectrum.

In 1994 Kivshar *et al.*[24] showed that the variation in the arrival time of dark solitons due to random changes in group velocity was smaller by a factor of $\sqrt{2}$ than for bright solitons. However, this is still enough to cause a large unwanted increase in the bit-error rate of a long-haul system, and some method of suppressing the cubic growth in the variance of pulse arrival times needs to be developed.

The use of filters[70], and more especially sliding filters[67] has been shown to produce a dramatic reduction in the timing jitter experienced by bright solitons, in particular reducing the growth from cubic to linear in form. The use of sliding filters, (essentially a technique where the system is arranged so as to have a small change in central frequency for each filter in a transmission line relative to the previous one) did not seem appropriate for dark solitons, whose central frequency is fixed, but investigating the effect of a chain of identical filters on dark soliton jitter seemed to be a suitable first step.

6.3.2 Numerical model used to analyse dark soliton jitter.

Because Gordon-Haus jitter results from an essentially random source, any analysis of its suppression or otherwise must use a large number of samples to ensure that results observed are statistically significant. All values given here (unless stated otherwise) are the result of finding the variance in pulse position of around 200 pairs of either bright or dark pulses. The software to perform this analysis was written specifically for this task, and the key features of the code are discussed below.

For the bright soliton case, for each sample at each stage of propagation, the points of full width half maximum power were located, and the centre of mass found between these points taken to be the position of the pulse peak. The centre of mass was defined, for a bright soliton, as

$$C_{mass\_bright} = \frac{\sum_{-n/2}^{n/2} t|u|^2 dt}{\sum_{-n/2}^{n/2} |u|^2 dt} \tag{6.5}$$

where n is the full width at half maximum point, the centre of the pulse corresponds to $t = 0$ and t represents the discrete time samples of the numerical system. $|u|^2$ is the power in a given sample t.

For the case of dark solitons, the centre of 'negative mass' was found, that is the power in each sample was subtracted from the background power at half the maximum depth (an arbitrarily selected definition), and the resulting value added to the sum so far. This definition of pulse position maximised the contribution to the total around the centre of the soliton while minimising the contribution from the edges of the sample, and was found to provide a more accurate value for the exact centre than a simple centre of mass calculation.

To allow for easy comparison with previous work by others in the field the simu-

lations were done assuming amplification was distributed along the transmission line, that is the solitons did not experience any loss during propagation. Noise was added at regular intervals, the distance between stages being defined as the amplifier spacing. It has been shown[71] that this has no effect on the observed jitter, compared to other systems for introducing noise, and is convenient from a numerical point of view. Each simulation used a different seed value to initialise the random number generator.

Using the definition of noise power given in equation 6.2, the noise field amplitude added to each sample was calculated as

$$N_s = N_{sp} * P_n/A \tag{6.6}$$

where A is the effective core area of the fibre and N_{sp} is the spontaneous emission factor associated with the amplifier. An ideal amplifier will have a value of 1 for N_{sp}, a more realistic value is 1.5, and this is the value which has been used in the work described here.

The noise was launched in the time domain, a field with amplitude N_s and random phase being added to each discrete element. The code to provide random number generation was standard, the rest of the additional code to simulate this type of amplifier was written specifically for this work.

6.3.3 Numerical demonstrations of jitter and jitter reduction techniques for bright and dark solitons.

Preliminary work was concerned with verifying that the modelling techniques used could reproduce previous work. Figure 6.13 shows the observed variance in pulse arrival times for equivalent bright and dark soliton systems. The growth in each case is cubic, but with the average jitter of a dark soliton at any point during propagation being less by a factor of $\sqrt{2}$ than that for bright, as expected.

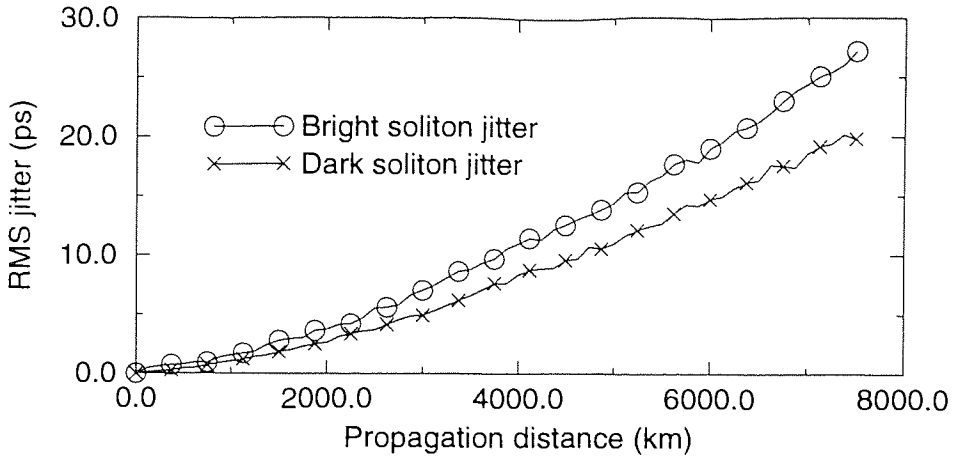

Figure 6.13: The standard deviation in pulse position from the initial conditions for equivalent bright and dark solitons experiencing Gordon-Haus jitter.

In this, and all the following examples, the solitons used had a full width at half maximum of 80ps, in a system with a dispersion of $\pm$20ps/nm, with amplifiers every 12.5km. These figures were chosen for their compatibility with earlier work on bright soliton jitter, with the first results being compared to ensure that the model was correct.

Figure 6.14 demonstrates the benefit to bright soliton jitter of periodic filtering. The timing variation has been almost completely eliminated, with the cubic growth reduced to linear.

Figure 6.15 shows the jitter observed in dark solitons in a system identical to that used in the simulations above, other than that the sign of dispersion is reversed. Not only is the jitter not reduced, but if the curve is compared to that in figure 6.13, it can be seen that as the filter bandwidth is reduced the jitter actually becomes worse, and the variation in dark soliton arrival time increases. The variance is no longer cubic, in the example shown the best curve fit to the observed standard deviation gives an exponent of 1.777, corresponding to a growth in the variance in arrival times of not 3 but 3.555. This is dramatically

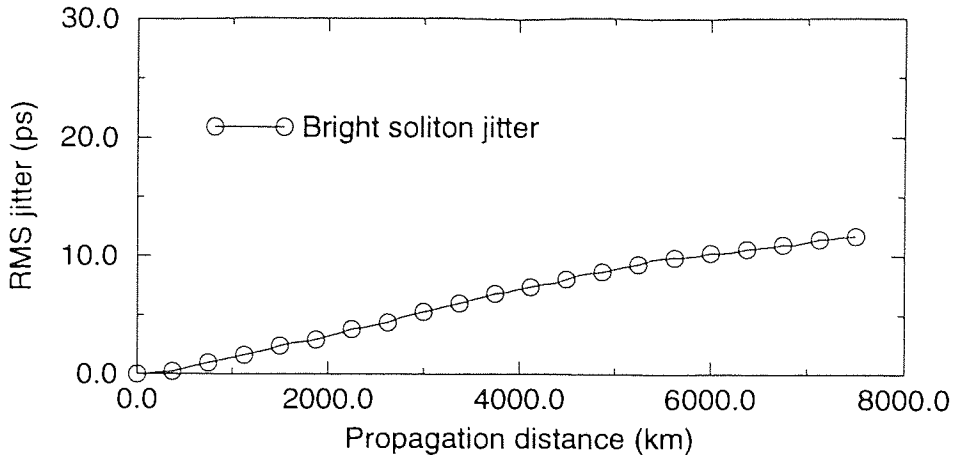

Figure 6.14: The standard deviation in pulse position from the initial conditions experienced by bright solitons when 0.075THz filters are included in the transmission line. Note that the increase in deviation is now linear.

different to the response of bright solitons, and has very serious implications for any future dark soliton communication systems.

The reasons for this behaviour are not clearly understood. It is possible to demonstrate mathematically that the action of a filter has no effect on the motion of a black soliton. However, when noise is added to the system, the soliton is no longer black, but grey, with the noise producing a slight change in phase and amplitude, and therefore group velocity. As was demonstrated in section 6.1.3, the speed of a grey soliton with respect to the background is increased by spectral filtering. In this case any small decrease in soliton depth (ie reduction in blackness) and simultaneous increase in speed produced by the superposition of noise on the spectrum is enhanced by the filtering. Decreases in speed, or equivalently increases in depth due to the same mechanism will be suppressed somewhat, and so the net effect of filtering will be to increase the jitter.

This counter-intuitive result shows yet again that the behaviour of dark solitons

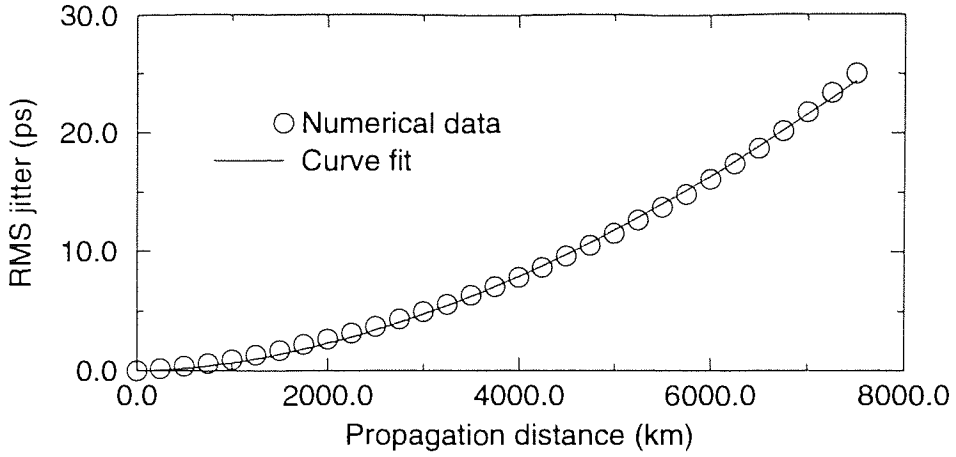

Figure 6.15: The standard deviation in pulse position from the initial conditions experienced by black solitons when 0.075THz real filters are included in the transmission line.

cannot be predicted a priori from a knowledge of the bright soliton response to a particular perturbation. In this case the difference is not a result of the large cw signal associated with dark solitons, but with the direct relationship between the dark soliton amplitude, phase and velocity at any point.

It is reasonable to consider that the phase response of the filters used may be more important for dark solitons than bright, because of the asymmetric phase profile associated with dark solitons, and when complex filters of the form:

$$H(f) = \frac{1}{1 + i\left(2\frac{f - f_0}{f_b}\right)} \tag{6.7}$$

were used in the simulations, a small difference could be seen between the behaviours observed (see figure 6.16). However, the difference lies within the bounds of numerical error, and cannot be considered to be statistically significant. The result is included here for completeness.

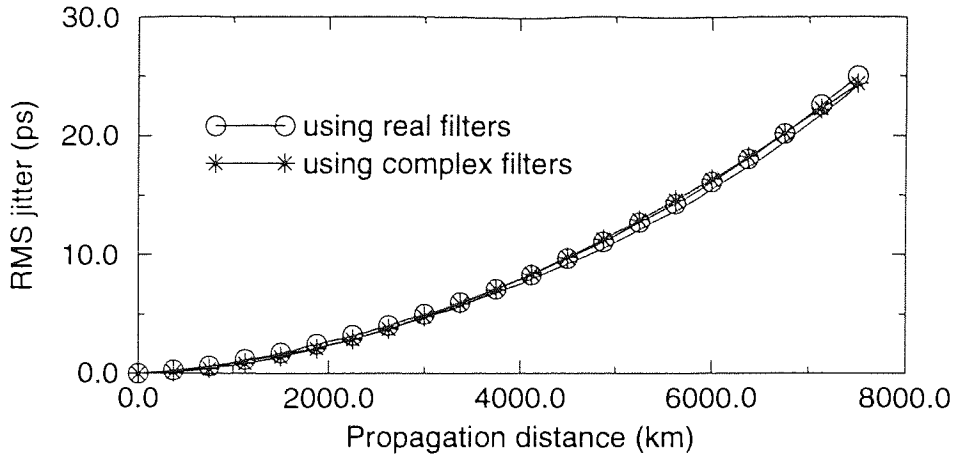

Figure 6.16: The standard deviation in pulse position when black solitons are filtered with 0.075THz real and complex filters.

6.4 Temporal phase modulation

Temporal phase modulation has been shown[68] to provide a simple technique for controlling the position of bright solitons, and the analytical study suggested that it would be equally successful when applied to the problem of dark soliton control. This section describes work done in collaboration with N.J. Smith, who has performed the mathematical analysis of the response of dark solitons to temporal phase modulation.

6.4.1 Mathematical analysis.

When a modulator with function $M(u)$ is inserted into the transmission line, the equation describing propagation in the normal dispersion regime becomes:

$$i\frac{\partial u'}{\partial z'} + \frac{\beta_2}{2}\frac{\partial^2 u'}{\partial t'^2} - \gamma_{NL}|u'|^2u' = M'(u') \equiv \frac{\Phi}{l_m}\cos(\omega_m t')u' \qquad (6.8)$$

Under the standard transformations (see chapter 1.4.1 $t = t'/\tau$, $z = \beta_2$, z'/τ^2, $u = \tau u'\sqrt{\gamma_{NL}/\beta_2}$, this becomes

$$i\frac{\partial u}{\partial z} + \frac{1}{2}\frac{\partial^2 u}{\partial t^2} - |u|^2 u = M(u) = \frac{\Phi\tau^2}{\beta_2 l_m}\cos(\omega_m \tau t)u \tag{6.9}$$

In the absence of modulation ($M(u) = 0$), the dark soliton solution to this equation can be written as,

$$u_s(z,t) = u_0 e^{-iz}(\eta \tanh(Z) - i\Omega) \tag{6.10}$$

$$Z = \eta(t - \Omega Z) \tag{6.11}$$

In this normalised form it is easy to see why the dark soliton can be described as a one parameter pulse. The soliton's velocity and amplitude are related by $\Omega = \sin\phi$, $\eta = \cos\phi$, such that $\eta^2 + \Omega^2 = 1$. In this analysis we are concerned with the variation in the parameter ϕ when a modulation of the form $M(u)$ is applied.

The perturbational methods of Kivshar[72] can be used to give the motion of the parameter ϕ as,

$$\frac{d\phi}{dz} = \frac{1}{2\cos^2\phi\sin\phi}\mathrm{Re}\int_{-\infty}^{\infty} M(u)\frac{du_s}{dz}dt \tag{6.12}$$

After substituting for the functions, and setting $Z \equiv \eta(t-T)$, where $\partial T/\partial z = \Omega$, the integral may be evaluated by parts to yield:

$$\frac{d\phi}{dz} = \frac{\Phi\tau^2}{2\beta_2 l_m}\left(\frac{\omega_m\tau}{\eta}\right)\frac{\pi\sin(\omega_m\tau T)}{\sinh(\pi\omega_m\tau/2\eta)} \tag{6.13}$$

$$\frac{dT}{dz} = \Omega \tag{6.14}$$

For nearly black solitons, that is those with a small value of ϕ, the pulses will perform simple harmonic motion about the centre of modulation. Although movement is not completely suppressed, it is now controlled and the pulse position is constrained within a defined window. The period of the SHM depends on the peak phase of the modulation applied.

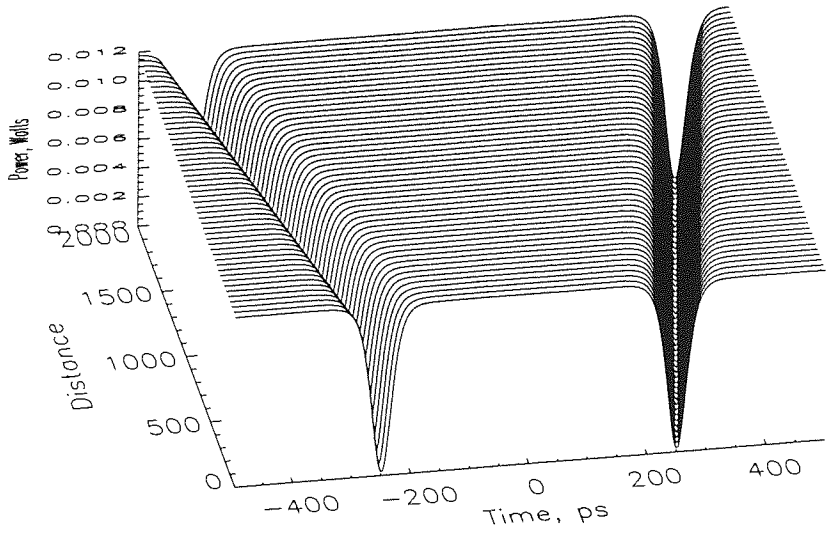

Figure 6.17: The propagation of a pair of 99% grey solitons.

These results have been confirmed by another group using a different analytical technique to demonstrate control of the soliton's motion [73]. However, neither method considers the effect of the periodic phase modulation on the 'cw' background which supports the solitons, nor the interactions between the two parts of the field.

6.4.2 Numerical simulations of phase modulation as a control mechanism.

To confirm the predictions of the theory presented above, a series of numerical simulations were performed, using different values for the parameters associated with the applied phase modulation $M(u)$. Both the peak phase excursion, and the frequency of the modulation could be changed. The modulator spacing used was 20km, with a dispersion of -1ps/nm.km. To avoid complication the propagation was assumed to be loss-free. A pair of grey solitons were used had a contrast ratio of 95%, and were initialised to be travelling away from each other, with an initial pulse separation of 500ps.

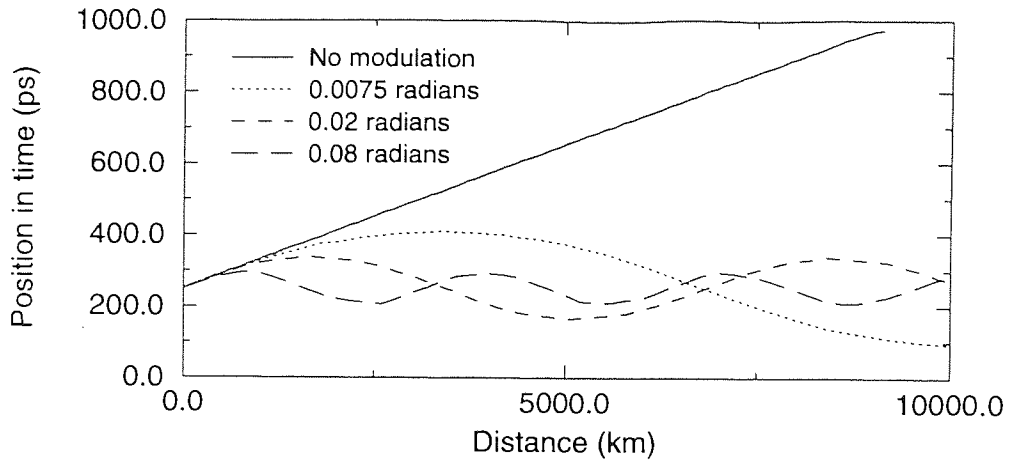

Figure 6.18: The position of a grey soliton in the time window when a variety of different phase modulations are applied.

Figure 6.17 shows the propagation of a pair of grey solitons as described above, in the absence of any control mechanism. Figure 6.18 shows the position of the centre of one of the solitons in this propagation (solid line), and the effect on pulse position of applying a phase modulation with peak excursion of 0.0075 radians (dotted line). The peaks of the modulation coincided with the centres of the pulses. The pulses move apart more slowly, but eventually escape the well created by the modulation, going on to collide in the centre of the window.

Increasing the phase excursion to 0.02 radians constrains the motion more successfully(figure 6.18 dashed line), and increasing it again to 0.08 radians is yet more successful (dot-dashed line). However, up to this point, we have only been concerned with the position of the soliton. Figures 6.19 to 6.21 show the complete evolution of the pulses whose positions were shown in figure 6.18.

Additional effects of the modulation can clearly be seen on the cw background, and although increasing the strength of the modulation produces good position control, this is at the expense of a large amount of perturbation to the background.

The concern over the large amount of observed modulation (bearing in mind

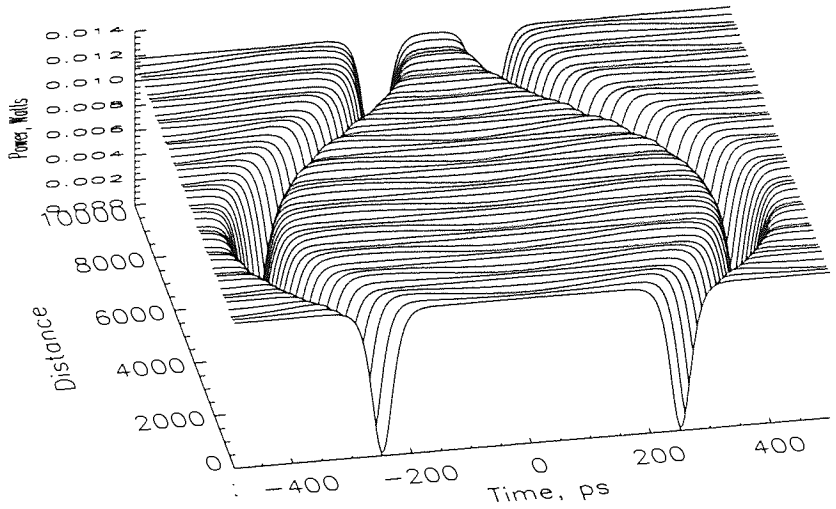

Figure 6.19: The evolution of a pair of grey solitons following propagation in a system including 0.0075 radians phase modulation, at the same frequency as the pulse repetition rate.

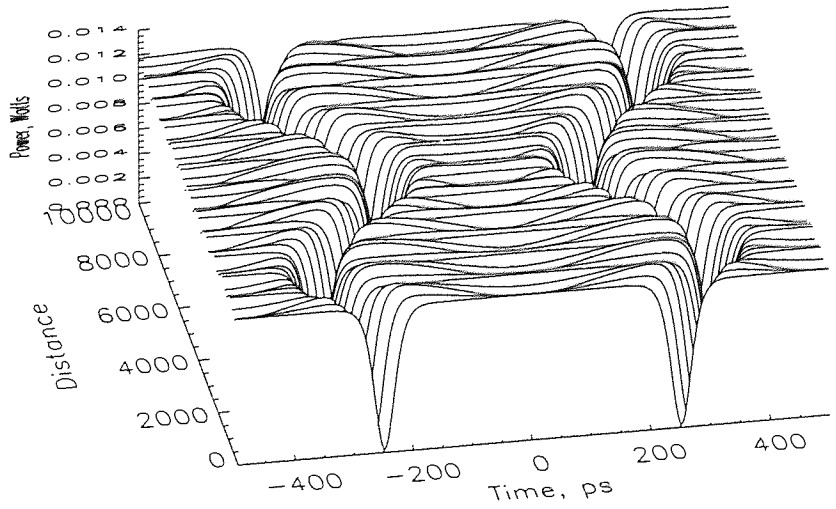

Figure 6.20: The evolution of a pair of grey solitons following propagation in a system including 0.02 radians phase modulation, at the same frequency as the pulse repetition rate.

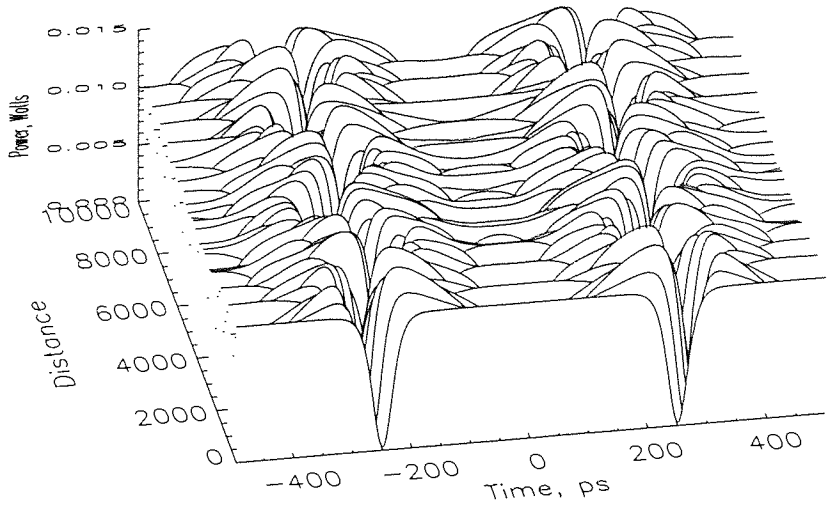

Figure 6.21: The evolution of a pair of grey solitons following propagation in a system including 0.08 radians phase modulation, at the same frequency as the pulse repetition rate.

that the soliton itself appears to maintain its integrity) is because in typical communication systems the presence or absence of a pulse within a bit interval is determined by the total energy detected. As the variation produced by the unwanted modulation grows to be a significant percentage of the total energy in the window, the chances of errors in reception are very much increased. If phase modulation is to be used as a control mechanism, then some method must be found of smoothing out the background disturbances, possibly using an amplifier with a nonlinear response, or some similar amplitude sensitive device. This could have a response such that power levels of the order of the CW level cause saturation, effectively flattening any disturbances to the background; and a response at low power levels such that the signal experiences loss, to keep the centre of the soliton itself as dark as possible.

6.5 Conclusions

It is clear from the results discussed in this chapter that the bright soliton control techniques of spectral filtering and temporal phase modulation cannot be directly applied to dark solitons. Periodic filtering has been shown to be advantageous in suppressing spectral sidebands, providing the filter used is not too strong. However, bright solitons can withstand much more extreme spectral filtering whilst maintaining their pulse shape.

A second, and more serious disadvantage of the response of dark solitons to periodic spectral filtering is that grey solitons (as opposed to 100%, or black solitons) will suffer a change in velocity as a result of any filtering. The black soliton is an ideal solution, and in realistic, noisy systems, all dark solitons will in fact be grey, even if by only a fraction of a percent. In situations where the timing of the pulses is critical, as is the case in most communications systems then the presence of in-line spectral filters will result in transmission errors due to this effect.

To assess the significance of these results, a study of the effectiveness of filtering in various situations was undertaken. The benefits in reducing sideband growth have already been mentioned, however, a more important use would be in the suppression or reduction of Gordon-Haus jitter. In-line filtering is known to be extremely beneficial to bright solitons in noisy systems, reducing the growth in the variance of pulse arrival times from a cubic to linear. However, Gordon-Haus jitter by its nature will act upon black solitons with the same velocity as the background to produce very dark grey solitons of random depth and velocity. Filtering will enhance this effect, and rather than reducing the jitter, it was shown that the variance in pulse arrival time increased with increasingly narrow filters. A possible alternative technique has been suggested, using nonlinear gain to control the jitter [74]. This has yet to be demonstrated experimentally.

Moving on to other control techniques, temporal phase modulation was shown to be beneficial to a small extent in controlling the motion of grey solitons and a paper has been published on this subject [73]. However, the authors have not taken into account the additional modulation produced by this technique may render it unsuitable for use in a communications system, unless some method is found of controlling the cw background supporting the soliton. Once again, the conclusion is that to remove the cw part of the field by some renormalisation process may seriously compromises the validity of any results, and should be justified in detail.

Work is now being carried out elsewhere into the possible advantages of using some form of amplitude sensitive element to provide control functions for dark solitons.[75] This approach affects the parameter Ω defined in section 6.4.1 directly, via the soliton depth, and so may have greater potential for this particular problem. A possible technique may be to use nonlinear optical loop mirrors (see section 1.3.2) to provide passive control, after reference [76].

Chapter 7

Conclusions

Many of the key features of dark solitons with respect to telecommunications may be illustrated using the results in this thesis. Firstly, the controlled generation of dark solitons is by no means so straightforward as for bright solitons, partly because both the amplitude and phase profiles must be created, and partly because pulses which are absences of light do not lend themselves well to spontaneous formation within either pulsed or cw laser cavities.

Aside from the difficulties of generation using standard techniques, the propagation properties of dark solitons are significantly different to those of bright solitons in many respects. Having a shorter soliton period means they are more susceptible to those disturbances which occur over a similar length scale. In addition, the presence of the cw background makes an important contribution to the response to many perturbations, the case considered here being of sideband formation due to periodic amplitude variation. The sidebands formed in bright soliton systems grow linearly, due to a resonance between the soliton and radiation shed during each cycle. In dark soliton systems, the sideband growth is exponential, with the resonant sideband growth being enhanced by a four-wave mixing process with the background, which is also undergoing the

periodic perturbation.

Another important difference between dark and bright solitons is the response of each to standard (bright soliton) control systems. In particular, spectral filtering, which has been remarkably successful in controlling jitter in bright solitons, actually exacerbates the problem when applied to dark solitons suffering from jitter.

The main conclusion of all of these results, and those of the other workers in the field, is that although dark solitons show enhanced stability to some disturbances, there are as many situations where this is not so. Comparisons between bright and dark solitons depend very very sensitively on the exact system being considered, and either can be shown to be superior with careful selection of system parameters.

Developing the study of dark solitons from the work presented here would require a shift in focus, with less emphasis on the equivalence or otherwise with bright solitons, and more on specific features of dark solitons. An interesting development would be to compare them, instead, with NRZ systems.

Recent experiments[77] with improving transmission in NRZ systems have included synchronous phase steps of π at the bit rate, with some success. It is possible that this engineering solution is approaching the same conclusions as mathematical analyses have suggested, that the optimum pulse-shape for stable transmission in the normal dispersion regime includes both amplitude and phase components.

The potential of dark soliton communication systems is still unknown. It has been shown here that there are many features of their behaviour which render them particularly suitable for certain situations. It is even possible that dark soliton systems are already being implemented, having evolved by trial and

error from more traditional systems. This work has indicated a number of important areas which should be considered, and with the advent of more reliable generation and modulation techniques the future of some communications may well not be bright, but dark.

Bibliography

[1] D. Gloge. Weakly guiding fibres. *Appl. Opt.*, 10(10):2252–2258, October 1971.

[2] B. J. Ainslie. A review of the fabrication and properties of erbium-doped fibres for optical amplifiers. *J. Lightwave Technol.*, 9(2):220–227, February 1991.

[3] E. Desurvire, J. R. Simpson, and P. C. Becker. High gain erbium-doped travelling wave fibre amplifier. *Opt. Lett.*, 12(11):888–890, November 1987.

[4] E. M. Dianov, L. M. Ivanov, P. V. Mamyshev, and A. M. Prokhorov. Efficient compression of high-energy laser pulses. *IEEE J. Quantum Electron.*, 25(4):828–835, April 1989.

[5] P. D. Maker and R. W. Terhune. Study of optical effects due to an induced polarisation third order in the electric field strength. *Phys. Rev. A*, 137(3):801–818, February 1965.

[6] Robert Hellwarth, Joel Cherlow, and Tien-Tsai Yang. Origin and frequency dependence of nonlinear opical susceptibilities of glasses. *Phys. Rev. B*, 11(2):964–967, January 1975.

[7] Govind P. Agrawal. *Nonlinear Fiber Optics.* Academic Press, 1989.

[8] N. J. Doran and David Wood. Non-linear optical loop mirror. *Opt. Lett.*, 13(1):56–58, January 1988.

[9] B. K. Nayar, K. J. Blow, and N. J. Doran. All-optical switching in nl fibre loop mirror devices. *Optical Computing and Processing*, 1(1):81–89, 1991.

[10] K. Smith, N. J. Doran, and P. G. J. Wigley. Pulse shaping, compression, and pedestal suppression employing a nonlinear optical loop mirror. *Opt. Lett.*, 15(22):1294–1296, November 1990.

[11] K. J. Blow, N. J. Doran, B. K. Nayar, and B. P. Nelson. Two-wavelength operation of the nonlinear fibre loop mirror. *Opt. Lett.*, 15(4):248–250, February 1990.

[12] V. E. Zakharov and A. B. Shabat. Interaction between solitons in a stable medium. *Sov. Phys. JETP*, 37(5):823–830, November 1973.

[13] A. Hasegawa and F. Tappert. Transmission of stationary nonlinear optical pulses in dispersive dielectric fibres. I. anomalous dispersion. *Appl. Phys. Lett.*, 23(3):142–144, August 1973.

[14] A. Hasegawa and F. Tappert. Transmission of stationary nonlinear optical pulses in dispersive dielectric fibres. II. normal dispersion. *Appl. Phys. Lett.*, 23(3):142–144, August 1973.

[15] A. Hasegawa and Y. Kodama. *Solitons in Optical Communications*. Oxford Series in Optical and Imaging Sciences. Clarendon Press, Oxford, 1995.

[16] L. F. Mollenauer, R. H. Stolen, and J. P. Gordon. Experimental observation of picosecond pulse narrowing and solitons in optical fibres. *Phys. Rev. Lett.*, 45(13):1095–1098, September 1980.

[17] K. J. Blow and N. J. Doran. Average soliton dynamics and the operation of soliton systems with lumped amplifiers. *IEEE Photonics Tech. Lett.*, 3(4):369–371, April 1991.

[18] A. Hasegawa and Y. Kodoma. Guiding-centre soliton. *Phys. Rev. Lett.*, 66:161–164, 1991.

[19] D. Anderson and M. Lisak. Bandwidth limits due to incoherent soliton interaction in optical fibre communication systems. *Phys. Rev. A*, 32:2270–2274, 1985.

[20] C. Desem and P. L. Chu. Soliton interaction in the presence of loss and periodic amplification in optical fibres. *Opt. Lett.*, 12:349, 1987.

[21] Yuri S. Kivshar. Dark solitons in non-linear optics. *IEEE J. Quantum Electron.*, 29(1):250, January 1993.

[22] W. Zhao and E. Bourkoff. Generation, propagation and amplification of dark solitons. *J. Opt. Soc. Am. B*, 9(7):1134, July 1992.

[23] W. Zhao and E. Bourkoff. Interactions between dark solitons. *Opt. Lett.*, 14(24):1371–1373, December 1989.

[24] Yu. S. Kivshar, M. Haelterman, Ph. Emplit, and J.-P. Hamaide. Gordon-Haus effect on dark solitons. *Opt. Lett.*, 19(1):1–3, January 1994.

[25] C. R. Menyuk and A. M. Rubenchik. Efect of brillouin scattering on optical fibre communication using solitons. *Electron. Lett.*, 30(16):1324–1326, August 1994.

[26] F. M. Knox, P. Harper, P. N. Kean, N. J. Doran, and I. Bennion. Low jitter long distance pulse transmission near net fibre dispersion zero wavelength. *Electron. Lett.*, 31(17):1467–1468, August 1995.

[27] J. Satsuma and N. Yajima. erm ... *Progr. Theor. Phys. Suppl*, 55:284, 1974.

[28] S. A. Gredeskul and Yu. S. Kivshar. Generation of dark solitons in optical fibres. *Phys. Rev. Lett.*, 62(8):977, January 1989.

[29] Sergei A. Gredeskul and Yuri S. Kivshar. Dark soliton generation in optical fibres. *Opt. Lett.*, 14(15):805, August 1989.

[30] G. L. Diankov and I. M. Uzunov. Soliton interaction of dark pulses on a background of finite width in optical fibre. *Opt. Commun.*, 117:424–430, June 1995.

[31] Yu. S. Kivshar. On the soliton generation in optical fibres. *J. Phys. A: Math. Gen.*, 22:337–340, 1989.

[32] K. J. Blow and N. J. Doran. Multiple dark soliton solutions of the nonlinear schroedinger equation. *Phys. Lett.*, 107A(2):55–58, January 1985.

[33] M. Lisak, D. Anderson, and B. A. Malomed. Dissipative damping of dark solitons in optical fibres. *Opt. Lett.*, 16(24):1936–1938, December 1991.

[34] W. J. Tomlinson et al. Dark optical solitons with finite-width background pulses. *J. Opt. Soc. Am. B*, 6(3):329, March 1989.

[35] J. A Giannini and R. I. Joseph. The propagation of bright and dark solitons in lossy optical fibres. *IEEE J. Quantum Electron.*, 26(12):2109–2114, December 1990.

[36] R. H. Stolen and E. P. Ippen. Raman gain in glass optical waveguides. *Appl. Phys. Lett.*, 22:276, 1973.

[37] A. M. Weiner, R. N. Thurston, W. J. Tomlinson, J. P. Heritage, D. E Leaird, and E. M. Kirschner. Temporal and spectral self-shifts of dark optical solitons. *Opt. Lett.*, 14(16):868, August 1989.

[38] Yuri S. Kivshar and Vsevolod V. Afanasjev. Decay of dark solitons due to the stimulated raman effect. *Opt. Lett.*, 16(5):285–287, March 1991.

[39] Ivan M. Uzunov and Vladimir S. Gerdjikov. Self-frequency shift of dark solitons in optical fibres. *Phys. Rev. A*, 47(2):1582–1585, February 1993.

[40] J. P. Gordon. Interaction forces among solitons in optical fibres. *Opt. Lett.*, 8(11):596–598, November 1983.

[41] R. N. Thurston and A. M. Weiner. Collisions of dark solitons in optical fibres. *J. Opt. Soc. Am. B*, 8(2):471–477, February 1991.

[42] Yuri S. Kivshar. Pertubation-induced dynamics of small-amplitude dark optical sltions. *Opt. Lett.*, 15(22):1273–1275, November 1990.

[43] J. P. Heritage, A. M. Weiner, and R. N. Thurston. Picosecond pulse shaping by spectral phase and amplitude manipulation. *Opt. Lett.*, 10(12):609–611, December 1985.

[44] P. Emplit et al. Picosecond steps and dark pulses through nonlinear single mode, fibres. *Opt. Commun.*, 62(6):374–375, June 1987.

[45] D. Krokel et al. Dark pulse propagation in optical fibres. *Phys. Rev. Lett.*, 60(1):29, January 1988.

[46] A. M. Weiner, J. P. Heritage, R. J. Hawkins, R. N. Thurston, E. M. Kirschner, D. E. Leaird, and W. J. Tomlinson. Experimental observation of the fundmental dark soliton in optical fibres. *Phys. Rev. Lett.*, 61(21):2445, November 1988.

[47] Ph. Emplit, M. Haelterman, and J. P. Hamaide. Picosecond dark soliton over a 1km fibre at 850nm. *Opt. Lett.*, 18(13):1047–1049, July 1993.

[48] Joshua E. Rothenberg. Dark soliton trains formed by visible pulse collisions in optical fibres. *Opt. Commun.*, 82(1,2):107–111, April 1991.

[49] Yuri S. Kivshar and Xiaoping Yang. Dark solitons on backgrounds of finite extent. *Opt. Commun.*, 107:93–98, April 1994.

[50] E. M. Dianov, P. V. Mamyshev, A. M. Prokhorov, and S. V. Chernikov. Generation of a train of fundamental solitons at a high repetition rate in optical fibres. *Opt. Lett.*, 14(18):1008–1010, September 1989.

[51] W. Zhao and E. Bourkoff. Generation of dark solitons under a cw background using waveguide electro-optic modulators. *Opt. Lett.*, 15(8):405–407, April 1990.

[52] Yuri. S. Kivshar and S. A. Gredeskul. Dark solitons produced by phase steps in nonlinear optical fibres. *Opt. Commun.*, 79(5):285, November 1990.

[53] M. Haelterman and Ph. Emplit. Optical dark soliton trains generated by passive spectral techniques. *Electron. Lett.*, 29(4):356, February 1993.

[54] D. J. Richardson, R. P. Chamberlain, L. Dong, and D. N. Payne. Experimental demonstration of 100ghz dark soliton generation and propagation using a dispersion decreasing fibre. *Electron. Lett.*, 30(16):1326–1327, August 1994.

[55] M. Nakazawa and K. Suzuki. Generation of a pseudo-random dark soliton data train and its coherent detection by one-bit-shifting with a mach-zender interferometer. *Electron. Lett.*, 31(13):1084–1085, June 95.

[56] M. Nakazawa and K. Suzuki. 10gbit/s pseudo-random dark soliton data transmission over 1200km. *Electron. Lett.*, 31(13):1076–1077, June 1995.

[57] K. M. Allen, N. J. Doran, and J. A. R. Williams. The generation of quasi-continuous trains of dark soliton-like pulses. Nonlinear Guided-wave

Phenomena Technical Digest 1993 Vol 15 (Optical Society of America, Washington, D.C.), pp 378-381), September 1993.

[58] J. A. R. Williams, K. M. Allen, N. J. Doran, and Ph. Emplit. The generation of quasi-continuous trains of dark soliton-like pulses. *Opt. Commun.*, 112:333–338, December 1994.

[59] Joshua E. Rothenberg and Harley K. Heinrich. Observation of the formation of dark soliton trains in optical fibres. *Opt. Lett.*, 17(4):261–263, February 1992.

[60] D. M. Pataca, M. L. Rocha, R. Kashyap, and K. Smith. Bright and dark pulse generation in an optically modelocked fibre laser at 1.3μm. *Electron. Lett.*, 31(1):35–36, January 1995.

[61] K. M. Allen, N. J. Smith, N. J. Doran, and J. A. R. Williams. Dark soliton sideband formation and stability in periodically amplified systems. *Opt. Lett.*, 19(24):2086–2088, December 1994.

[62] N. J. Smith, K. J. Blow, and I. Andonovic. Sideband generation through perturbations to the average soliton model. *J. Lightwave Technol.*, 10(10):1329–1333, October 1992.

[63] F. Matera, A. Mecozzi, M. Romagnoli, and M. Settembre. Sideband instability induce by periodic power variation in long distance fibre links. *Opt. Lett.*, 18(18):1499–1501, September 1993.

[64] Yijiang Chen and Javid Atai. Absorption and amplification of dark solitons. *Opt. Lett.*, 16(24):1933–1935, December 1991.

[65] D. J. Richardson, R. I. Laming, D. N. Payne, V. J. Matsas, and M. W. Philips. Pulse repetition rates in passive, self-starting, femtosecond soliton laser. *Electron. Lett.*, 27:194–197, 1991.

[66] A. Mecozzi, J. D. Moores, H. A. Haus, and Y. Lai. Modulation and filtering control of soliton transmission. *J. Opt. Soc. Am. B*, 9(8):1350–1357, August 1992.

[67] L. F. Mollenauer, J. P. Gordon, and S. G. Evangelides. The sliding-frequency guiding filter: an improved form of soliton jitter control. *Opt. Lett.*, 17(22):1575–1577, November 1992.

[68] N. J. Smith, N. J. Doran, K. J. Blow, and W. J. Firth. Gordon-Haus jitter suppression using a single phase modulator. *Electron. Lett.*, 30(12):987–988, 1994.

[69] J. P. Gordon and H. A. Haus. Random walk of coherently amplified solitons in optical fibre transmission. *Opt. Lett.*, 11(10):665–667, October 1986.

[70] D. Marcuse. Simulations to demonstrate reduction of the Gordon-Haus effect. *Opt. Lett.*, 17(1):34–36, January 1992.

[71] J.P.Hamaide, Ph. Emplit, and M. Haelterman. Dark soliton jitter in amplified optical transmission systems. *Opt. Lett.*, 16(20):1578–1580, October 1991.

[72] Yuri S. Kivshar and Xiaoping Yang. Pertubation-induced dynamics of dark solitons. *Phys. Rev. E*, 49(2):1657–1669, February 1994.

[73] A. Maruta and Y. Kodama. Suppression of interactions between adjacent optical dark pulses by means of synchronised phase modulation. *Opt. Lett.*, 20(17):1752–1754, September 1995.

[74] M. Masumoto, H. Ikeda, and A. Hasegawa. Reduction of Gordon-Haus effect on dark solitons by means of nonlinear gain. *Electron. Lett.*, 31(6):482–483, March 1995.

[75] Hiroki Ikeda, Masayuki Matsumoto, and Akira Hasegawa. Transmission control of dark solitons by means of nonlinear gain. *Opt. Lett.*, 20(10):1113–1115, May 1995.

[76] N. J. Smith and N. J. Doran. Picosecond soliton propagation using nonlinear optical loop mirrors as intensity filters. *Electron. Lett.*, 30(13):1084–1085, June 1994.

[77] Neal S. Bergano, C. R. Davidson, A. M. Vengsarkar, B. M. Nyman, S. G. Evangelides, J. M. Darcie, M. Ma, J. D. Evankow, P. C. Corbett, M. A. Mills, G. A Ferguson, J. R. Pedrazzani, J. A. Nagel, J. L. Zyskind, J. W. Sulhoff, and A. J. Lucero. 100 gb/s wdm transmission of twenty 5 gb/s nrz data channels over transoceanic distances using a gain-flattened amplifier chain. In *Post-deadline Papers*, volume 3, pages 967–970. IMEC, IMEC vzw, INTEC-department, Sint-Pietersnieustraat 41, B-9000 Gent, Belgium, September 1995.